

Old Dominion University

ODU Digital Commons

Mechanical & Aerospace Engineering Theses & Dissertations

Mechanical & Aerospace Engineering

Spring 5-2023

E-Cadherin Force Transmission and Stiffness Sensing

Mazen Mezher

Old Dominion University, mmezh001@odu.edu

Follow this and additional works at: https://digitalcommons.odu.edu/mae_etds



Part of the [Cell Biology Commons](#), [Mechanical Engineering Commons](#), and the [Molecular Biology Commons](#)

Recommended Citation

Mezher, Mazen. "E-Cadherin Force Transmission and Stiffness Sensing" (2023). Doctor of Philosophy (PhD), Dissertation, Mechanical & Aerospace Engineering, Old Dominion University, DOI: 10.25777/yxrf-jt17
https://digitalcommons.odu.edu/mae_etds/358

This Dissertation is brought to you for free and open access by the Mechanical & Aerospace Engineering at ODU Digital Commons. It has been accepted for inclusion in Mechanical & Aerospace Engineering Theses & Dissertations by an authorized administrator of ODU Digital Commons. For more information, please contact digitalcommons@odu.edu.

E-CADHERIN FORCE TRANSMISSION AND STIFFNESS SENSING

by

Mazen Mezher

B.S., June 2014, Holy Spirit University of Kaslik, Lebanon

M.S, June 2016, Holy Spirit University of Kaslik, Lebanon

A Dissertation Submitted to the Faculty of
Old Dominion University in Partial Fulfillment of the
Requirements of the Degree of

DOCTOR OF PHILOSOPHY

MECHANICAL ENGINEERING

OLD DOMINION UNIVERSITY

May 2023

Approved by:

Venkat Maruthamuthu (Director)

Sharan Asundi (Member)

Stacie Ringleb (Member)

Guijun Wang (Member)

ABSTRACT

E-CADHERIN FORCE TRANSMISSION AND STIFFNESS SENSING

Mazen Mezher
Old Dominion University, 2023
Director: Dr. Venkat Maruthamuthu

E-cadherin is the chief mediator of cell-cell adhesion between epithelial cells and is a known mechanosensor. Force transmission and stiffness sensing are two crucial aspects of E-cadherin mechanobiology.

E-cadherin has an extracellular adhesive region, a transmembrane region and an intracellular region that binds to adhesion-associated proteins. Here, we assessed how different factors affect the level of force transmission (i) from inside the cell such as adhesion-associated proteins, (ii) on the cell membrane, such as growth factor receptors and (iii) outside the cell, such as different binding partners in adhesion. To study the level of force transmission inside the cell, we studied the role of vinculin and α -catenin in transmitting endogenous forces at cell-cell contacts. We found that vinculin, not α -catenin, is pivotal for transmitting high endogenous forces at cell-cell contacts through E-cadherin. To study how the level of force transmission is affected by factors on the cell membrane, we investigated the effect of EGFR on the intercellular forces transmitted at cell-cell contacts. We found that EGFR activity significantly affects the level of intercellular forces. In order to understand how the level of force transmission depends on binding partners from outside the cell, we studied homophilic and heterophilic interactions of cadherins. We found that the intercellular tension for the heterophilic E-cad/N-cad interaction is higher than the homophilic E-cad/E-cad interaction. Additionally, we also devised a modified traction force

microscopy method using a novel, simple strategy for coincident immunofluorescence and traction force microscopy.

Moreover, E-cadherin adhesions reside in a microenvironment that is comprised of adjacent epithelial cells. We found that E-cadherin adhesions change their organization depending on the magnitude of the epithelial cell-like elasticity of their microenvironment. Such E-cadherin adhesions were of two types: linear shaped adhesions and irregularly shaped adhesions. We found that linear adhesions were dependent on formin-dependent linear actin bundles and irregular adhesions were dependent on high local actin density. Thus, we found that actin is a crucial determinant of how E-cadherin adhesions are organized in response to cell-like soft microenvironments. All these findings have important implications for tissue development (morphogenesis), dysregulation (such as during cancer progression) as well as tissue engineering.

Copyright, 2023, by Mazen Mezher, All Rights Reserved.

This dissertation is dedicated to my parents.

ACKNOWLEDGMENTS

I would like to express my sincere gratefulness and my genuine appreciation to my advisor Dr. Venkat Maruthamuthu for his tremendous assistance and valuable guidance throughout my Ph.D. career. In addition, I would like to thank him for his motivation, devotion, commitment, and determination which have helped me achieve my goals and build my research career.

Besides my advisor, I would like to thank Dr. Sharan Asundi, Dr. Stacie Ringleb, and Dr. Guijun Wang for their insightful advices and continuous encouragement.

Finally, I am extremely grateful for my parents and my siblings for their unconditional love, care, and support. My deepest gratitude goes to my dad in heaven who is my forever spiritual guidance and I dedicate all my efforts, achievements, and my accomplishments to him.

TABLE OF CONTENTS

	Page
LIST OF FIGURES	ix
LIST OF TABLES	xvi
INTRODUCTION	1
1.1 Cell Adhesion.....	1
1.2 Cadherins and Cell-Cell Adhesion.....	2
1.3 Integrins and Cell-ECM Adhesion.....	4
1.4 Importance of Cell Adhesion and Force Transmission.....	5
1.5 Role of Intracellular Adhesion-associated Proteins in Cellular Mechanotransduction.....	6
1.6 Measuring Cell-ECM Traction Forces Using Traction Force Microscopy.....	7
1.7 Determination of Forces Transmitted at Cell-Cell Contacts.....	9
1.8 Aspects of E-cadherin mechanobiology of interest	10
VINCULIN IS ESSENTIAL FOR HIGH ENDOGENOUS FORCE TRANSMISSION AT CELL-CELL CONTACTS	12
2.1 Introduction.....	12
2.2 Methods.....	15
2.2.1 Cell Culture	15
2.2.2 Live Cell Imaging and Immunofluorescence	15
2.2.3 Preparation of Qgel substrate	16
2.2.4 Traction Force Measurement	16
2.2.5 Biaxial Stretch.....	17
2.2.6 Statistical Analysis.....	17
2.3 Results and Discussion	18
2.4 Conclusion	32
SIMPLE STRATEGY FOR COINCIDENT TRACTION FORCE MICROSCOPY AND IMMUNOFLUORESCENCE TECHNIQUE	33
3.1 Introduction.....	33
2.2 Methods.....	35
3.2.1 Preparation of NuSil Substrate.....	35
3.2.2 Reference bead image	35
3.2.3 Traction Force Microscopy and Immunofluorescence.....	36

3.3	Results and Discussion	37
3.4	Detailed Experimental Protocol for Coincident Immunofluorescence and TFM (IF-TFM).....	42
3.4.1	Stitching Protocol.....	45
3.4.2	Protocol to Determine YAP Ratio	46
3.5	Conclusion	51
E-CADHERIN STIFFNESS SENSING AND FACTORS AFFECTING FORCE TRANSMISSION		52
4.1	Introduction.....	52
4.2	Methods.....	55
4.2.1	Cell Culture.....	55
4.2.2	Biomimetic E-cadherin Glass Substrate Preparation	56
4.2.3	Biomimetic E-cadherin Soft Substrate Preparation	56
4.2.4	Immunofluorescence and Drug Treatment.....	57
4.3	Results and Discussion.....	58
4.3.1	Formation of undesirable focal adhesions on E-cadherin-Fc glass substrate.....	58
4.3.2	Absence of focal adhesions on E-cadherin-Fc glass substrate.....	60
4.3.3	Avoiding focal adhesions on E-cadherin-Fc substrate using integrin inhibitors.....	63
4.3.4	Effect of E-cadherin cell-like elastic substrates on the organization of E-cadherin adhesions.....	65
4.3.5	Localization of phospho-myosin in cells on E-cadherin coated cell-like substrates.....	72
4.3.6	Organization of F-actin in cells on E-cadherin coated cell-like substrates	73
4.3.7	Effect of myosin inhibition on E-cadherin adhesions in cells on E-cadherin coated cell-like substrates.....	74
4.3.8	Effect of formin inhibition on the actin organization of cells on E-cadherin coated cell-like substrates.....	75
4.3.9	Effect of Arp2/3 inhibition on the actin organization in cells on E-cadherin coated cell-like substrates.....	77
4.3.10	Effect of Rho-activation on cells plated on E-cadherin-coated soft substrate	79
4.3.11	Soft silicones as possible candidates for E-cadherin coated substrates – Rheology	80
4.3.12	E-cadherin force transmission regulation at the cell membrane and from outside the cell.....	85
4.4	Conclusion	91
CONCLUSION.....		94
REFERENCES.....		98
VITA.....		108

LIST OF FIGURES

Figure 1: A schematic depiction of the transmembrane protein E-cadherin at the cell-cell contact linked to the actomyosin network.	3
Figure 2: A schematic depiction of integrin and focal adhesion proteins and their linkage to the actomyosin network	5
Figure 3: schematic description of the experimental setup of traction force microscopy (TFM). During day 1: The substrate is prepared with fluorescent beads and then cells are plated on the substrate. During day 2: A fluorescence microscope is used to capture two images: the cell image and the corresponding stressed bead image. Then, the cells are disintegrated, and a relaxed bead image is taken. From the stressed bead image and the relaxed bead image, TFM analysis yields the traction stresses exerted by cells.	8
Figure 4: Schematic depicting the key mechanical roles of adhesion proteins. Adhesion proteins enable force transmission at cell-cell contact and enhance the adhesion strength by the recruitment of specific proteins like vinculin under force	13
Figure 5: Schematic description of the multiple pathways by which force can be transmitted through E-cadherin to F-actin. (X may be a protein such as afadin or EPLIN).	14
Figure 6: Absence of vinculin in MDCK vinculin KO cells. (A) Immunofluorescence images of MDCK and (B) MDCK vinculin KO cells stained for vinculin. Scale bar: 5 μ m.	19
Figure 7: Traction forces within a single cell. (A) Traction stresses exerted by a single MDCK cell (top, left) and (B) an MDCK vinculin KO cell (bottom, left) on the ECM. Traction stress vectors are overlaid (red arrows). Heat-scale map of the traction magnitude for a single MDCK cell (top, right) and MDCK vinculin KO (bottom, right). Scale bar is 5 μ m. Red arrow: 400 Pa.	19
Figure 8: Distribution of the strain energy for MDCK and MDCK vinculin KO single cells. Bar represents the mean value.	20
Figure 9: Loss of vinculin leads to a severe decrease in inter-cellular forces. (A) Traction stresses of an MDCK cell pair (top, left) and (B) an MDCK vinculin KO cell pair (bottom, left). Traction stress vectors are overlaid (red arrows.). Heat-scale map of the traction magnitude for MDCK cell pair (top, right) and MDCK vinculin KO (bottom, right). Scale bar is 5 μ m. Red arrow: 400 Pa.	21

Figure 10: Distribution of the intercellular forces for MDCK and MDCK vinculin KO cell pairs. Bar represents the mean value. 22

Figure 11: Loss of α -catenin does not lead to a significant decrease in inter-cellular forces. (A) Traction stresses of MDCK α -catenin cell pair (top, left) and (B) MDCK α -catDVBS in α -catenin KO cell pair (bottom, left). Traction stress vectors are overlaid (red arrows.). Heat-scale map of the traction magnitude for MDCK α -catenin KO cell pair (top, right) and MDCK α -catDVBS in α -catenin KO (bottom, right). Scale bar is 5 μ m. Red arrow: 400 Pa. 24

Figure 12: Distribution of the intercellular forces for MDCK α -catenin KO and MDCK α -catDVBS in α -catenin KO cell pair. Bar represents the mean value. 25

Figure 13: Loss of both α -catenin and vinculin leads to a severe decrease in inter-cellular forces. (A) Traction stresses of MDCK α -catenin KO & vinculin KO cell pair. Traction stress vectors are overlaid (red arrows). Heat-scale map of the traction magnitude for MDCK α -catenin & vinculin KO cell pair. Scale bar is 5 μ m. Black arrow: 400 Pa. 26

Figure 14: Distribution of the intercellular forces for MDCK and MDCK α -catenin & vinculin KO cell pairs. Bar represents the mean value. 26

Figure 15: (A) MDCK cells before stretch and (B) after full stretch. (C) plasma membrane staining for MDCK before stretch and (D) after stretch. Scale bar: 10 μ m. 28

Figure 16: (A) MDCK vinculin KO before stretch and (B) after full stretch. (C) plasma membrane staining for MDCK vinculin KO before stretch and (D) after stretch. Scale bar: 10 μ m. 28

Figure 17: Fraction of cell-cell contacts ruptured as a function of strain (%). Each data point is the mean \pm standard deviation (SD) for two cell islands for MDCK vinculin KO cells (306 cell-cell contacts) and four cell islands for MDCK (378 cell-cell contacts). 29

Figure 18: Traction stresses of MDCK cell island (top, left) and MDCK α -catenin knock out (KO) rescued with α -catenin CA cell island (bottom, left). Traction stress vectors are overlaid (red arrows). Heat-scale map of the traction magnitude for MDCK cell island (top, right) and MDCK α -catenin Knock out (KO) rescued with α -catenin CA cell island (bottom, right). Black arrow: 400 Pa. 30

Figure 19: Box plot comparison of the traction magnitude distribution for MDCK parental control and MDCK α -catenin knock out (KO) rescued with α -catenin CA cell islands. Statistical properties are as follows: mean (open square), box (25/75% quartile), whisker (5/95% quartile), diagonal cross (maximum/minimum). There was no statistical difference ($p > 0.05$) observed for traction

magnitudes between MDCK parental control and MDCK α -catenin knock out (KO) rescued with α -catenin CA conditions. 31

Figure 20: Schematic depiction of our methods for coincident traction force and immunofluorescence data collection. (A) Collagen I substrate with fluorescent beads plated on Qgel silicone substrate. (B) Region of the substrate selected near the center and imaged using Tile Scan in fluorescence microscopy. (C) Stitched bead image composed of several reference bead images in absence of cell generated forces taken from the tile scanned region of panel (B). (D) Cells are plated on the substrate. (E) After overnight incubation, cells and deformed bead images within the tile scanned region near the center of substrate are imaged using fluorescent microscopy. (F, right) Traction Force Microscopy (TFM) procedure can be done after using cross-correlation using MATLAB where a reference bead image can be matched with the deformed bead image (E) in order to get the traction force map. Subsequently, the immunofluorescence (IF) image of the same cell can be obtained (F) after fixing and staining the cells. 38

Figure 21: Coincident traction force maps and immunofluorescence images. (A) Stitched reference bead image. (B, left) A431 cell phase image. (B, right) Deformed/stressed bead image. (C) Traction stresses of A431 single cell (left). Traction stress vectors are overlaid (red arrows.). Heat-scale map of the traction magnitude for A431 single cell (right). Scale bar is 5 μ m. Red arrow: 500 Pa. (D) Immunofluorescence images for an A431 cell stained for actin, DAPI, and YAP. 40

Figure 22: Single cell strain energy vs YAP ratio. Average ratio of YAP for single cells was 1.03 ± 0.02 42

Figure 23: Inter-cellular force vs YAP ratio for cell pairs. Average ratio of YAP for cell pairs was 1.03 ± 0.03 42

Figure 24: Formation of not well-developed E-cadherin adhesions but prominent focal adhesions on E-cadherin-Fc glass substrate in the presence of fetal bovine serum. (A-C) Immunofluorescence images of C2BBE cells on E-cadherin glass substrate stained for (A) β -catenin (marking E-cadherin adhesions), (B) paxillin (marking focal adhesions), and (C) phalloidin (marking actin cytoskeleton). All scale bars are 5 μ m. 59

Figure 25: Presence of BSA does not preclude the formation of focal adhesions on E-cadherin glass substrate. (A-C) Representative immunofluorescence images of C2BBE cells on E-cadherin glass substrate that includes 10 mg/mL BSA blocking step and stained for (A) β -catenin (marking E-cadherin adhesions), (B) paxillin (marking focal adhesions), and (C) phalloidin (marking actin cytoskeleton). Focal adhesions marked by paxillin were prominent even in the presence of BSA blocking. All scale bars are 5 μ m. 60

Figure 26: Formation of well-developed E-cadherin adhesions with absence of focal adhesions on E-cadherin-Fc glass substrate in serum free medium. (A-C) Immunofluorescence images of

C2BBe cells on E-cadherin glass substrate stained for (A) β -catenin (marking E-cadherin adhesions), (B) paxillin (marking focal adhesions), and (C) phalloidin (marking actin cytoskeleton). All scale bars are 5 μ m. 61

Figure 27: Formation of well-developed E-cadherin adhesions on E-cadherin-Fc glass substrate in serum free medium. (A-C) Immunofluorescence images of A431 cells on E-cadherin glass substrate stained for (A) phalloidin (marking actin cytoskeleton), (B) β -catenin (marking E-cadherin adhesions), and (C) paxillin (marking focal adhesions). All scale bars are 5 μ m. 62

Figure 28: Cell viability is not affected during the experimental time course in the absence of serum. (A) C2BBe cell island at time 0 hour cultured in media with 5% FBS. Same C2BBe cell island after being in culture in serum free medium for 2 hours (B) and 4hrs (C). All scale bars are 10 μ m. 63

Figure 29: Actin-associated E-cadherin adhesion morphologies after treatment with integrin inhibitors in the presence of fetal bovine serum. (A-F) Immunofluorescence images of C2BBe cells on glass substrate stained for (A, D) phalloidin (marking actin cytoskeleton), (B, E) β -catenin (marking E-cadherin adhesions), and (C, F) paxillin (marking focal adhesions). (B) E-cadherin adhesions associated with actin foci along circumferential structures of F-actin. (E) E-cadherin associated with the ends of radial orientation of F-actin structures. All scale bars are 5 μ m. 64

Figure 30: Actin-associated E-cadherin adhesion morphologies after treatment with integrin inhibitors in the absence of fetal bovine serum. (A-F) Immunofluorescence images of C2BBe cells on glass substrate stained for (A, D) phalloidin (marking actin cytoskeleton), (B, E) β -catenin (marking E-cadherin adhesions), and (C, F) paxillin (marking focal adhesions). (B) E-cadherin adhesions associated with actin foci along circumferential structures of F-actin. (E) E-cadherin associated with the ends of radial orientation of F-actin structures. All scale bars are 5 μ m. 65

Figure 31: Formation of not well-developed E-cadherin adhesions but prominent focal adhesions on cell-like soft substrate in the presence of fetal bovine serum after overnight incubation. (A-C) Immunofluorescence images of C2BBe cells on 2.4 kPa E-cadherin soft substrate stained for (A) phalloidin (marking the actin cytoskeleton), (B) β -catenin (marking E-cadherin adhesions), and (C) paxillin (marking focal adhesions). All scale bars are 5 μ m 67

Figure 32: Actin associated with linear E-cadherin morphologies on 0.3 kPa E-cadherin substrates. (A-C) representative immunofluorescence images of C2BBe cells on 0.3 kPa E-cadherin substrate stained for (A) phalloidin (marking actin cytoskeleton) and (B) β -catenin (marking E-cadherin adhesions), and (C) paxillin (marking focal adhesions). (B) Linear E-cadherin associated with the ends of radial orientation of F-actin structures. All scale bars are 5 μ m 68

Figure 33: Actin associated with linear E-cadherin morphologies on 2.4 kPa E-cadherin substrates. (A-C) representative immunofluorescence images of C2BBe cells on 2.4 kPa E-cadherin substrate

stained for (A) phalloidin (marking actin cytoskeleton) and (B) β -catenin (marking E-cadherin adhesions), and (C) paxillin (marking focal adhesions). (B) Linear E-cadherin associated with the ends of radial orientation of F-actin structures. All scale bars are 5 μ m. 69

Figure 34: Actin associated with irregular E-cadherin morphologies on 0.3 kPa E-cadherin substrates. (A-C) representative immunofluorescence images of C2BBe cells on 0.3 kPa E-cadherin substrate stained for (A) phalloidin (marking actin cytoskeleton) and (B) β -catenin (marking E-cadherin adhesions), and (C) paxillin (marking focal adhesions). (B) Irregular E-cadherin adhesions associated with actin foci along circumferential structures of F-actin. All scale bars are 5 μ m..... 70

Figure 35: Actin associated with irregular E-cadherin morphologies on 2.4 kPa E-cadherin substrates. (A-C) representative immunofluorescence images of C2BBe cells on 2.4 kPa E-cadherin substrate stained for (A) phalloidin (marking actin cytoskeleton) and (B) β -catenin (marking E-cadherin adhesions), and (C) paxillin (marking focal adhesions). (B) Irregular E-cadherin adhesions associated with actin foci along circumferential structures of F-actin. All scale bars are 5 μ m..... 71

Figure 36: Presence of irregular adhesions associated with circumferential actin foci and linear E-cadherin adhesions associated with radial actin. (A-D) Immunofluorescence images of C2BBe cells on 2.4 kPa soft substrate stained for (A, C) phalloidin (marking actin cytoskeleton), and (B, D) cytoplasmic domain of E-cadherin. (B) E-cadherin adhesions associated with actin foci along circumferential structures of F-actin. (D) E-cadherin associated with the ends of radial orientation of F-actin structures. All scale bars are 5 μ m. 72

Figure 37: Circumferential actin foci does not colocalize with phospho-myosin. (A-C) representative immunofluorescence images of C2BBe cells on 2.4 kPa E-cadherin substrate stained for (A) phalloidin (marking actin cytoskeleton) and (B) β -catenin (marking E-cadherin adhesions), and (C) phospho-myosin. All scale bars are 5 μ m..... 73

Figure 38: High local actin density supports irregular E-cadherin adhesions on soft substrates. (A-C) representative immunofluorescence images of C2BBe cells on 2.4 kPa E-cadherin substrate treated with Jasplakinolide and stained for (A) phalloidin (marking actin cytoskeleton) and (B) β -catenin (marking E-cadherin adhesions), and (C) paxillin. All scale bars are 5 μ m 74

Figure 39: Blebbistatin treatment does not eliminate E-cadherin irregular adhesions but leads to loss of linear adhesions. (A-D) representative immunofluorescence images of C2BBe cells on 2.4 kPa E-cadherin substrate treated with blebbistatin and stained for (A, C) phalloidin (marking actin cytoskeleton) and (B, D) β -catenin (marking E-cadherin adhesions). All scale bars are 5 μ m.... 75

Figure 40: Formin activity is crucial for the formation of linear E-cadherin adhesions associated with the ends of radial orientation of F-actin structures on cell-like soft E-cadherin substrates. (A-

F) representative immunofluorescence images of C2BBe cells on 2.4 kPa E-cadherin substrate treated with DMSO (A, B, C) and SMIFH2 (D, E, F) and stained for (A, D) phalloidin (marking actin cytoskeleton) and (B, E) β -catenin (marking E-cadherin adhesions), and (C, F) paxillin. All scale bars are 5 μ m. 76

Figure 41: Formin activity is crucial for the formation of linear E-cadherin adhesions on sub-kPa substrates. (A-C) representative immunofluorescence images of C2BBe cells on 0.3 kPa E-cadherin substrate treated with SMIFH2 and stained for (A) phalloidin (marking actin cytoskeleton) and (B) β -catenin (marking E-cadherin adhesions), and (C) paxillin. All scale bars are 5 μ m. 77

Figure 42: E-cadherin adhesions on cell-like substrates are independent of Arp2/3 actin nucleator. (A-B) Representative immunofluorescence images of C2BBe cells on 2.4 kPa E-cadherin substrate treated with CK-666 and stained for (A) phalloidin (marking actin cytoskeleton) and (B) β -catenin (marking E-cadherin adhesions). All scale bars are 5 μ m. 78

Figure 43: E-cadherin adhesions are localized with actin clumps even under arp2/3 inhibition. (A-B) representative immunofluorescence images of C2BBe cells on 8.7 kPa E-cadherin substrate treated with CK-666 and stained for (A) phalloidin (marking actin cytoskeleton) and (B) β -catenin (marking E-cadherin adhesions). All scale bars are 5 μ m. 79

Figure 44: Rho activator promotes the formation of smaller irregular E-cadherin adhesions at regions of high actin density. (A-C) representative immunofluorescence images of C2BBe cells on 2.4 kPa E-cadherin substrate treated with Rho activator and stained for (A) phalloidin (marking actin cytoskeleton) and (B) β -catenin (marking E-cadherin adhesions), and (C) paxillin. All scale bars are 5 μ m. 80

Figure 45: Mechanical properties of NuSil 1.1 with 0% Sylgard 184 with frequency sweep test at 0.5 % strain. Storage modulus, G' , and loss modulus, G'' , in kPa versus angular frequency, ω , in rad/sec. All data points are mean \pm SD. 82

Figure 46: Mechanical properties of NuSil 1.1 with 0.15% Sylgard 184 with frequency sweep test at 0.5 % strain. Storage modulus, G' , and loss modulus, G'' , in kPa versus angular frequency, ω , in rad/sec. All data points are mean \pm SD. 82

Figure 47: Mechanical properties of NuSil 1.1 with 0.5% Sylgard 184 with frequency sweep test at 0.5 % strain. Storage modulus, G' , and loss modulus, G'' , in kPa versus angular frequency, ω , in rad/sec. All data points are mean \pm SD. 83

Figure 48: Mechanical properties of NuSil 1.1 with 1% Sylgard 184 with frequency sweep test at 0.5 % strain. Storage modulus, G' , and loss modulus, G'' , in kPa versus angular frequency, ω , in rad/sec. All data points are mean \pm SD. 83

Figure 49: Mechanical properties of NuSil 1.1 with 2.5% Sylgard 184 with frequency sweep test at 0.5 % strain. Storage modulus, G' , and loss modulus, G'' , in kPa versus angular frequency, ω , in rad/sec. All data points are mean \pm SD. 84

Figure 50: Mechanical properties of NuSil 1.1 with 0.55% Sylgard 184 with frequency sweep test at 0.5 % strain. Storage modulus, G' , and loss modulus, G'' , in kPa versus angular frequency, ω , in rad/sec. All data points are mean \pm SD. 85

Figure 51: Inhibition of EGFR leads to a decrease in inter-cellular forces. (A) Traction stresses of A431 cell pair (top, left) and A431 cell pair treated with EGFR inhibitor (bottom, left). Traction stress vectors are overlaid (red arrows.). Heat-scale map of the traction magnitude for A431 cell pair (top, right) and A431 cell pair treated with EGFR inhibitor (bottom, right). Scale bar is 5 μ m. Red arrow: 400 Pa. (B) Dot plot of the intercellular forces for A431 cell pair and A431 cell pair treated with EGFR inhibitor cell pairs. Black bar represents the mean value. ($P = 2 \times 10^{-7}$). 87

Figure 52: Heterophilic interaction between A431D cells leads to higher inter-cellular forces compared to homophilic interactions between A431D cells. (A) Traction stresses of A431D cell pair transfected with N-cadherin (top, left), A431D cell pair transfected with E-cadherin (middle, left), and A431D heterogeneous (bottom, left). Traction stress vectors are overlaid (red arrows.). Heat-scale map of the traction magnitude for A431 cell pair transfected with N-cadherin (top, right), A431D cell pair transfected with E-cadherin (middle, right), and A431D heterophilic cell pair (bottom, right). Scale bar is 5 μ m. Red arrow: 400 Pa. (B) Dot plot of the intercellular forces for A431D cell pair transfected with N-cadherin, A431D cell pair transfected with E-cadherin, and A431D heterophilic. Black bar represents the mean value. (** corresponds to $p < 0.01$). 90

LIST OF TABLES

1. Mechanical properties of NuSil soft silicones with 0%, 0.15%, 0.5%, 1%, and 2.5% Sylgard 184. A table of storage modulus, G' , with mean \pm standard deviation and elastic modulus, E , in kPa.....	84
---	----

CHAPTER 1

INTRODUCTION

Cells are the basic units of all living bodies. In epithelial tissues, cells physically cohere together in order to form a well-organized multicellular structure. Cells adhere to each other through cell-cell junctions, or through the connection to the extracellular matrix (ECM), a network of polysaccharide chains and proteins, secreted by the cells. The junctions between cells allow them to exchange many signals by creating pathways for communication and to form a stable junction that allows the epithelial cells to form tissues in the body. Cell adhesion has a crucial role in the development of tissues, and it stimulates signals that control tissue differentiation, migration, and survival of the cells. In this chapter, I provide a general overview of cell adhesion and the methods used to measure forces transmitted through cell-cell contacts and forces exerted by cells on the extracellular matrix.

1.1 Cell Adhesion

Cell adhesion is the process by which a single cell physically interacts with neighboring cells or with the extracellular matrix. Cell junctions are contact sites that join the surfaces of two adjacent cells or the surfaces of a cell and the extracellular matrix. In epithelial tissues, cells form an epithelial cell sheet where cells are closely bound together. The extracellular matrix closest to epithelial cells consists of a thin layer called basal lamina that underlies one face of the epithelial sheet. Within the epithelium, the cells are directly attached to one another by cell-cell junctions, where the cytoskeletal filaments are anchored and transfer stresses from one adhesion site to another across the interior of each cell. The junctions between adjacent cells or between cells and extracellular matrix have several structures and many functions. In general, there are four classes

of cell junctions: (i) Anchoring junctions that are attached to cytoskeletal filaments inside the cell and include both cell-cell adhesions and cell-matrix adhesions. (ii) Occluding junctions seal the gaps between epithelial cells and make a cell sheet that serves as a selectively permeable barrier. (iii) Channel-forming junctions link the cytoplasm of adjacent cells by creating passageways for small molecules and ions to pass from one cell to another. (iv) Signal-relaying junctions transmit signals between two cells through their plasma membrane at cell-cell adhesion site [1]. Different techniques have been applied to analyze cell adhesion in order to determine the adhesion properties of normal cells [2]. Several studies have demonstrated that cell adhesion is important for tissue integrity [3], migration [4] and wound healing [5]. Improved knowledge of cell adhesion can improve drug delivery systems [6] and suggest means of attenuating cancer cell metastasis [7]. Understanding cell adhesion can also help develop novel biomaterials that enhance the design of implanted sensors and artificial tissue constructs [8]. It is also crucial for finding treatments for diseases such as kidney disease [9], or Alzheimer's disease [10].

1.2 Cadherins and Cell-Cell Adhesion

Cadherins are cell surface proteins that are dependent on Ca^{2+} ions. Several classical cadherins were discovered and were named according to the main body tissues in which they were found. E-cadherin is present in epithelial tissues, N-cadherin is present in neural tissues, VE-cadherin is present in endothelial tissues. In epithelial tissues, the main classical type of cadherin that mediates interactions at the cell-cell contact is E-cadherin. E-cadherin has an extracellular region, a transmembrane region and an intracellular region. The extracellular region of E-cadherin of one cell binds homophilically to the extracellular region of E-cadherin of the neighboring cell, however the intracellular region of E-cadherin binds to p120-catenin and β -catenin. β -catenin in turn binds to α -catenin. E-cadherin also binds to actin filaments through the catenin complex on

both sides of the junction at the cell-cell contact (Figure 1). The tension exerted through E-cadherin is produced by the actomyosin complex. E-cadherin plays an important role in influencing morphogenetic changes, differentiation, and remodeling [11]. The contacts between neighboring cells with cadherin junctions are mechanically active structures. Cadherin adhesion couples the contractile cortices of neighboring cells in order to provide tension transmission at the adhesion site [12]. The regulation of cell-cell junction dynamics is influenced by the actin cytoskeleton that is associated with E-cadherin adhesion receptors [13]. An intact actin cytoskeleton is required for a functional cadherin adhesion. Physical coupling with the actin cytoskeleton is very important for cadherins to establish junctions that resist mechanical stress.

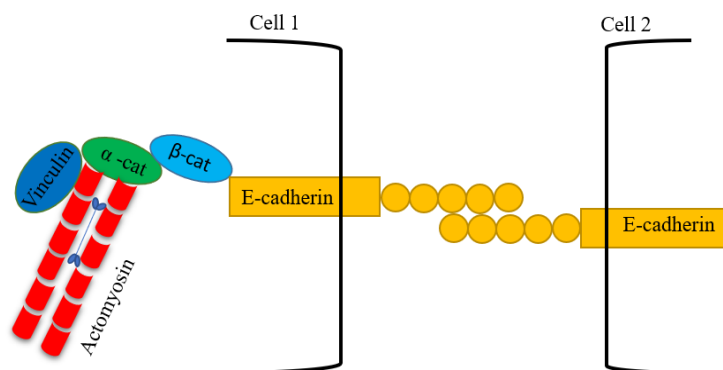


Figure 1: A schematic depiction of the transmembrane protein E-cadherin at the cell-cell contact linked to the actomyosin network.

1.3 Integrins and Cell-ECM Adhesion

Integrin is a matrix receptor molecule composed of two noncovalently associated glycoproteins called the α and β subunits. Integrin heterodimerization occurs intracellularly prior to the transport to the plasma membrane surface. In vertebrates, the family of integrins is composed of 18 α subunits and 8 β subunits that can form 24 different heterodimers [14]. The head of the integrin attaches to an extracellular matrix protein such as fibronectin or laminin, and the intracellular tail of the integrin binds directly to a set of intracellular anchorage proteins to form focal adhesions [1]. Focal adhesions help to reinforce the linkage between the extracellular matrix and the actin filament and include proteins such as vinculin and paxillin (Figure 2). Focal adhesion proteins act as mechano-sensors that allow cells to respond to matrices of various molecular and physical properties. Several types of cell-ECM adhesions are defined by their subcellular location, composition, and size. Focal complexes, which are smaller than focal adhesions, are located at the periphery of migrating or spreading cells. They are regulated by small G-proteins that regulate and control actin dynamics such Cdc42 and Rac, and lead to larger focal adhesions that are regulated by Rho activity. Integrins can be activated in two different ways, either from a cytoplasmic signal or from the extracellular matrix. Inside-out signaling occurs when integrins become activated in response to a cytoplasmic signal (talin binding) [15]. Outside-in signaling occurs when external signals from ligand binding activate integrin [16]. Integrins transmit molecular and mechanical signals across the cell membrane in both directions. This influences cell behavior, from survival and proliferation to guidance of migration and cell polarity [17]. Defects in integrin-based adhesion leads to genetic diseases including kidney and skin disease [18]. Several studies have shown that sensing of the microenvironmental stiffness through integrins regulates cell morphology and cell migration [19]. Moreover, studies have demonstrated that the cell spread area

is influenced by the molecular tension at integrin-ECM bonds [20,21,22]. For instance, cells with larger molecular tension (high forces across proteins) have larger spreading area [23].

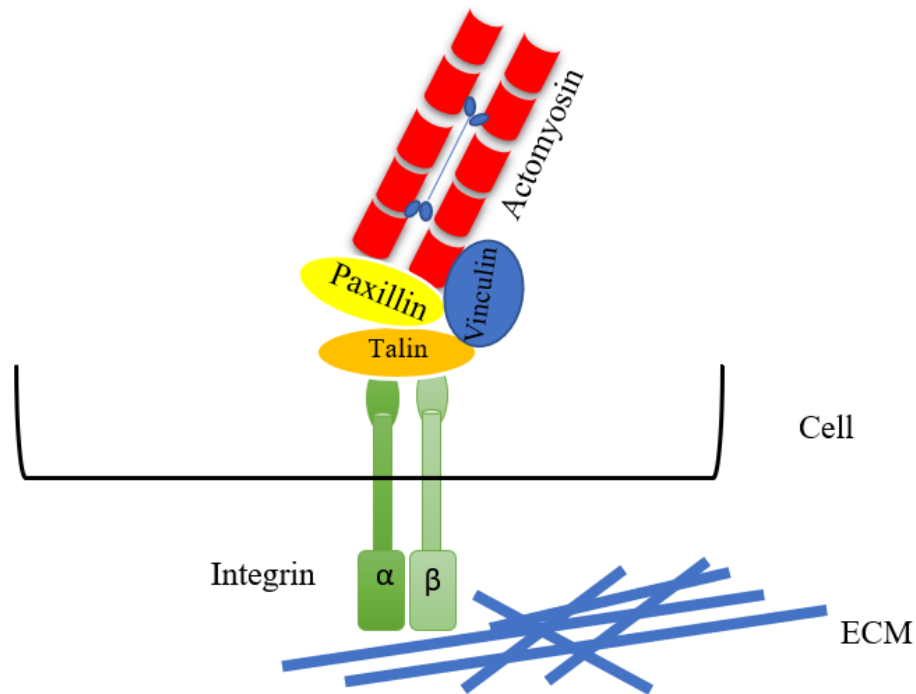


Figure 2: A schematic depiction of integrin and focal adhesion proteins and their linkage to the actomyosin network.

1.4 Importance of Cell Adhesion and Force Transmission

In epithelial tissues, cells are in contact with neighboring cells and with the extracellular matrix. Cells are contractile and are subjected to stretching, compression, and shear forces. Forces are both generated internally within the cell by the cytoskeleton and exerted externally by adjacent cells and the extracellular matrix. Internal forces are generated by the actomyosin network that is composed of non-muscle myosin II motor linked to filamentous actin (F-actin). The actomyosin

network is crucial for providing structural integrity by linking different parts of the cell membrane and the cell membrane to the nucleus of the cell. External forces are either transmitted between two adjacent cells through intracellular and intercellular proteins such as cadherins and between the cell and the extracellular matrix through proteins such as integrins. Forces are transmitted through cell-cell adhesion clusters consisting of E-cadherin that bind to β -catenin, which in turn binds to α -catenin and mediate interaction with the actin cytoskeleton inside the cell [24]. When the linkage between the actomyosin machinery and the adhesions are strong, the transmission of forces is more efficient. Force transmission is crucial for cell adhesion [25], cell division, cell migration, morphogenesis and tissue integrity [26]. Dysregulation in force transmission may result in tissue stiffening, wound healing failure and cancer.

1.5 Role of Intracellular Adhesion-associated Proteins in Cellular Mechanotransduction

Cells sense and respond to forces by converting the mechanical information into biochemical signals that produce specific cellular responses - this process is called mechanotransduction. Intracellular adhesion-associated proteins play an important role in cell-cell adhesion and in cell-ECM adhesion. To study how cellular functions are regulated by mechanical forces, cells should not be considered as isolated units, but their physical contact with adjacent cells or the extracellular matrix needs to be considered. The structural organization of the cell is affected by the adhesion of cells to the extracellular matrix. For instance, bonding and clustering of integrins against the ECM ligands influence cell shape and cytoskeletal architecture [27]. At cell-cell adhesion sites, catenins and other intracellular proteins regulate force transmission. Knock out of α -catenin in cells alters the force response and reduces the affinity of E-cadherin [28]. Therefore, α -catenin contributes to strengthening adhesions and modulating the transmission of forces especially during collective cell migration. Upon knocking out β -catenin, adherens

junctions become very weak in response to the application of external stress [29,30]. Adherens junctional tension is reduced after the direct or indirect depletion of RhoA [31]. The contractility of actomyosin is the origin of the pulling forces on the adhesion sites. Tensile stress at cell-cell contacts is sensed by the intracellular proteins of the cadherin-catenin family: tension reveals binding sites of α -catenin, leading to the recruitment of vinculin, which provides further binding sites for actin filaments. The recruitment of vinculin is thus expected to reinforce junctions at the cell-cell contact and strengthen the mechanical properties of adhesion sites [24].

1.6 Measuring Cell-ECM Traction Forces Using Traction Force Microscopy

Cells constantly experience internal and external forces. Mechanical forces can be measured using several methods that can vary in their assumptions and in the experimental setup. Mechanical forces transmitted through cell-ECM have an impact on several cell processes. Therefore, it is crucial to understand and quantify cell-ECM forces. Traction force microscopy (TFM) is one quantitative method that is used to measure mechanical forces exerted by the cells on an elastic substrate [32]. In this method, a soft substrate (polyacrylamide or soft silicone) is used as a substrate for cells in order to measure the mechanical forces transmitted by the cells (Figure 3). Traction Force Microscopy (TFM) characterizes the deformation of a flexible substrate coated with fluorescent marker beads caused by the forces exerted by the cells onto the substrate (Figure3). The substrate deformation is captured by the bead displacement field that is generated from the comparison of the positions of the fluorescent marker beads on a stressed substrate (caused by cell force exertion) against the positions of the fluorescent marker beads on a relaxed substrate (in the absence of cells). This approach uses the bead deformation field to quantify the traction forces by using a computational method that employs elasticity theory. The traction force (F) is obtained by solving the Boussinesq equation: $X=GF$ in which X is the displacement vector

field and G is Green's function that takes into consideration all the mechanical properties. Computationally, one can solve the Boussinesq equation in Fourier space in what is called Fourier Transform Traction Cytometry (FTTC). Here, the traction forces are solved in Fourier space and the values of the traction forces are then calculated by implementing an inverse Fourier Transform. *In vitro*, several studies have demonstrated that high traction forces exerted on cell-ECM contacts can impact cell-cell contacts [33]. Therefore, the actomyosin tension at adherens junctions depends on traction forces at the cell-ECM interface. Adaptive transmission of forces is fundamentally important for the movements of the cells, changes in cell shape and tissue morphogenesis. Thus, measuring these forces using TFM is essential to understanding their role in cell function.

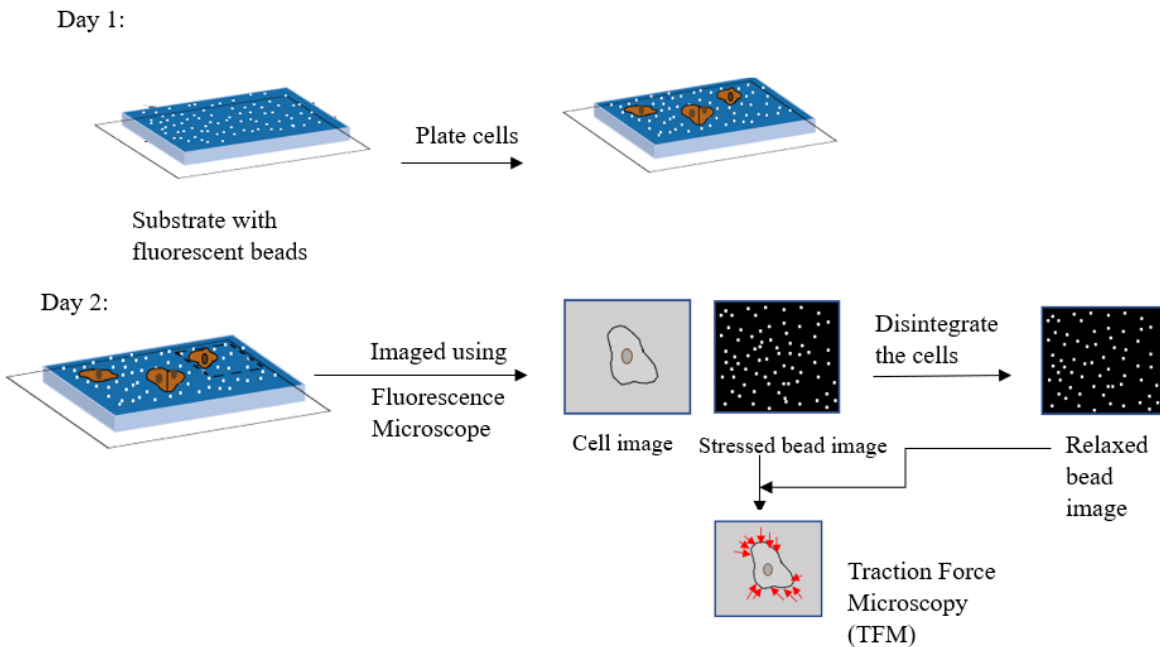


Figure 3: schematic description of the experimental setup of traction force microscopy (TFM). During day 1: The substrate is prepared with fluorescent beads and then cells are plated on the substrate. During day 2: A fluorescence microscope is used to capture two images: the cell image

and the corresponding stressed bead image. Then, the cells are disintegrated, and a relaxed bead image is taken. From the stressed bead image and the relaxed bead image, TFM analysis yields the traction stresses exerted by cells.

1.7 Determination of Forces Transmitted at Cell-Cell Contacts

Different methods have been used to measure forces transmitted at cell-cell adhesions. Inter-cellular forces exerted between two adjacent cells at a single cell-cell contact can be measured using an approach called the traction force imbalance method (TFIM). This technique is based on measuring the traction forces underneath a pair of cells, using traction force microscopy (TFM) followed by computing the forces exerted at cell-cell contact employing physical force imbalance [33]. For an isolated single cell, the only forces acting on the cell are the forces exerted by the substrate on the cell which are reaction forces to the forces exerted by the cell on the substrate (called traction forces). It has been shown that the sum of all traction forces exerted by a single cell sum close to zero, with a small force imbalance of $5 \pm 3\%$ [33]. If we take a cell pair as a whole, the force balance was like that observed in single cells. If we take a cell pair and consider a single cell within a cell pair, the imbalance for a single cell in a cell pair was larger than the imbalance for the entire cell pair as a whole. It has been reported that this imbalance reflects the forces exerted at cell-cell contacts by neighboring cell i.e., intercellular forces between neighboring cells. Previous studies referred to this way of deducing the intercellular forces as the traction force imbalance method (TFIM). Intercellular forces are essential for understanding various biological and physical processes, such as mitosis, cell migration, stem cell self-renewal and differentiation. Thus, using TFM, followed by TFIM to quantify inter-cellular forces opens

the door to understanding the factors that affect it and thereby affect the mechanical function of E-cadherin mediated cell-cell contacts.

1.8 Aspects of E-cadherin mechanobiology of interest

Previous studies showed that the modulation of E-cadherin adhesion can play an important role in the progression of cancer [35]. It has been suggested that E-cadherin adhesions can be modulated by inside-out signaling [35]. Mechanosensitivity at cell-cell contacts is also crucial for maintaining tissue architecture, morphogenesis [26], and plays a role in disease progression [34]. Since human epithelial cancer cells are softer than benign cells [36], E-cadherin mechanosensing of cell elasticity can play a role in this context. Therefore, we raised the question of whether E-cadherin-based adhesions can sense elasticity within the same range of that of epithelial cells that surround them (chapter 4). E-cadherins are epithelial mechanosensors that sense mechanical forces at intercellular junctions and convert junctional tension to biochemical signals inside the cell. However, what factors determine the level of forces transmitted in the first place is unclear. E-cadherin- β -catenin- α -catenin can bind directly to the actin cytoskeleton, with increased binding of α -catenin to F-actin under tension [37,38,39]. In addition, E-cadherin can bind to the actin cytoskeleton through other adhesion-associated intracellular proteins [40,41,42]. To study the level of force transmission through E-cadherin, we wanted to explore the role of vinculin and α -catenin in transmitting endogenous forces at cell-cell contacts (chapter 2). Previous reports showed that Epidermal Growth Factor Receptor (EGFR) is a key factor in the E-cadherin force transduction machinery [43]. Thus, we asked how the inhibition of EGFR will affect the level of force transmission at cell-cell contacts (chapter 4). It has been shown E-cadherin can also bind to other cadherins like N-cadherin – for eg., forces can be transmitted by heterophilic interactions between E-cadherin at the cancer cell membrane and N-cadherin at the Cancer Associated Fibroblasts

(CAFs) [44]. Therefore, we studied homophilic and heterophilic interactions of cadherins (chapter 4), all on epithelial cells, in order to understand how the level of force transmission through E-cadherin depends on binding partners from outside the cell. The level of force transmission at cell-cell contacts was quantified based on experimental measurements using traction force microscopy (TFM). However, this method requires cell removal and no further post-processing procedures can be done. Therefore, we devised a modified traction force microscopy method using a novel, simple strategy for coincident immunofluorescence and traction force microscopy in order to enable wider use of TFM. This approach is detailed in chapter 3.

CHAPTER 2

VINCULIN IS ESSENTIAL FOR HIGH ENDOGENOUS FORCE TRANSMISSION AT CELL-CELL CONTACTS

2.1 Introduction

In epithelial tissues, cells exert forces on neighboring cells and the extracellular matrix (ECM). These cells stick to each other as well as to the extracellular matrix through transmembrane proteins. E-cadherin is the major transmembrane protein that mediates cell-cell adhesions. E-cadherin adhesions play an important role in the function and integrity of cell-cell contacts. During pathological events, forces transmitted at cell-cell contacts may change. During cancer metastasis, tumor cells break away from the primary tumor and invade surrounding tissues. Tissue morphogenesis is also dependent on tension transmitted through cell-cell contacts and on the dynamic activity of cell-cell adhesion proteins. Assessing endogenous force transmission at cell-cell contacts and the stability of these contacts when subjected to external forces is essential to understand the role of adhesion proteins in many physiological and pathological processes.

At cell-cell contacts, E-cadherin from one cell binds homophilically to E-cadherin from a neighboring cell. The intracellular domain of E-cadherin binds to β -catenin which in turn binds to α -catenin. The ternary E-cadherin/ β -catenin/ α -catenin complexes bind directly and indirectly to the actin cytoskeleton. The cadherin-catenin complex forms stable bonds with F-actin under force [45,46,47]. Several other adhesion-associated proteins such as vinculin, α -actinin, and ZO-1 connect the E-cadherin-catenin complex to the actin cytoskeleton (Figure 4).

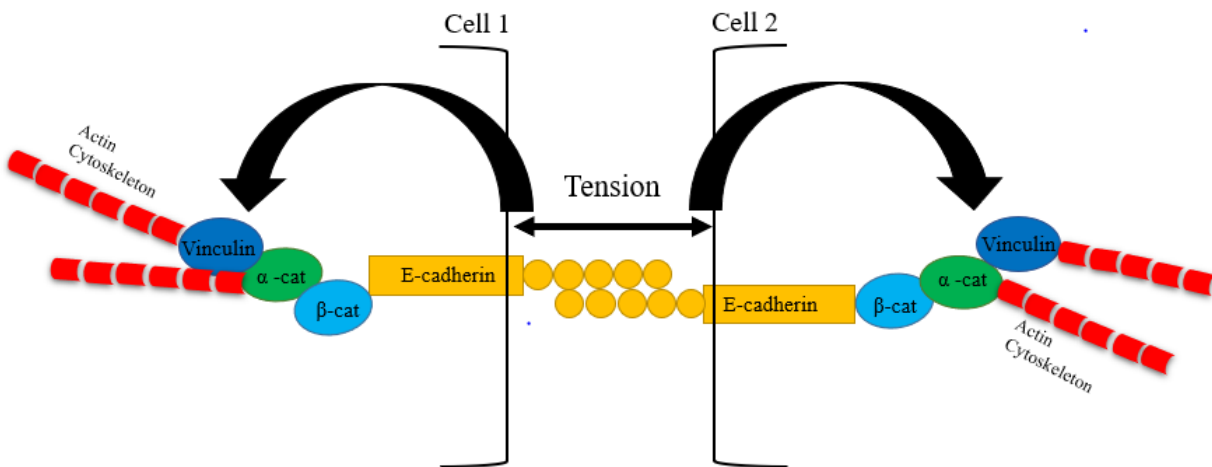


Figure 4: Schematic depicting the key mechanical roles of adhesion proteins. Adhesion proteins enable force transmission at cell-cell contact and enhance the adhesion strength by the recruitment of specific proteins like vinculin under force.

In addition, a previous study showed that the protein afadin links the actin cytoskeleton to adherens junctions [48]. EPLIN [49] and the formin Fmn1 [50] also serve as linkers of the cadherin-catenin complex to the actin cytoskeleton (Figure 5). It has been shown that α -catenin is a stretch-activable sensor that connects the cadherin complex to actin and is a necessary player in mechanotransduction at cell-cell contacts [51]. Tension at cell-cell junctions unfolds α -catenin and leads to the recruitment of vinculin which in turn depends on non-muscle myosin II activity [52]. Therefore, vinculin reinforces cell-cell junctions and plays an important role in force transmission. However, it is still unknown how vinculin impacts the endogenous forces between cells relative to other proteins and by how much cell-to-cell force transmission is affected in the absence of vinculin.

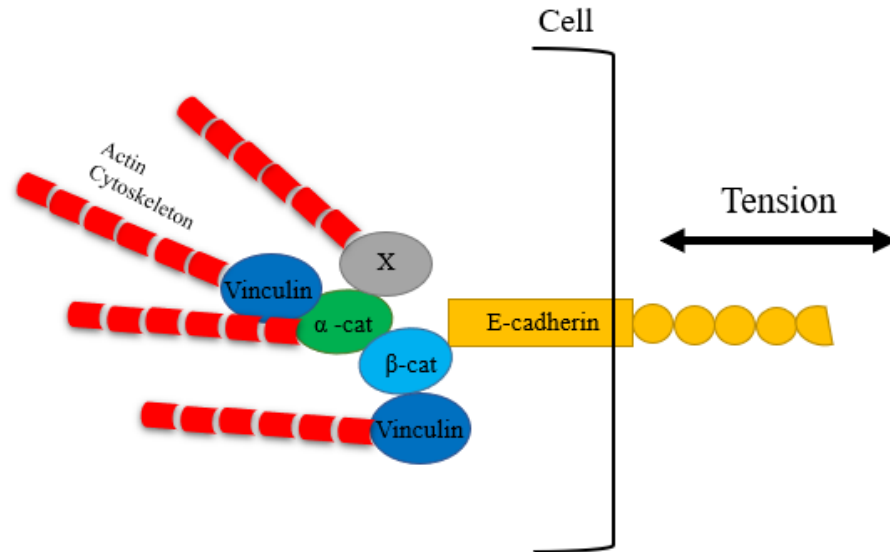


Figure 5: Schematic description of the multiple pathways by which force can be transmitted through E-cadherin to F-actin. (X may be a protein such as afadin or EPLIN).

Cell-cell adhesion proteins are involved in transmitting mechanical forces from one cell to a neighboring cell as well as maintaining the adhesion strength at cell-cell contacts. Several methods have been used to assess the function of cell-cell adhesion associated proteins in force transmission by using biochemical methods, cadherin-coated beads, cadherin coated substrates, or the Förster Resonance Energy Transfer (FRET) technique [53,54,55,56], without quantifying the total forces transmitted between epithelial cells. Therefore, measuring the endogenous force transmitted at cell-cell contacts is crucial for understanding the effect of perturbations of intracellular proteins that are involved in the adhesion systems at cell-cell contacts. Also, identifying the adhesion strength of lateral cell-cell contacts is very important to assess the strength of these adhesions while bearing exogenous force.

2.2 Methods

2.2.1 Cell Culture

Madin-Darby Canine Kidney (MDCK) II cells were cultured in Dulbecco's modified Eagle's medium (Corning Inc., Corning NY) containing 10% fetal bovine serum (Corning Inc., Corning NY), L-glutamine, and 1 % Penicillin/Streptomycin at 37°C, under 5 % CO₂. MDCK cells were plated overnight onto collagen I-coated soft silicone atop 22 mm square No.1.5 coverslips in 35 mm culture dishes and then used for experiments.

2.2.2 Live Cell Imaging and Immunofluorescence

Leica DMI8 epifluorescence microscope (Leica Microsystems, Buffalo Grove, IL) was used to image living and fixed cells. The microscope is equipped with an airstream incubator (Nevteck, Williamsville, VA) in order to maintain the temperature at 37°C during the process of imaging living cells. Images are taken using a 10 x 0.3 NA objective, HQ2-cooled CCD camera (Andor Technology, Belfast, UK), and an airstream incubator (Nevtek, Williamsville, VA). MDCK cells were fixed utilizing 4% paraformaldehyde (Electron Microscopy Sciences, Hatfield, PA) in 1.5% Bovine Serum Albumin and 0.5% Triton in CB buffer. The actin cytoskeleton was stained using Alexa-488 Phalloidin from Thermo Fisher Scientific (Eugene,OR).. Rabbit anti vinculin (catalogue# ab129002) from Abcam (Waltham,MA) and mouse anti β -catenin (catalogue# 610153) from BD transduction laboratories (Franklin Lakes, NJ) were used to stain vinculin and β -catenin respectively.

2.2.3 Preparation of Qgel substrate

Qgel (CHT USA Inc, Cassopolis, MI) was prepared using a mixture of two solutions Qgel 300A and Qgel 300B at a 1:2.2 ratio. The Qgel mixture is cured using a heater at 100⁰ C for an hour. After curing, the Qgel mixture is exposed to 305 nm UV light (UVP cross-linker, Analytik Jena AG, Upland, CA) for five minutes. A solution of 0.65 mg/ml carboxyl red fluorescent beads of diameter 0.44 μ m (Spherotech Inc., Lake Forest, IL) was coupled to the top surface of the Qgel silicone surface with 10 mg/ml 1-Ethyl-3-(3-Dimethylaminopropyl) Carbodiimide, 5 Vmg/ml N-Hydroxysuccinimide chemistry and 0.017 mg/ml collagen I for 30 minutes at room temperature. For MDCK α -catenin knock out (KO) cells rescued with conformationally active (CA) α -catenin cell islands, we used 1 mg/ml fibronectin (Millipore Sigma, Burlington, MA) instead of collagen I in the mixture. Then, Qgel substrate was washed with Dulbecco's Phosphate-Buffered Saline (DPBS) for five minutes and the substrate was ready to be used for plating cells. The Qgel silicone substrate had a mean Young's modulus of 8.7 kPa determined by shear rheology using a Modular Compact Rheometer MCR 302 (Anton Paar).

2.2.4 Traction Force Measurement

A phase image of each MDCK cell or cell pair along with the corresponding image of beads beneath were first recorded. After the cells were disintegrated using 1% sodium dodecyl sulfate, an image of the beads on the relaxed substrate were recorded. The stressed bead images (in the presence of cells) and the relaxed bead images (in the absence of cells) were aligned using an ImageJ plugin [57]. The displacement field was then computed using mpiv, scripted in MATLAB (MathWorks, Natick, MA) as before [58]. From the bead displacement, traction stresses are then reconstructed using regularized Fourier Transform Traction Cytometry that uses the

Boussinesq solution, such as in previously published work [58,59]. The Traction Force Imbalance Method refers to the computation of the inter-cellular force at a cell-cell contact within a cell pair from the vector sum of traction forces under each cell within the cell pair. For MDCK α -catenin knock out (KO) cells rescued with conformationally active (CA) α -catenin (CA α -catenin) cell islands, the traction stress magnitudes higher than 50 Pa were plotted using Mathematica (Wolfram Research, Champaign, IL).

2.2.5 Biaxial Stretch

A silicone sheet was exposed to 305 nm UV light for five minutes. Then incubated with Collagen I at 37°C, under 5% CO₂ for 15 minutes. Then, the sheet was washed for five minutes with Dulbecco's Phosphate-Buffered Saline (DPBS). MDCK cells were plated on the silicone sheet in the presence of Dulbecco's modified Eagle's (DMEM) medium and kept overnight in the incubator. After overnight incubation, the DMEM medium is replaced with 1:200 CellBrite labeling solution in DMEM. MDCK cells were incubated with the staining medium for 30 minutes at 37°C. Next, the staining medium was aspirated and replaced with normal growth DMEM medium and HEPES buffer. Next, the silicone sheet was placed inside the well of the biaxial cell stretcher. MDCK cells islands were imaged using Leica DMI8 epifluorescence microscope equipped with an airstream heater. A phase and a CellBrite plasma membrane image were taken for every stretching step.

2.2.6 Statistical Analysis

For statistical analysis, a t-test was used to compare wildtype and vinculin KO single cell data and Analysis of Variance (ANOVA) was used for multiple comparisons of all different cell pair data, with * indicating $p < 0.05$, ** indicating $p < 0.01$ and *** indicating $p < 0.001$.

2.3 Results and Discussion

Under the action of forces through E-cadherin at cell-cell junctions, α -catenin undergoes conformational changes and vinculin is recruited at the cell-cell contact to reinforce adherens junctions. Therefore, we wanted to check if vinculin is an important factor in maintaining high levels of forces at cell-cell contacts or if its influence on intercellular forces is minimal. We used Madin-Darby Canine Kidney (MDCK) cells in which vinculin was knocked out (KO) using CRISPR/Cas-9. To ensure that vinculin was completely knocked out in MDCK cells, we stained for vinculin using immunofluorescence. In MDCK wildtype (WT) cells, vinculin was present at cell-cell contacts and the cell-ECM interface (Figure 6), however, in MDCK vinculin KO cells, vinculin was completely absent (Figure 6). Previous reports [60,61], showed that absence of vinculin in fibroblasts decreases the traction forces exerted by these cells on the extracellular matrix (ECM). In contrast, the absence of vinculin in mesenchymal cells did not considerably decrease traction forces [62]. Thus, we plated MDCK vinculin KO cells on collagen-I-coated Qgel silicone soft substrates (Young's modulus 8.7 kPa). Then, we measured the traction forces exerted by these cells onto the ECM using traction force microscopy (Figure 7). We found that MDCK vinculin KO cells exerted lesser traction forces compared to MDCK WT cells. The strain energy for MDCK vinculin KO cells was 10.5 ± 6.1 fJ, however the strain energy for MDCK WT was 22.2 ± 16.3 fJ (Figure 8).

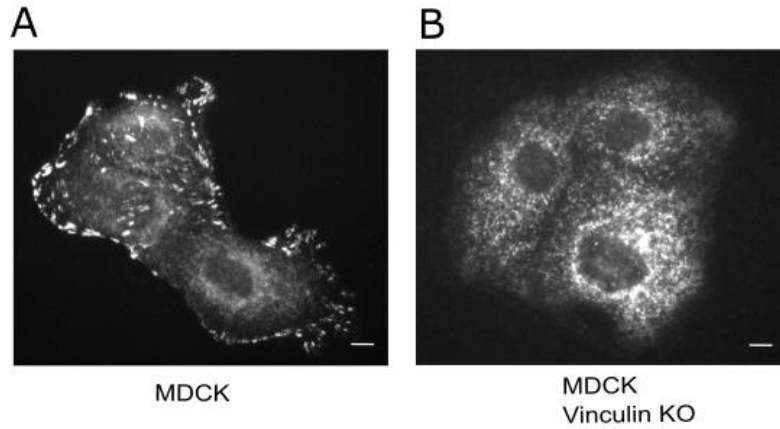


Figure 6: Absence of vinculin in MDCK vinculin KO cells. (A) Immunofluorescence images of MDCK and (B) MDCK vinculin KO cells stained for vinculin. Scale bar: 5 μ m.

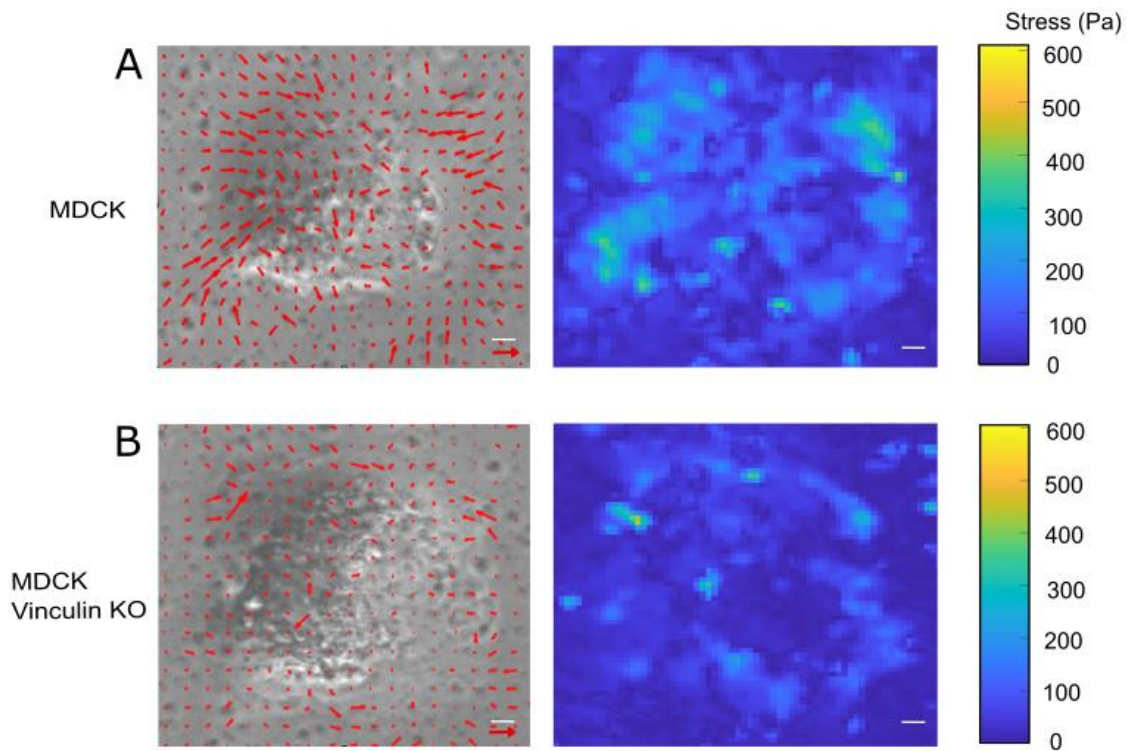


Figure 7: Traction forces within a single cell. (A) Traction stresses exerted by a single MDCK cell (top, left) and (B) an MDCK vinculin KO cell (bottom, left) on the ECM. Traction stress vectors

are overlaid (red arrows). Heat-scale map of the traction magnitude for a single MDCK cell (top, right) and MDCK vinculin KO (bottom, right). Scale bar is 5 μm . Red arrow: 400 Pa.

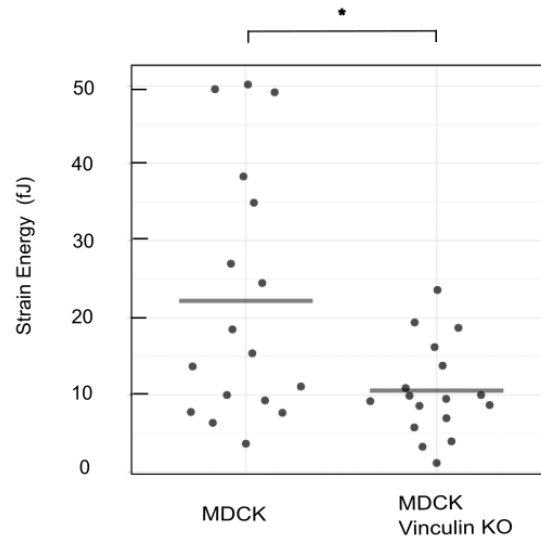


Figure 8: Distribution of the strain energy for MDCK and MDCK vinculin KO single cells. Bar represents the mean value.

Then, we wanted to check the effect of the absence of vinculin on the endogenous force transmitted at cell-cell contacts. Therefore, we plated MDCK vinculin KO and MDCK WT cell pairs on collagen-I-coated Qgel silicone soft substrates and measured the inter-cellular forces using the Traction Force Imbalance Method (TFIM) [63]. For an isolated cell, the vector sum of the reaction forces exerted by the substrate on the cell is zero (within experimental error) because of physical force balance. Every reaction force has an equal and opposite traction force exerted by the cell on the substrate, therefore all the traction forces also sum to zero (within experimental error). However, the vector sum of the reaction forces for a single within a cell pair is not zero.

Therefore, there should be another force that counterbalances the reaction forces – this is the inter-cellular force. Previous reports have used the Traction Force Imbalance Method (TFIM) to measure the force between endothelial cell pairs [63], epithelial cell pairs [59] and within epithelial cell sheets. Here, we quantified the traction forces for MDCK WT and MDCK vinculin KO cell pairs, and then computed the intercellular force for MDCK WT and MDCK vinculin KO cell pairs using TFIM (Figure 9). We found that the inter-cellular force at cell-cell contacts was significantly less for MDCK vinculin KO compared to MDCK WT cell pairs. The corresponding cell-cell tension was 51 ± 24 nN for MDCK WT cell pairs versus 23 ± 12 nN for vinculin KO cell pairs (Figure 10). Therefore, the absence of vinculin prohibits cells from exerting high endogenous tension at cell-cell contacts.

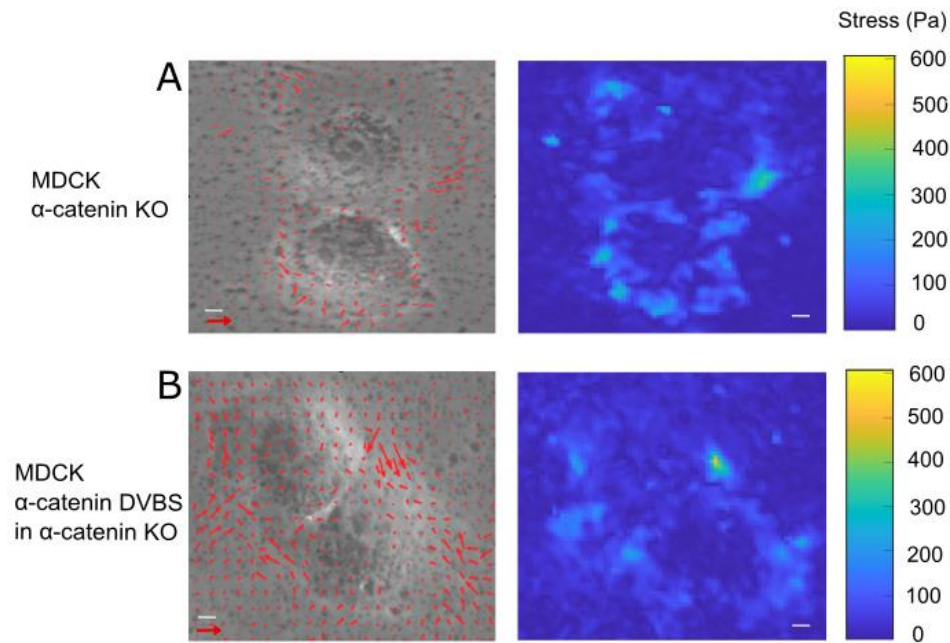


Figure 9: Loss of vinculin leads to a severe decrease in inter-cellular forces. (A) Traction stresses of an MDCK cell pair (top, left) and (B) an MDCK vinculin KO cell pair (bottom, left). Traction

stress vectors are overlaid (red arrows.). Heat-scale map of the traction magnitude for MDCK cell pair (top, right) and MDCK vinculin KO (bottom, right). Scale bar is 5 μm . Red arrow: 400 Pa.

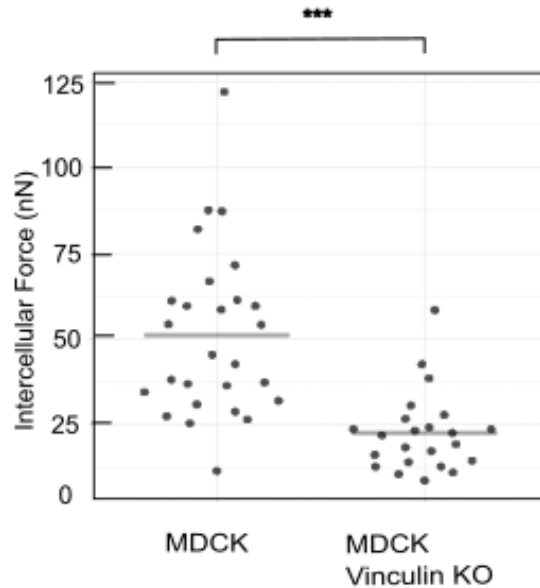


Figure 10: Distribution of the intercellular forces for MDCK and MDCK vinculin KO cell pairs. Bar represents the mean value.

Since α -catenin stretches under forces and it recruits vinculin at cell-cell contacts, we assumed that α -catenin would at least have similar importance as vinculin in transmitting forces at cell-cell contacts. In addition, the E-cadherin-catenin complex binds to F-actin through several intracellular proteins such as vinculin, F-actin binding proteins afadin, EPLIN, and tight junction protein ZO-1. This also made us think that α -catenin would play an important role in force transmission through cell-cell contacts. Therefore, we expected that the endogenous forces through cell-cell contacts of MDCK α -catenin KO cells would be drastically lesser than the endogenous forces of MDCK vinculin KO cells. We quantified the traction forces for MDCK α -catenin KO

cell pairs and then we calculated the intercellular forces for MDCK α -catenin KO cell pairs using TFIM (Figure 11). Surprisingly, we found that the intercellular force for MDCK α -catenin KO cells was 39 ± 23 nN which was not significantly lesser than for MDCK WT contacts (Figure 12). Our results are consistent with previous reports in which they found that knocking down α -catenin leads to a very minor decrease in cell-cell tension. Also, MDCK α -catenin KO cells were shown to exert less traction forces on E-cadherin-coated substrates compared to MDCK WT cells [64].

Knowing that α -catenin has many binding partner proteins, we checked the role of α -catenin-vinculin interaction by exogenously expressing α -catenin lacking the WILLYWILD site (VBS), α -catenin- Δ VBS, in MDCK α -catenin KO cells. We measured the traction forces for MDCK α -catenin- Δ VBS cell pairs (Figure 11) and then quantified the inter-cellular forces using the Traction Force Imbalance Method (TFIM). We found that the inter-cellular force for MDCK α -catenin- Δ VBS cell pairs was 36 ± 20 nN, which was not statistically significantly lesser than the inter-cellular force for MDCK WT cell pairs (Figure 12). This result suggests that, in the absence of α -catenin, or in the presence of α -catenin lacking the vinculin binding site, the inter-cellular forces at cell-cell contacts were slightly reduced compared to the WT case. Our finding is consistent with a previous study [64] showing that the traction forces on E-cadherin coated substrates of α -catenin- Δ VBS and α -catenin KO cells were similar.

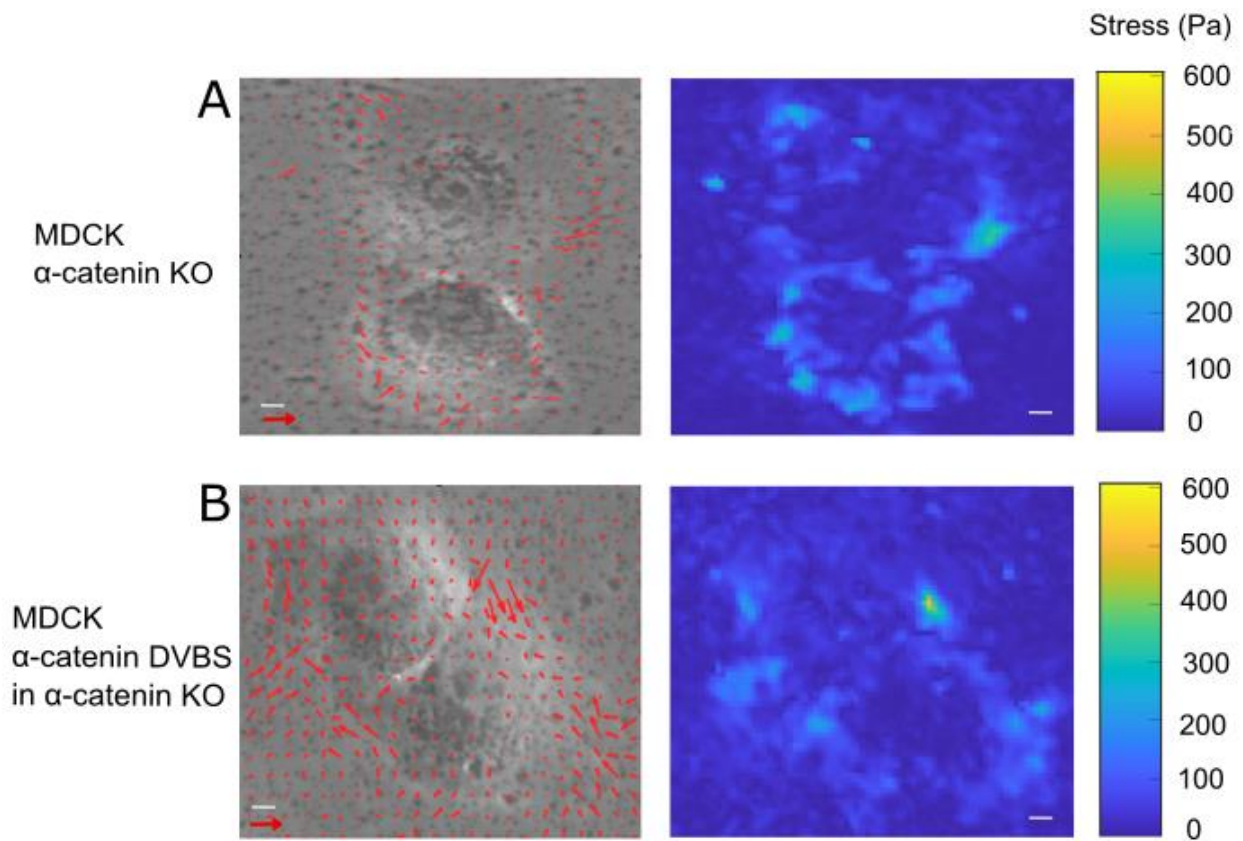


Figure 11: Loss of α -catenin does not lead to a significant decrease in inter-cellular forces. (A) Traction stresses of MDCK α -catenin cell pair (top, left) and (B) MDCK α -catDVBS in α -catenin KO cell pair (bottom, left). Traction stress vectors are overlaid (red arrows.). Heat-scale map of the traction magnitude for MDCK α -catenin KO cell pair (top, right) and MDCK α -catDVBS in α -catenin KO (bottom, right). Scale bar is 5 μm . Red arrow: 400 Pa.

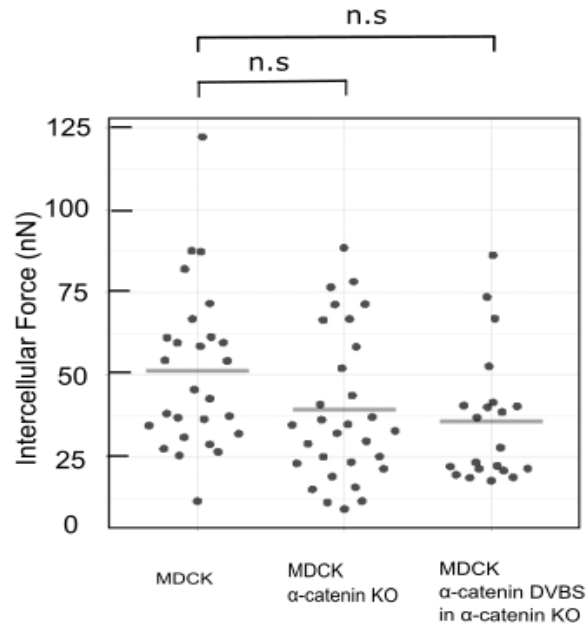


Figure 12: Distribution of the intercellular forces for MDCK α -catenin KO and MDCK α -catDVBS in α -catenin KO cell pair. Bar represents the mean value.

Next, we checked if knocking out both α -catenin and vinculin in MDCK cells would lead to a significant decrease in inter-cellular forces. We measured the traction forces for MDCK α -catenin-vinculin double KO cell pairs and we quantified the inter-cellular forces using TFIM (Figure 13). We found that the inter-cellular force for MDCK α -catenin-vinculin double KO cell pairs was 21 ± 15 nN (Figure 14). This was similar to the inter-cellular forces of MDCK vinculin KO cells and drastically less than the inter-cellular force of MDCK WT cell pairs. Therefore, we confirmed that vinculin, and not α -catenin, is responsible for transmitting high endogenous forces at cell-cell contacts.

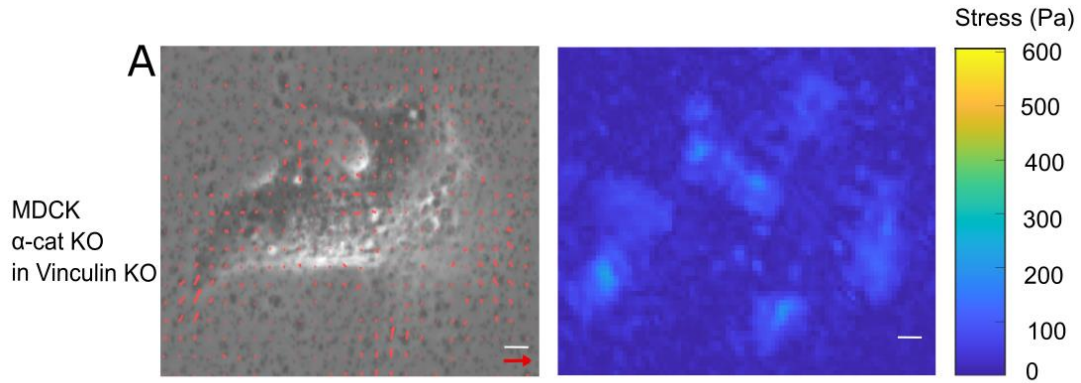


Figure 13: Loss of both α -catenin and vinculin leads to a severe decrease in inter-cellular forces.

(A) Traction stresses of MDCK α -catenin KO & vinculin KO cell pair. Traction stress vectors are overlaid (red arrows). Heat-scale map of the traction magnitude for MDCK α -catenin & vinculin KO cell pair. Scale bar is 5 μ m. Black arrow: 400 Pa.

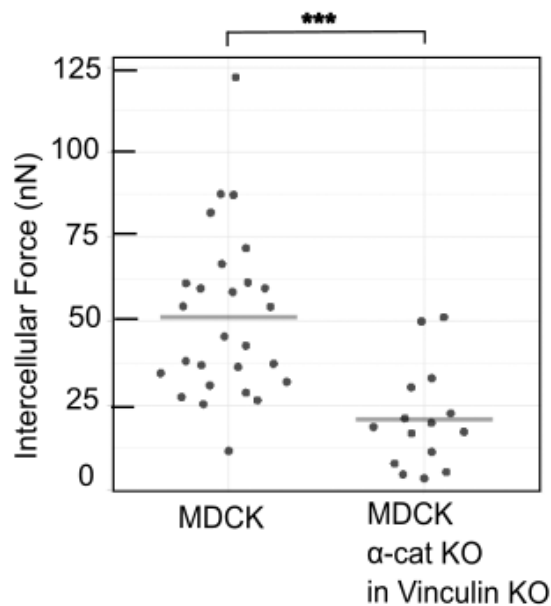


Figure 14: Distribution of the intercellular forces for MDCK and MDCK α -catenin & vinculin KO cell pairs. Bar represents the mean value.

Then, we wanted to check the role of vinculin in protecting the integrity of cell-cell contacts under exogenous mechanical challenges. For this purpose, we used a biaxial stretcher which allows us to test the integrity of cell-cell contacts while applying external stretch over a small duration of time. We used a collagen-coated silicone sheet on which we plated either MDCK cells (Figure 15) or MDCK vinculin KO cells (Figure 16) overnight. We used a fluorescence stain for the plasma membrane, Cellbrite, in order to carefully monitor the fraction of ruptured contacts as a function of time. We subjected MDCK cells or MDCK vinculin KO cells to a large external stretch and found that both MDCK and MDCK vinculin KO cell-cell contacts ruptured over time while remaining adhered to the collagen-I substrate. Therefore, we were able to test the effect of knocking out vinculin on the integrity of cell-cell contacts under mechanical challenges. The fraction of ruptured cell-cell contacts for MDCK vinculin KO cells was over twice the fraction of that for MDCK cells (Figure 17). Therefore, vinculin is important for protecting and maintaining the integrity of cell-cell contacts under mechanical challenges, as well as transmitting high endogenous forces at cell-cell contacts. Our finding is consistent with the results of previous studies using detached cell sheets [65] E-cadherin coated substrates [66], and suspended doublets [67], suggesting that vinculin is crucial for maintaining the integrity of cell-cell contacts

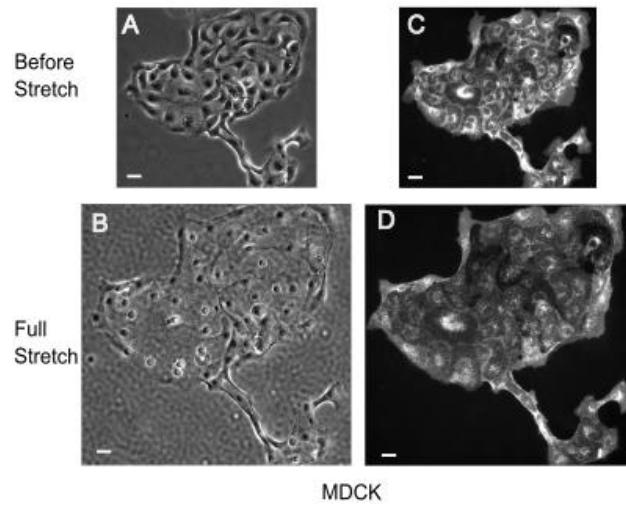


Figure 15: (A) MDCK cells before stretch and (B) after full stretch. (C) plasma membrane staining for MDCK before stretch and (D) after stretch. Scale bar: 10 μ m.

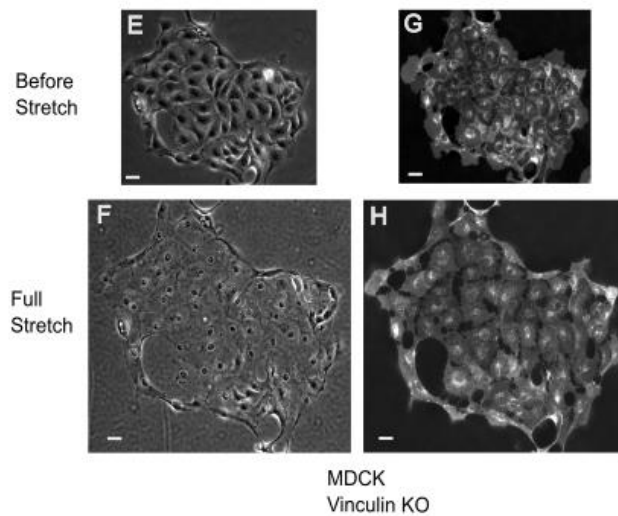


Figure 16: (A) MDCK vinculin KO before stretch and (B) after full stretch. (C) plasma membrane staining for MDCK vinculin KO before stretch and (D) after stretch. Scale bar: 10 μ m.

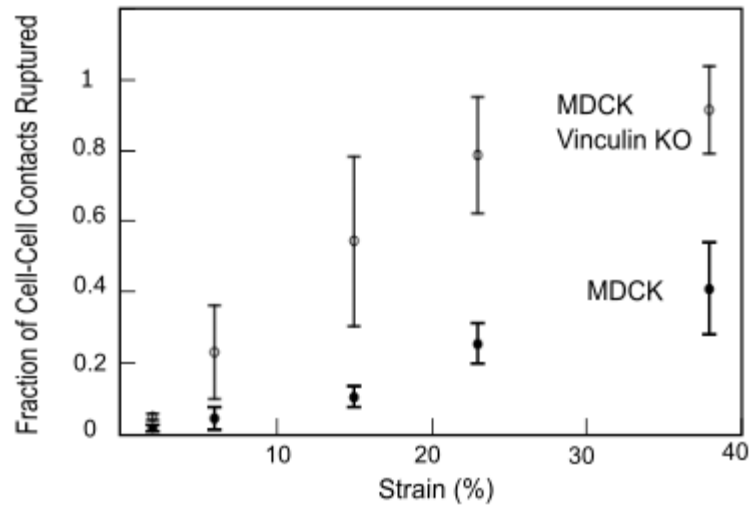


Figure 17: Fraction of cell-cell contacts ruptured as a function of strain (%). Each data point is the mean \pm standard deviation (SD) for two cell islands for MDCK vinculin KO cells (306 cell-cell contacts) and four cell islands for MDCK (378 cell-cell contacts).

To further test whether changing the recruitment of vinculin to cell-cell contacts has an adverse effect at the cell-ECM contact, we used MDCK cells and MDCK α -catenin knock out (KO) cells rescued with the conformationally active (CA) α -catenin mutant that was previously shown to enhance the recruitment of vinculin to adherens junctions [68]. A previous report showed that MDCK α -catenin knock out (KO) cells rescued with CA α -catenin exhibited severe impairment of focal adhesions [69]. Therefore, to determine if MDCK α -catenin knock out (KO) cells rescued with CA α -catenin alters traction forces, we tested the traction forces exerted by small islands of MDCK α -catenin knock out (KO) rescued with CA α -catenin or WT α -catenin onto fibronectin-coated Qgel silicone soft substrates (Figure 18).

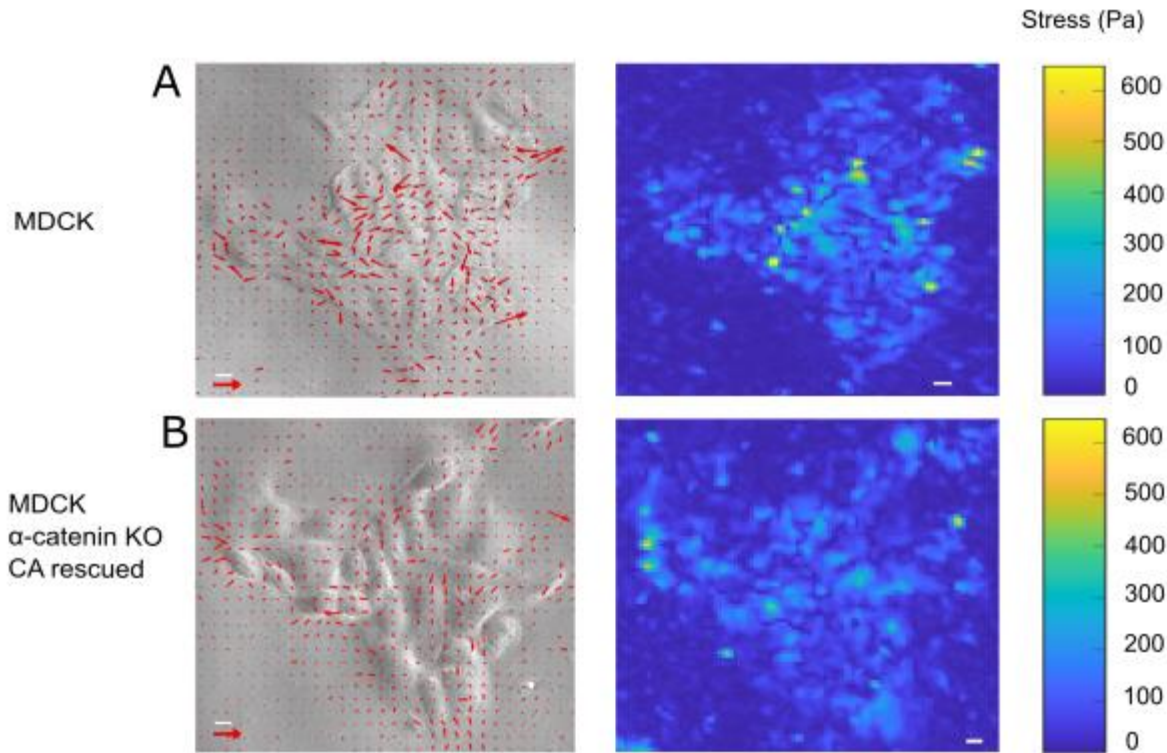


Figure 18: Traction stresses of MDCK cell island (top, left) and MDCK α -catenin knock out (KO) rescued with α -catenin CA cell island (bottom, left). Traction stress vectors are overlaid (red arrows). Heat-scale map of the traction magnitude for MDCK cell island (top, right) and MDCK α -catenin Knock out (KO) rescued with α -catenin CA cell island (bottom, right). Black arrow: 400 Pa.

We found that there was no difference between the traction forces of MDCK α -catenin knock out (KO) cells rescued with α -catenin CA or α -catenin WT (Figure 19). Therefore, we concluded that the overall traction forces for both MDCK α -catenin knock out (KO) rescued with α -catenin CA or α -catenin WT were not reduced, while MDCK α -catenin knock out (KO) rescued with α -catenin CA induced a severe impairment of focal adhesion formation [69]. Our results

suggests that increased recruitment of vinculin to cell-cell contacts does not affect traction forces at the cell-ECM contact.

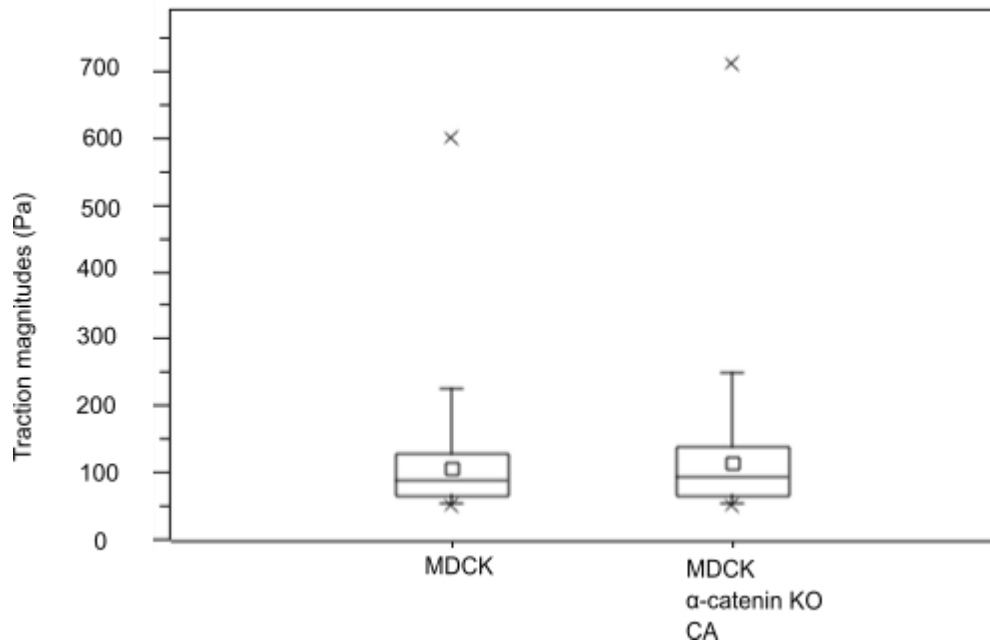


Figure 19: Box plot comparison of the traction magnitude distribution for MDCK parental control and MDCK α -catenin knock out (KO) rescued with α -catenin CA cell islands. Statistical properties are as follows: mean (open square), box (25/75% quartile), whisker (5/95% quartile), diagonal cross (maximum/minimum). There was no statistical difference ($p > 0.05$) observed for traction magnitudes between MDCK parental control and MDCK α -catenin knock out (KO) rescued with α -catenin CA conditions.

2.4 Conclusion

Transmission of forces at cell-cell contacts is crucial for tissue shape changes during physiological and pathological processes and adult tissue repair. Transmission of forces between cells is mediated through E-cadherin based adhesions. Here, we found that vinculin is very important for transmitting high endogenous forces at cell-cell contacts as well as maintaining the integrity of cell-cell contacts under mechanical forces. Also, we found that the α -catenin-vinculin interaction or α -catenin's interaction with other proteins such as EPLIN, afadin, and tight junction protein ZO-1 don't play a pivotal role in transmitting high endogenous forces through cell-cell contacts. Our results are consistent with previous work suggesting that, once vinculin is activated, β -catenin forms a direct structural connection with vinculin in order to support mechanical tension and stabilize cadherin-catenin complexes. Also, another previous study showed that vinculin plays an essential role in establishing and regulating cell-cell adhesions through E-cadherin through a direct contact with β -catenin [70]. There is evidence that vinculin and α -catenin bind to the same N-terminal region of β -catenin [66,70,71] But in α -catenin knock down (KD) cells, vinculin is displaced from β -catenin, suggesting that vinculin may transmit forces at cell-cell contacts through E-cadherin using other intermediate molecular linkers like myosin VI as showed in a previous report [72]. Once activated, vinculin plays a major role at cell-cell contacts. Our results are consistent with previous studies that showed that vinculin protects cell-cell contacts from rupturing not only in epithelial cells but also in cardiac tissues [73] and in endothelial cell junction during dynamic events like vascular lumen formation [74].

CHAPTER 3

SIMPLE STRATEGY FOR COINCIDENT TRACTION FORCE MICROSCOPY AND IMMUNOFLUORESCENCE TECHNIQUE

3.1 Introduction

The mechanical link between cells and their surroundings is pivotal to understand several biological processes during tissue repair or pathology. Cells generate and exert forces on their surroundings, through non-muscle myosin motors that walk on the actin cytoskeleton, causing contractility of the cells. Forces are transmitted to their extracellular microenvironments through focal adhesion proteins, allowing cell shape changes [75]. Also, cells sense and respond to forces by converting forces to biochemical signals. Traction force microscopy (TFM) is the principal technique used to quantify the forces exerted by the cells on the substrate.

In the last few decades, several protocols have been used to measure the traction forces based on the optical detection of force-dependent substrate deformation [76,77,78]. Lower-resolution discrete methods [79,80] such as cells lying on a bed of microneedles, can estimate forces from a single image but they limit cell spreading and adhesions [78,81,82,83]. Continuum TFM approaches utilize elastic soft substrates coated with well dispersed fluorescent beads [84,85,86]. These methods require a reference image which is typically obtained after the cells are disintegrated. To overcome these limits, several attempts have been made to come up with reference-free methods. One approach is the micro-patterning of adhesive islands [87,88] – however, this method was hampered by poor spatial resolution. Molecular methods [89] like DNA-based force sensors are not able to provide information about the direction of forces. The

so-called confocal traction force microscopy (cTFM) uses very precise electrohydrodynamic nanodrip-printing of quantum dots into a monocrystalline layer [90,91,92,93,94]. cTFM solved the issues encountered in previous approaches but it involves an advanced setup that is out of the reach of most labs.

Yes-Associated Protein (YAP) is a transcriptional co-regulator that promotes transcription of genes, including those which regulates proliferation and apoptosis during organ development. YAP respond to multiple biochemical signals and convert them into biological effects in a way that is specific for each cell type and mechanical stress [95]. YAP respond to several mechanical inputs such as topology and rigidity of ECM [96,97] and shear stress [98,99,100]. YAP is considered as a universal mechanoeffector and mechanotransducer. The subcellular localization and activity of YAP is influenced by mechanical stimuli. It has been shown that YAP is localized in the cytoplasm when cells express low levels of physical and mechanical cues such as cells attached to soft ECM [95] . However, YAP is localized in the nucleus when cells perceive high physical and mechanical cues such as cells experiencing cytoskeletal force or cultured on rigid substrates [95]. Further studies using genomics techniques showed that genes activity that regulates the division and contraction of epithelial cells is regulated by YAP [101]. YAP controls the production phosphorylated myosin light chain (pMLC) this is essential to generate mechanical forces so the cells can properly contract. Therefore, it is important to study the distribution of YAP in the cells along with assessing the force transmission of the cells in order to find a relationship between YAP nuclear recruitment and tractions forces exerted by the cells. Immunofluorescence is usually used to determine YAP ratio and it is incompatible with conventional TFM.

Despite progress, the important limitation of requiring the removal of cells to get the relaxed substrate image is a disruptive step after which no further post-processing experimental

procedures can be done with cells. Here, we have devised a simple strategy for coincident traction force microscopy and immunofluorescence in which we can quantify traction forces without disintegrating the cells and then assess the localization of proteins in cells using immunofluorescence.

2.2 Methods

3.2.1 Preparation of NuSil Substrate

NuSil soft silicone was prepared using A and B solutions at a 1:1 ratio along with 0.55% Sylgard 184 crosslinker. This NuSil mixture is cured using an oven at 100⁰ C for three hours. NuSil mixture is exposed to 305nm UV light (UVP cross-linker, Analytik Jena AG, Upland, CA) for five minutes. A solution of 0.65mg/ml carboxyl red fluorescent beads of 0.44 μ m diameter was coupled to the top surface of the NuSil gel surface with 10 mg/ml 1-Ethyl-3-(3-Dimethylaminopropyl) Carbodiimide, 5 mg/ml N-Hydroxysuccinimide chemistry and 0.017 mg/ml collagen I for 30 minutes. Then, the NuSil substrate is washed two times with Dulbecco's Phosphate-Buffered Saline (DPBS) for five minutes.

3.2.2 Reference bead image

The top corner of the bottom part of the substrate's coverslip was marked with a marker. The substrate's coverslip was placed face up inside a chamber that had marks on each side. The microscope stage insert was also marked on each side with marks so that the marks on the chamber were aligned with the marks on the microscope stage when placing the chamber on the stage. A square region was selected by the mark on the bottom part of the glass coverslip and a 10 x 10 frame was manually imaged using the "Tile-Scan" feature (that is routinely available with many microscopes software) with 10% overlap between individual frames in the tile scan. After taking

100 reference bead images of the relaxed substrate (in the absence of cells), all the reference bead images are stitched together using the “Grid/Selection stitching” plugin in Fiji software (<https://imagej.net/plugins/grid-collection-stitching>) [102] .

3.2.3 Traction Force Microscopy and Immunofluorescence

After overnight incubation, A431 cells plated on the substrate (on a coverslip) were placed inside the chamber with normal growth DMEM medium and 10 mM HEPES buffer. The chamber and the microscopic stage were aligned as described in the previous section – 2.2.2 Reference bead image. Following the mark on the bottom part of the glass coverslip, the same 10x10 square region frame was then scanned using a Leica DMI8 epifluorescence microscope equipped with an airstream incubator to maintain the temperature at 37⁰ C while imaging living cells. All bead images taken from the 10 x 10 frame were stitched together using Fiji. Since the cell phase and corresponding bead images are taken after overnight incubation, with the chamber placed on the microscope stage a second time after taking the reference bead images, the stressed bead image and the reference bead image will be slightly rotated with respect to each other. For aligning the bead images for rotation, we use the “Stackreg” plugin in ImageJ (<https://imagej.nih.gov/ij/plugins/>) [103]. The traction forces of A431 cells are quantified using traction force microscopy for single cells and TFM followed by the traction force imbalance method for cell pairs as discussed in Chapter 2. Cell images and their corresponding bead images were taken within the same frame. Each phase image of a cell and its corresponding bead image are now grouped together, with the same bead image frame taken from the same spot of the previous reference stitched bead image. (For example, if we find a cell within frame number 30, we take the cell phase image and its correspondent bead image and we group them with the bead

frame number 30 taken from the 100 reference bead images that formed the stitched reference bead image).

A431 cells were fixed while keeping the chamber on the stage using 4% paraformaldehyde (Electron Microscopy Sciences, Hatfield, PA) in 1.5% Bovine Serum Albumin and 0.5% Triton in CB (cytoskeletal buffer). The actin cytoskeleton was stained using Alexa-488 conjugated phalloidin from Thermo Fisher Scientific (Waltham, MA) in the Cy5 channel. Mouse anti-YAP from Santa Cruz Biotechnology (Dallas, TX) was used to stain and image YAP in the green channel.

3.3 Results and Discussion

Our simple strategy for coincident immunofluorescence and traction force microscopy requires the collection of reference bead image images at the beginning of the TFM experiment (Figure 20A). All reference bead images are stitched together to make one large stitched reference bead image frame (Figure 20B) After stitching all the reference bead images, the typical TFM experiment is performed in which a cell image and a deformed bead image (Figure 20E) are taken for each single cell or cell pairs within the frame selected in (Figure 20B). Our approach does not require the disintegration of cells, which allows obtaining protein localization from cells post-traction force data collection (Figure 20F).

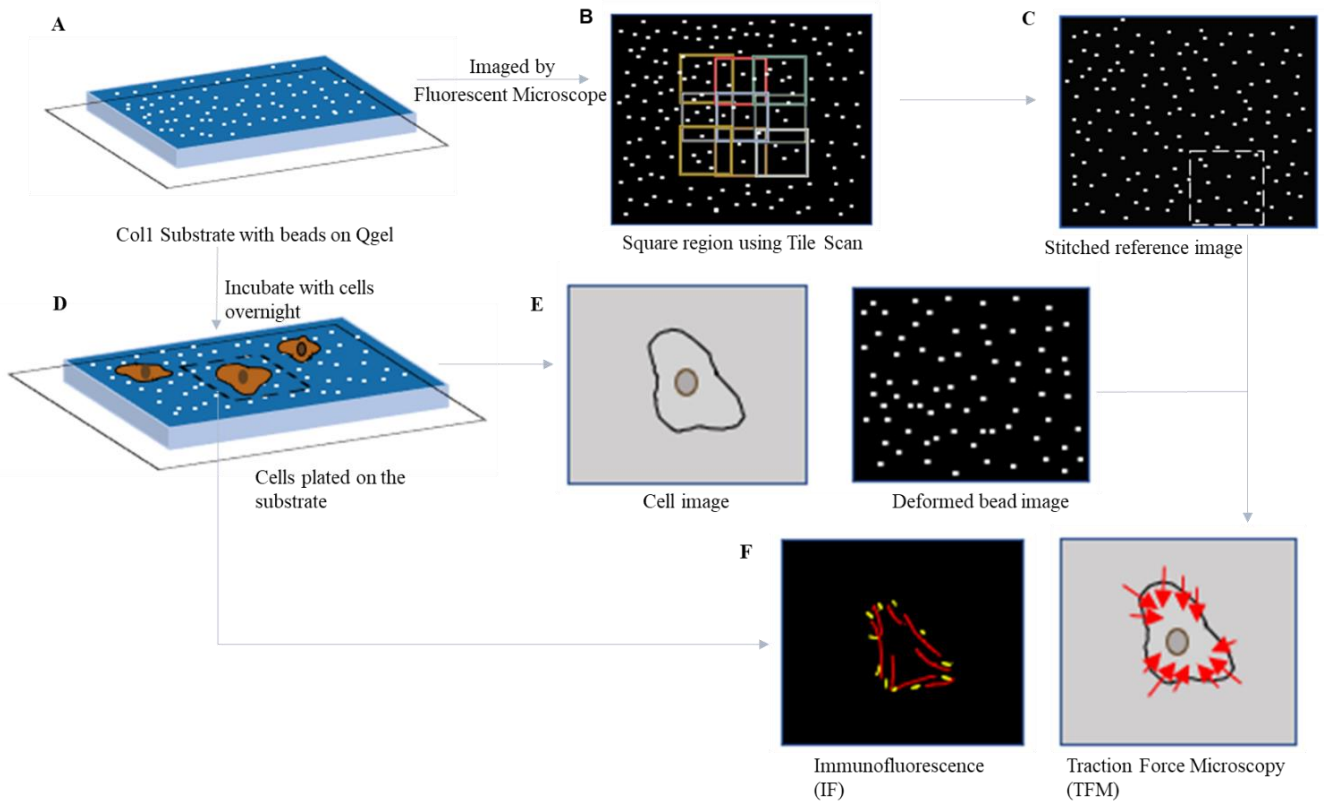


Figure 20: Schematic depiction of our methods for coincident traction force and immunofluorescence data collection. (A) Collagen I substrate with fluorescent beads plated on Qgel silicone substrate. (B) Region of the substrate selected near the center and imaged using Tile Scan in fluorescence microscopy. (C) Stitched bead image composed of several reference bead images in absence of cell generated forces taken from the tile scanned region of panel (B). (D) Cells are plated on the substrate. (E) After overnight incubation, cells and deformed bead images within the tile scanned region near the center of substrate are imaged using fluorescent microscopy. (F, right) Traction Force Microscopy (TFM) procedure can be done after using cross-correlation using MATLAB where a reference bead image can be matched with the deformed bead image (E) in order to get the traction force map. Subsequently, the immunofluorescence (IF) image of the same cell can be obtained (F) after fixing and staining the cells.

To apply this method, we used A431 epidermoid carcinoma cells expressing endogenous E-cadherin and high levels of Epidermal Growth Factor Receptor (EGFR). We plated the A431 cells on a NuSil 1:1, 0.55% Sylgard 184 substrate coated with collagen-I. We used coincident immunofluorescence and traction force microscopy in order to quantify the strain energy for A431 single cells and the inter-cellular forces for A431 cell pairs and coincidentally determine the YAP ratio via immunofluorescence for the same cells. First, we generated a reference stitched bead image (Figure 21A) using Fiji software (detailed steps in the following sections). In figure 21B, we see the image of a single A431 (Figure 21B, left) cell and the correspondent stressed bead image (Figure 21B, right). Using the reference stitched image and the stressed bead image, we were able to obtain the traction stress vectors (Figure 21C, left) and the heat map of traction magnitudes (Figure 21C, right). Then, we stained for the actin cytoskeleton using phalloidin (Figure 21D, left) the nucleus using DAPI (Figure 21D, middle), and YAP using an antibody for YAP (Figure 21D, right).

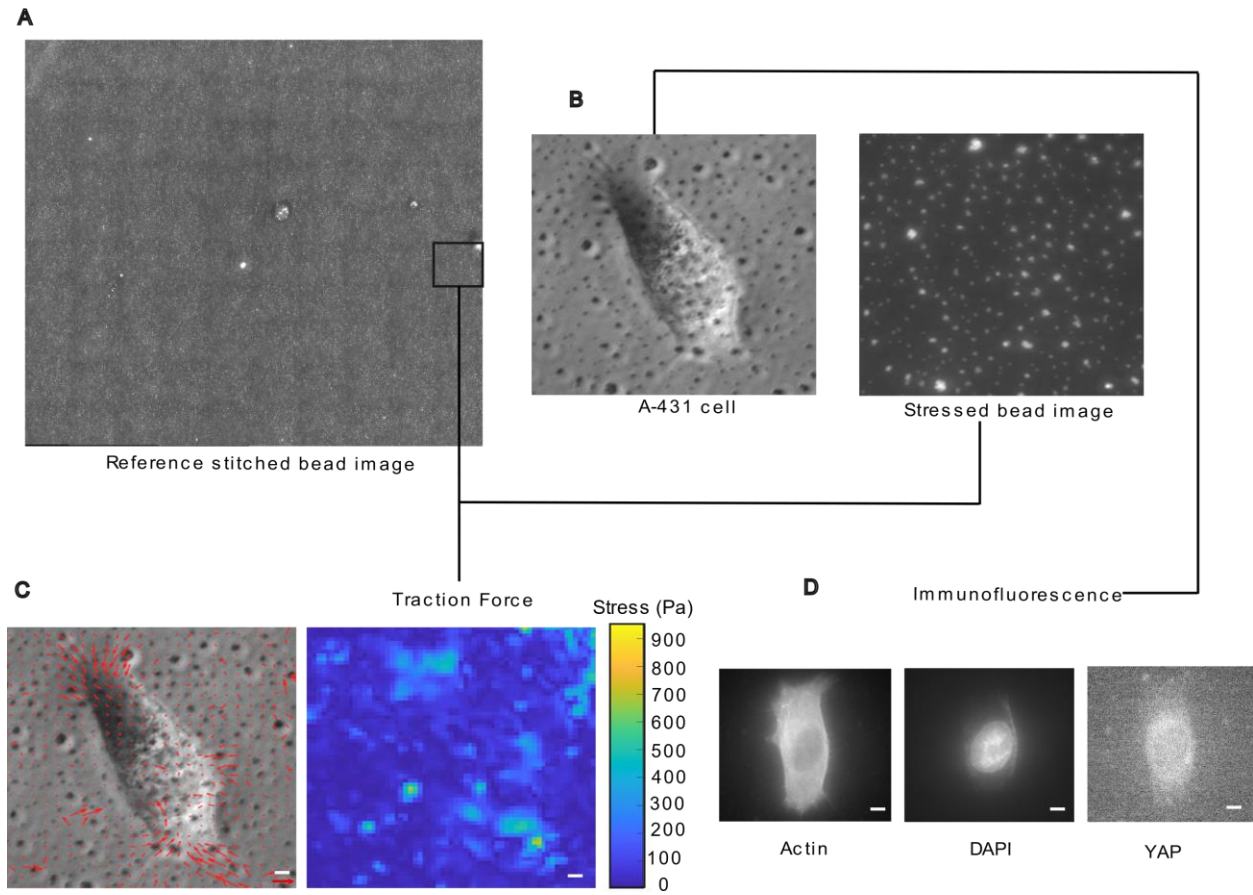


Figure 21: Coincident traction force maps and immunofluorescence images. (A) Stitched reference bead image. (B, left) A431 cell phase image. (B, right) Deformed/stressed bead image. (C) Traction stresses of A431 single cell (left). Traction stress vectors are overlaid (red arrows.). Heat-scale map of the traction magnitude for A431 single cell (right). Scale bar is 5 μm . Red arrow: 500 Pa. (D) Immunofluorescence images for an A431 cell stained for actin, DAPI, and YAP.

For each cell, we analyzed (using equation 1) the immunofluorescence images of YAP by quantifying the average intensity of YAP in the nucleus and the average intensity in the cytosol

(following equation 2) in order to study the degree of nuclear recruitment. The protocol for determining YAP ratio is detailed in the following sections.

Equation 1:

$$YAP\ Ratio = \frac{Intensity_{Nucleus}}{Intensity_{Cytosol}}$$

Equation2:

$$Intensity_{cytosol} = \frac{([Intensity_{Cell}Area_{Cell}] - [Intensity_{Nucleus}Area_{Nucleus}])}{Area_{Cytosol}}$$

For single cells, we plotted the strain energy (Y axis) versus YAP ratio (X axis) (Figure 22). For cell pairs, we plotted the inter-cellular force (Y axis) versus YAP ratio (X axis) (Figure 23).

The average YAP ratio for all 22 analyzed single cells was 1.03 ± 0.02 . For cell pairs, the average of the 10 cell pairs, i.e., 20 single cells (since each cell was analyzed as a single cell), was 1.03 with a standard deviation of ± 0.03 . We noticed that our YAP ratio is in a very narrow range. Only when we consider a substantial range, we may be able to see if there is a correlation between traction forces and the YAP ratio. To better understand the relationship between traction forces and YAP ratio, we can plate the cells on stiffer and softer substrates so that we can have a wide range of YAP ratios.

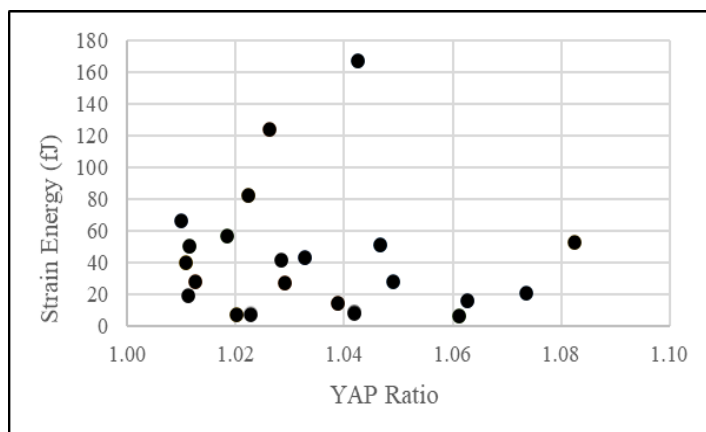


Figure 22: Single cell strain energy vs YAP ratio. Average ratio of YAP for single cells was 1.03 ± 0.02 .

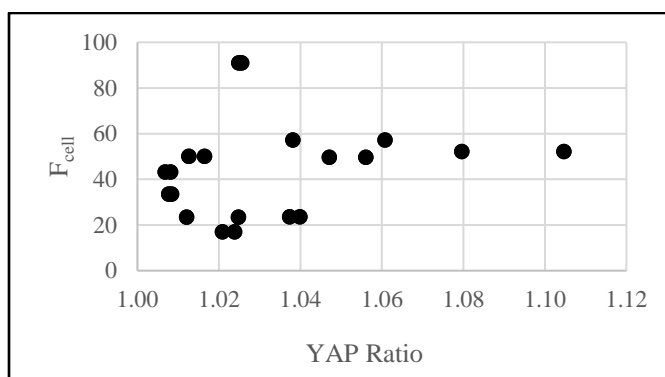



Figure 23: Inter-cellular force vs YAP ratio for cell pairs. Average ratio of YAP for cell pairs was 1.03 ± 0.03 .

3.4 Detailed Experimental Protocol for Coincident Immunofluorescence and TFM (IF-TFM)

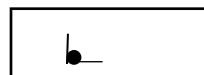
One of the results of this work was the development of the following step-by-step protocol that was developed so that it can be widely adopted by many other labs. Adoption of

this method can lead to novel insights from coincident immunofluorescence and TFM. The following is the detailed procedure for performing coincident immunofluorescence and TFM:

1. Prepare the NuSil A: B at a ratio 1:1 gel mixture with 0.55% Sylgard.
2. Mark the bottom part of the glass coverslip with: 
3. Add 0.1 g of the gel mixture on top of a 22 mm x 22 mm glass coverslip.
4. Place the glass coverslip with silicone in the degasser for about 5 minutes.
5. Cure the gel using a gravity convection oven at 100 °C for 3 hours.
6. Expose the NuSil substrate to 305 nm UV light for 5 minutes.
7. Prepare the bead solution: 10 mg EDC, 5 mg NHS, 200 μ L of 0.017 mg/ml collagen-1 solution and 130 μ L of 0.65mg/ml of 0.44 μ m red fluorescent beads in 2 mL DI water.
8. Add the bead solution to a 35 mm petri dish.
9. Incubate the glass coverslip face down for 30 minutes in the 35 mm petri dish containing the bead solution.
10. Wash the glass coverslip with 2 mL PBS for 5 minutes.
11. Place the glass coverslip in a chamber with 2 mL PBS.
12. Image the reference bead 10 x 10 frame by the marked small dot/circle.
13. Mark the stage of the microscope and the chamber such that the marks on the stage and the chamber are aligned.
14. Locate the first bead image by checking and noting the X and Y positions. Go to the 2nd bead image by adding 0.2 mm horizontally (X+0.2 mm), keep going till the 10th bead image. Go down to the 11th bead image by adding 0.15 mm vertically (Y+0.15 mm), keep going horizontally following the -0.2 mm increment till you reach the 20th bead image.

Follow the same trend till the 100th bead image (last bead image). Beads are stitched using Fiji (protocol is detailed in the next section).

15. Take the glass coverslip, wash two times with PBS for 3 minutes.
16. Plate cells on the glass coverslip.
17. Incubate overnight.
18. Place the glass coverslip in the chamber with DMEM + HEPES.
19. Place the chamber on the microscope such that the mark on the stage and the chamber are aligned.
20. Go to the same first bead image by the marked small dot/circle and match it with the reference bead image taken in step 12; if there is a single cell or a cell pair within the first frame, take the image of the bead and the cell. Go to the next frame (by adding 0.2 mm horizontally), if there is a single cell or a cell pair within the frame, take the image of the bead and the cell. Keep repeating the same process till the 10th bead image. Go down by 0.15 mm, make sure that the 11th bead image matches the 11th reference bead image taken in step 12; then, if there is a single cell or a cell pair within the frame, take the image of the bead and the cell. keep going horizontally following the 0.2 mm increment. Then, keep repeating the same process till the 20th frame. Follow the same trend till the 100th bead image (last bead image).
21. Keep the chamber on the stage, aspirate the DMEM+HEPES, add the fixing solution of the immunofluorescence (IF) protocol. Take the chamber to the lab bench, place the glass coverslip in a 2 mL petri dish, wash the glass coverslip three times with 2 mL PBS for 5 minutes. Continue the IF protocol (described in the methods section).
22. Seal the glass coverslip face down on a slide as follows.



23. Image the cells by going to the same first bead image following the small dot/circle and match it with the reference bead image taken in step 12. Within the first horizontal row of 10 bead images go to the specific bead frame where you found and imaged a single cell or cell pair (in step 20), make sure that the bead image matches the reference bead image and take the IF images. Move to the second row of bead images by adding 0.15 mm vertically and go to the specific bead frame where you found and imaged a single cell or cell pair (in step 20), make sure that the bead image matches the reference bead image and take the IF images. Keep going till the 10th row.

3.4.1 Stitching Protocol

In order to stitch all the reference bead images taken from the 10 x 10 frame, we used Fiji software (link in the section 3.22 under “Methods”.) The following is a detailed step-by-step protocol that was used in order to generate the stitched reference bead image shown in Figure 21A.

1. Save the 100 reference bead images; rename each image with an iterator in positions (such as Bead_(Tile1), Bead_(Tile2) and so on).
2. Use Fiji software and run the “Grid/Selection stitching” plugin in Fiji in order to stitch all the bead images together.
3. Choose the type and the order of the images depending on the sequence of the bead images initially saved.
4. Specify the “Grid size x” which is “10” and the “Grid size in Y” which is also “10”.
5. Adjust the “Tile overlap [%]” to “10” and indicate the “First file index i” to be “1”, since the index of the first bead image starts with the number “1”.
6. Select the “Directory” of the saved folder.

7. Select the “file names for tiles” by copying and pasting the title of the first bead image with a file extension at the end (“.tif” in our case). It is crucial to specify the part of the file name that iterates over to get all of the bead images, therefore replace the iteration number with “{i}” so that it becomes “Bead_(Tile{i}).tif”.
8. Select “Linear blending” option for the “Fusion method”.
9. Choose “Compute overlap (otherwise use approximate grid coordinates)” in order to calculate the overlap between images.
10. Select “Save computation time (but use more RAM)” from the “computation parameters” options.
11. Choose “Fuse and display” from “Image output” options.
12. Click “OK” and this will generate a stitched image composed of all the bead images.

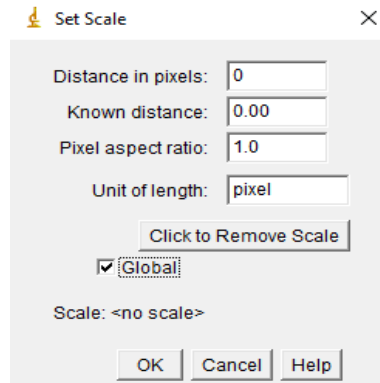
3.4.2 Protocol to Determine YAP Ratio

YAP ratio for single cells and cell pairs is determined using the following procedure:

1. Open IF folder containing the actin, DAPI, and YAP images.
2. Open the actin image and DAPI image in ImageJ
 - a. Highlight the actin and DAPI images in the file folder
 - i. Click and drag the images over the main ImageJ menu screen.
3. Open the same images again to have a total of 4 windows of images on screen
 - a. One can minimize DAPI images for now.
4. Ensure that the measurements are in pixels:
 - a. Analyze → Set Scale
 - i. Unit of length: pixel
 - ii. Click to Remove Scale

iii. Check Global

1. A quick check is to draw a line (or a box) from one end to the other from $X=0$ and $Y=0$ to the opposite end and read the width (w) and height (h) values. For 40x magnification, they should be $w = 1392$ and $h = 1040$ as shown at the bottom of the ImageJ window.



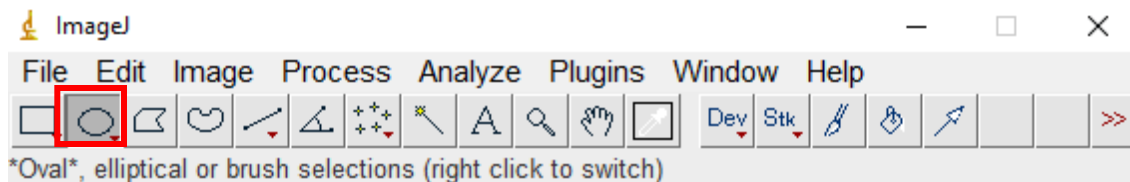
5. For better efficiency, create “Select None” and “Restore Selection” Shortcuts
 - a. Plugins → Shortcuts → Add plugin by name...
 - i. Shortcut: 0 (or any other unbound key of choice. I.e., 8,7,6, q, g, J, etc.)
 - ii. Command: Select None
 - b. Plugins → Shortcuts → Add plugin by name...
 - i. Shortcut: 9 (or any other unbound key of choice. I.e., 8,7,6, q, g, J, etc.)
 - ii. Command: Restore Selection
6. Zoom into one of the opened actin images so the cell occupies the entire ImageJ window by pressing the plus button (“=”)
7. Invert the color of only one of the IF images of actin
 - a. Edit → Invert
 - b. Never save the adjusted image unless you want to save in a separate folder, to avoid overwriting the main IF image.

- c. Can also adjust Brightness/Contrast to help visualize the outline (for both actin and DAPI for the main image that will be traced)

- i. Image → Adjust → Brightness/Contrast

8. Create an outline of the entire cell

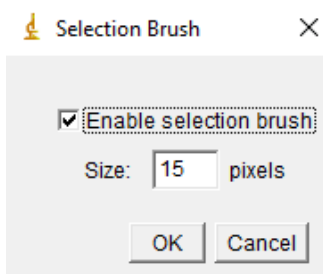
- a. Double click “*Oval*, elliptical or brush selections (right click to switch)”



- b. Check the “Enable selection brush” box and type in size of the circle

- i. Start with 100 to create a rough outline of the cell

- ii. Press “OK”



9. Click in the center of the cell and drag the circle to give a very rough outline of the cell.

10. Save the outline.

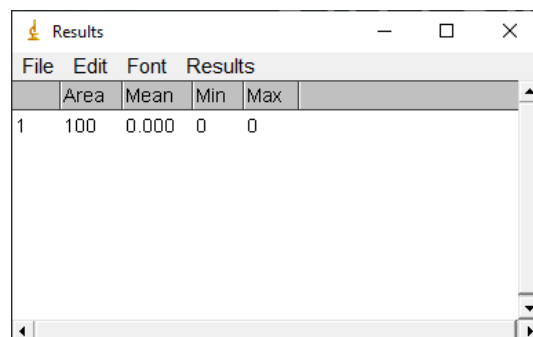
11. Slowly decrease the size of the Selection Brush to create a more detailed outline by following steps 8-11.

- a. Use any size you wish, but recommended circle sizes: 100, 50, 10, 5, 2, and 1.

12. Once having complete outline, save the outline.

- a. Click on the unaltered image.
 - b. Use the Restore Selection shortcut.
 - c. Edit → Clear outside.
 - d. File → Save as → .tiff.

13. Trace the outline for the nucleus (DAPI image) following steps 6-13 but can save the .tiff file into the same folder as the actin .tiff.
14. Place the outline of the cell onto the YAP image.
 - a. Open the “Clear outside” IF image of Actin in ImageJ.
 - i. One window opened.
 - b. Open the YAP IF image in ImageJ.
 - i. Two windows of images opened.
 - c. Click on the Actin window.
 - d. Click on the YAP window and press the “Restore Selection” shortcut button that was assigned in step 5.
15. Measure the amount of YAP.
 - a. With the Restored selection of Actin placed onto the YAP image, measure the intensity of the entire cell on the YAP image.
16. Analyze → Measure: Results window will open.
 - a. The “Mean” column is the average of the intensity.



	Area	Mean	Min	Max
1	100	0.000	0	0

17. Restore the nucleus selection onto the YAP image and measure the amount of YAP following steps 15-16 using the DAPI image.
18. Shift select the data in the “Results” window.

19. Do steps 1-3 and 6-19 for all single cells and cell pairs.

a. For cell pairs

i. analyze each cell individually, just label it as a number and A or B.

ii. Open a new image of the cell pair.

1. “Paste” the outline of the first fully traced cell using the “Restore Selection” tool.

2. Edit → Fill

a. Should turn white or may need to adjust the fill color

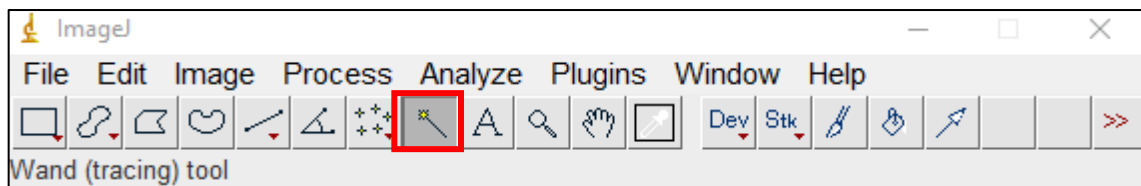
i. Edit → Selection → Properties → “Fill color:”
“none”

3. Use brush size 100 to get the part of the first cell (that is now white) and the entire second cell.

4. Edit → Clear Outside.

5. “Select None” Shortcut button.

6. Get the wand tool (red box).



7. Click the white area that was creating using “Fill”.

8. Edit → Clear.

9. Click around the perimeter of the roughly outlined cell until it is entirely selected.

10. Open a new Cell Pair image.

11. “Restore Selection” onto a new unedited cell image and repeat steps 6-19.

3.5 Conclusion

Traction force microscopy is an important method to enable the determination of forces exerted by cells on their surroundings. Here, we addressed one of the main limitations of traction force microscopy – the inability to obtain protein localization data from cells post-traction force data collection. We proposed and realized a simple strategy for coincident traction force microscopy and immunofluorescence. By collecting reference bead images before the TFM workflow, we obviate the need for cell disintegration to collect reference bead images. Our technique is an easy approach that does not require complicated procedures or advanced tools. It just requires an epifluorescence microscope and common image collection and processing techniques. Using our method, we were able to measure the strain energies for single cells and the inter-cellular forces for cell pairs, as well as determine the YAP ratio via immunofluorescence for the same cells. Further investigations can be done by plating single cells and cell pairs on softer/stiffer substrates so that we can have a wide range of YAP ratios to better understand the relationship between traction forces and the YAP ratio.

CHAPTER 4

E-CADHERIN STIFFNESS SENSING AND FACTORS AFFECTING FORCE TRANSMISSION

4.1 Introduction

In epithelial tissues, E-cadherin is the major transmembrane protein that mediates cell-cell adhesions. E-cadherin is responsible for maintaining the architecture of adult epithelial tissues as well as remodeling of tissues [104,105]. E-cadherin from one cell binds homophilically to E-cadherin from a neighboring cell at the cell-cell contact. Intracellularly, E-cadherin transmembrane proteins bind to the actin cytoskeleton through adaptor proteins. E-cadherin adhesions form trans-interaction clusters at cell-cell contacts and cis-dimer interactions within the surface of each epithelial cell [106]. The actin cytoskeleton forms a belt within each cell in an epithelial cell sheet and these belts are coupled to each other using E-cadherins that combine the adhesive and contractile responses of epithelial cells [107,108,109]. To decipher the role of E-cadherin adhesions in tissues, it is important to understand both their biochemical and biophysical aspects. Significantly, it has been shown that E-cadherin adhesions sense changes in junctional tension and associate with downstream signaling molecules [110], just like integrin-based adhesions do at cell-ECM contacts [27]. E-cadherin is a mechanosensor at cell-cell contacts and converts junctional tension to biochemical signals inside the cell. Mechanosensitivity at cell-cell contacts [111,112] and cell-extracellular matrix (ECM sites) [113] is important for maintaining the architecture of tissues, morphogenesis [114], and influences the progression of diseases [34]. It is known that adhesions through integrins are sensitive to elasticity within the range of that of the extracellular

matrix. However, it is still unclear if E-cadherin adhesions at cell-cell contacts can sense elasticity within the same range as that of the epithelial cells that surround them.

Sensing cell-like elasticity by E-cadherin may be essential for several processes such as wound healing [115] and the modulation of E-cadherin adhesion through inside-out signaling may play an important role in the progression of cancer [35,116]. Human epithelial cancer cells are considered as softer than benign epithelial cells [36], therefore E-cadherin mechanosensing of cell elasticity can play a role in this context. Different studies showed that cancer epithelial cells are softer than benign epithelial cells from the same tissue: The Young's modulus was 0.5 kPa for cancer vs 2 kPa for benign cells from lungs [117], 0.5 kPa for cancer vs 2 kPa for benign cells from breast [117], 0.5-1.1 kPa for cancer vs 2.5 kPa for benign cells from ovaries [118], 1.4 for cancer vs 2.2 kPa for benign cells from thyroid [119] 0.3-1.4 kPa for cancer vs 2.8 kPa for benign cells from prostate [120]. Therefore, we used E-cadherin coated soft substrates in the range of sub-kPa to a few-kPa to test if cells can sense the stiffness via E-cadherin on substrates within the range of cell-like elasticity.

In epithelial cell-cell contacts, E-cadherin adhesions exist among a complex network consisting of different cell-cell adhesion structures. E-cadherin adhesions are usually studied using a sheet of epithelial monolayers or islands that have numerous cell-cell contacts. There are four types of epithelial cell-cell junctions: (i) tight junctions, (ii) adherens junctions, (iii) desmosomes, and (iv) gap junctions [121]. Each junction has specific transmembrane proteins that connect cell-cell contacts. In tight junctions, claudin and occludin are the main transmembrane proteins that connect the junction between cells. In desmosomal junctions, desmoglein and desmocollin are the main desmosomal cadherins that are engaged in cell-cell adhesions. In adherens junctions, E-cadherins are the main transmembrane proteins at the cell-cell contact but there are other types of

cell-cell adhesions such as those mediated through nectins. Many groups have used cadherin-coated surfaces in order to enable the specific probing of cadherin [122,123,124,125,126]. E-cadherin consists of three regions: extracellular region, transmembrane region, and intracellular region. In order to study biochemical events specifically initiated by E-cadherin adhesion, we performed *in vitro* experiments using a glass coverslip coated with E-cadherin-Fc (i.e., the extracellular region of E-cadherin fused together with the Fc region). To be more specific, protein A is first coated on glass and E-cadherin-Fc is then coated on top of protein A [127]. It is important to note that E-cadherin adhesions here are more easily imaged in a 2D plane compared to native epithelial cell-cell contacts consisting of a very complex topology. Actin cytoskeleton closely regulates E-cadherin [128], with the archetypical apical band of E-cadherin around epithelial cells intimately juxtaposed to a related belt of actin cytoskeleton. E-cadherin on soft and flat substrates can allow us to see how the actin cytoskeleton is closely coupled to discrete E-cadherin adhesions at an interface with epithelial cell-like elasticity. To understand E-cadherin mechanobiology, flexible E-cadherin-coated substrates have been used *in-vitro* before. It has been shown that E-cadherin can differentiate between elastic moduli within the tens of kPa range [129] or between kPa and MPa elastic moduli. However, it is still unclear if E-cadherin adhesions can differentially sense elasticity within the same range as that of epithelial cells such as in the sub-kPa to few-kPa range. Moreover, the formation of discrete E-cadherin adhesions on substrates within a relevant range of elasticity has still not been reported. In this chapter, we address if the formation of E-cadherin adhesion relies on the sensing of epithelial cell-like stiffness and how these E-cadherin adhesions are supported by the actin cytoskeleton on such substrates.

To further understand E-cadherin mechanobiology, we are not only interested in checking whether E-cadherin senses epithelial cell-like stiffness but also assessing the level of force

transmission through E-cadherin adhesion complexes at cell-cell contacts. E-cadherin mechanotransduction loci sense mechanical forces at cell-cell contacts. Therefore, it is important to understand the factors that affect the levels of force transmitted through E-cadherin-based cell-cell contacts. Recent studies showed that two E-cadherin molecules and one monomer Epidermal Growth Factor Receptor (EGFR) molecule form a heterotrimeric complex at the plasma membrane [130]. Importantly, the Epidermal Growth Factor Receptor (EGFR) is involved in the force transduction mechanism at interepithelial junctions [130]. Therefore, we tested how perturbations of EGFR affect intercellular forces through E-cadherin-based cell-cell contacts.

Based on previous reports, it is known that force transmission is also mediated by heterophilic adhesion between E-cadherin and N-cadherin [44]. Heterophilic interaction between E-cadherin/N-cadherin has higher binding affinity compared to homophilic interaction [131] and junctions of E-cadherin from cancer cells and N-cadherin from fibroblasts have been shown to be involved in cancer progression [44]. Thus, we were interested in comparing force transmission at cell-cell contacts in epithelial cells through homophilic vs heterophilic cadherin interactions. Here, we do so by quantifying the inter-cellular forces of homophilic E-cadherin/E-cadherin interactions, homophilic N-cadherin/N-cadherin interactions, and heterophilic E-cadherin/N-cadherin interactions using A431D cells exogenously expressing either E-cadherin or N-cadherin.

4.2 Methods

4.2.1 Cell Culture

Dulbecco's modified Eagle's medium (Corning Inc., Corning NY) containing 10% fetal bovine serum (Corning Inc., Corning NY), L-glutamine, and 1% Penicillin/Streptomycin was used to culture C2BBE human colon epithelial cells under 5% CO₂ at 37°C. Versene, a trypsin-free

chelator-based cell dissociation reagent, from Thermo Fisher Scientific (Waltham, MA) was used during each experiment to detach cells from cell culture dishes. The experiments on the E-cad-coated surfaces were performed using the same media mentioned above, but without the fetal bovine serum, and the incubation time was 2 hours, under 5 % CO₂ at 37°C. The experiments with 15 uM Gefitinib EGFR inhibitor were performed in low serum (0.5 %), with 100 ng/ml EGFR inhibitor. The heterophilic experiments were seeded on the substrate with the presence of 400 µg/mL G418 (Geneticin) so that cells continue to express cadherins.

4.2.2 Biomimetic E-cadherin Glass Substrate Preparation

Glass substrates was prepared using a 22 mm x 22 mm glass coverslip that was incubated with 40 µL of 0.2 mg/mL protein-A from Prospec (Rehovot, Israel) for one hour. After three washing steps with DPBS (with Ca/Mg), the protein-A coated substrate was incubated with 20 µL of 0.1 mg/mL recombinant E-cadherin-Fc from Sino Biological (Beijing, China) for 2 hours at room temperature. Next, the glass coverslip was washed three times with DPBS (with Ca/Mg) for five minutes each time and then incubated with 20 µL of 1 mg/mL Fc fragment from Jackson ImmunoResearch (West Gove, PA) for 1 hour at room temperature. Lastly, the sample was washed again three times with DPBS (with Ca/Mg). Afterwards, the glass substrate was ready for cell plating.

4.2.3 Biomimetic E-cadherin Soft Substrate Preparation

NuSil soft silicone from NuSil Silicone Technologies (Carpinteria, CA) was prepared by mixing its A and B components in the ratio 2:3 and 2:7 by weight. A Modular Compact Rheometer (Austria, Europe) was used in order to measure the storage and loss shear moduli of each NuSil composition. The substrate was prepared using a 22 mm x 22 mm glass coverslip. About 100 µL

of NuSil soft silicone was poured onto the glass coverslip and cured using a hot plate at 100°C for 1 hour. Following that, the substrate was exposed for 5 minutes to 305 nm UV light (UVP cross-linker, Analytik Jena AG, Upland, CA). An aqueous solution containing 0.2 mg/mL protein-A from Prospecc (Rehovot, Israel), 10 mg/mL EDC (1-ethyl-3-(3-dimethylaminopropyl) carbodiimide hydrochloride), 5 mg/mL sulfo-NHS (N-hydroxysulfosuccinimide) chemistry were mixed to couple protein A to the substrate for an incubation time of 1 hour at room temperature. The substrate was then washed with Dulbecco's Phosphate-Buffered Saline (with calcium), then incubated with 0.1 mg/mL recombinant E-cadherin-Fc from Sino Biological (Beijing, China) for 2 hours at room temperature. After washing with Dulbecco's Phosphate-Buffered Saline (with calcium), the substrate was incubated with 1 mg/mL Fc fragment from Jackson ImmunoResearch (West Gove, PA) for 1 hour at room temperature. The cells were plated on the substrate after washing the substrate once more with Dulbecco's Phosphate-Buffered Saline (with calcium). The silicone substrate's Young's modulus for the experiments with C2BBe cells was determined to be 0.3 kPa and 2.4 kPa [132]. For all the experiments with A431 cells and A431D, the Young's modulus of NuSil 1:1 with 0.55% Sylgard 184 substrate was 6.603 ± 0.660 kPa.

4.2.4 Immunofluorescence and Drug Treatment

Proteins inside cells were stained using immunofluorescence in which cells were permeabilized and fixed for 15 minutes using buffer C (10 mM MES (2-morpholinoethanesulfonic acid), 138 mM KCL (pH 6.8), and 3 mM MgCl₂ with 0.5% (v/v) Triton-X, 1.5% (w/v) bovine serum albumin, and 4% paraformaldehyde. Cells were incubated face down with primary antibodies at 4°C overnight, then incubated with secondary antibodies at room temperature for 1 hour. Primary antibodies used were anti-β-catenin from BD biosciences (San Jose, CA), anti-paxillin from Abcam (Cambridge, UK), anti-phosphomyosin Light Chain 2 (Ser 19) from Cell

Signaling Technology (Danvers, MA), and anti-E-cadherin from Santa Cruz Biotechnology (Dallas, TX). DAPI from Biotium (Hayward, CA) and Alexa Fluor 488-conjugated phalloidin from Thermo Fisher Scientific (Waltham, MA) were used to stain the nucleus and the actin cytoskeleton, respectively. Secondary antibodies used were from Jackson ImmunoResearch (West Grove, PA). SMIFH2 inhibitor was used at 20 μ M for 2 hours and Jasplakinolide inhibitor was used at 1 nM for 1 hour. SMIFH2 and Jasplakinolide were from MilliporeSigma (Burlington, MA). SB 27005 and ATN161 were from Selleckchem (Houston, TX). rhEGF was from R&D systems (Minneapolis, MN).

4.3 Results and Discussion

4.3.1 Formation of undesirable focal adhesions on E-cadherin-Fc glass substrate

To study E-cadherin adhesions without other cell-cell adhesion structures, we first prepared an oriented and immobilized E-cadherin-Fc substrate using glass coverslips. The glass coverslip was incubated first with protein A, and then coated with recombinant E-cadherin-Fc onto protein A. Then, human epithelial C2BBe cells were plated on the E-cadherin substrate in growth cell culture medium with fetal bovine serum. Cells adhered to the substrate and spread well. Afterwards, immunofluorescence was used in order to check the formation of E-cadherin adhesions by staining for β -catenin that binds to the intracellular region of E-cadherin at a 1:1 stoichiometric ratio [133]. Also, immunofluorescence was used to check for focal adhesions by staining for paxillin. We aimed to prohibit the formation of focal adhesions in order to clearly attribute cell response to E-cadherin adhesions. However, when human epithelial C2BBe cells were plated in normal cell culture medium with fetal bovine serum, prominent focal adhesions were present in all cells (Figure 24).

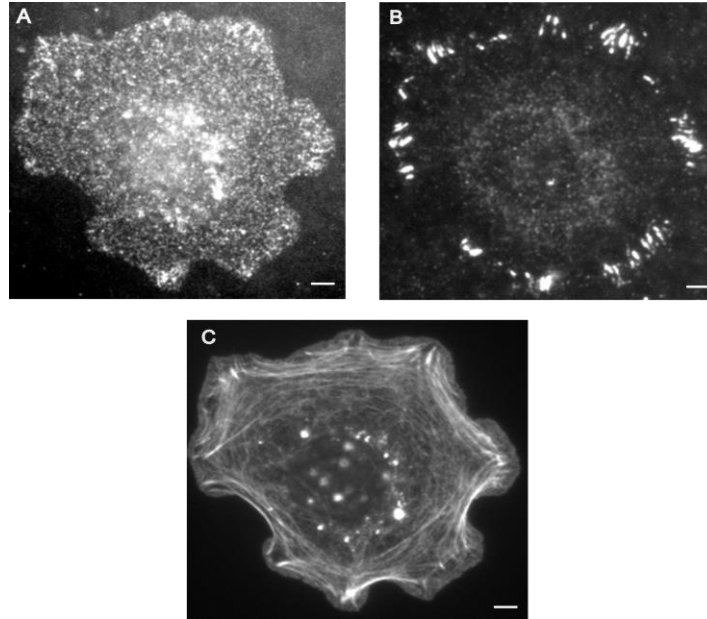


Figure 24: Formation of not well-developed E-cadherin adhesions but prominent focal adhesions on E-cadherin-Fc glass substrate in the presence of fetal bovine serum. (A-C) Immunofluorescence images of C2BBe cells on E-cadherin glass substrate stained for (A) β -catenin (marking E-cadherin adhesions), (B) paxillin (marking focal adhesions), and (C) phalloidin (marking actin cytoskeleton). All scale bars are 5 μ m.

Moreover, we tried to include a blocking step with bovine serum albumin (BSA), but the formation of focal adhesions was not prevented, as shown in Figure 25.

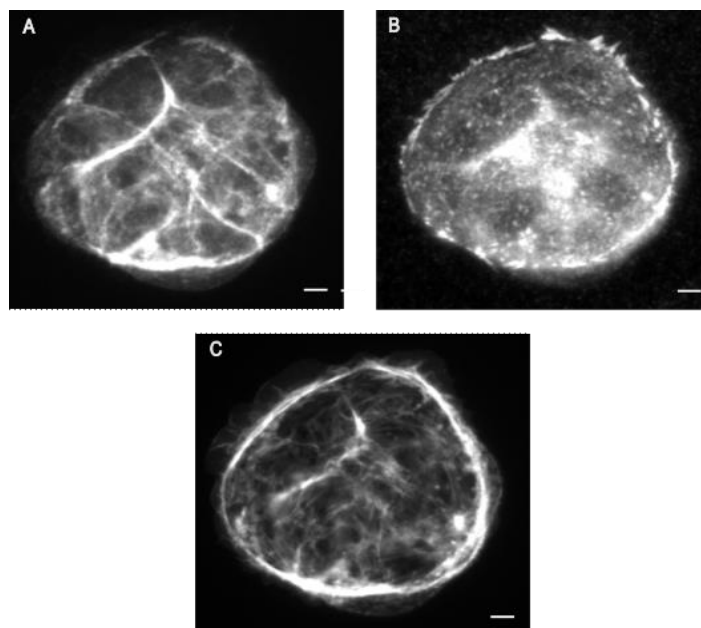


Figure 25: Presence of BSA does not preclude the formation of focal adhesions on E-cadherin glass substrate. (A-C) Representative immunofluorescence images of C2BBe cells on E-cadherin glass substrate that includes 10 mg/mL BSA blocking step and stained for (A) β -catenin (marking E-cadherin adhesions), (B) paxillin (marking focal adhesions), and (C) phalloidin (marking actin cytoskeleton). Focal adhesions marked by paxillin were prominent even in the presence of BSA blocking. All scale bars are 5 μ m.

4.3.2 Absence of focal adhesions on E-cadherin-Fc glass substrate

We thought that the extracellular matrix presents in fetal bovine serum could be leading to the formation of the unwanted focal adhesions. Therefore, we plated C2BBe human epithelial cells in growth culture medium that does not contain fetal bovine serum (serum-free) and found that focal adhesion formation was noticeably reduced with most of the cells (Figure 26).

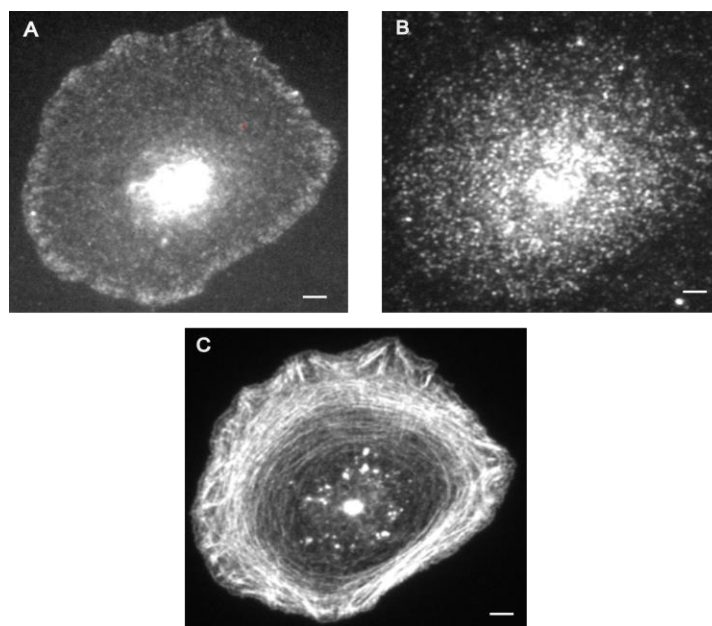


Figure 26: Formation of well-developed E-cadherin adhesions with absence of focal adhesions on E-cadherin-Fc glass substrate in serum free medium. (A-C) Immunofluorescence images of C2BBe cells on E-cadherin glass substrate stained for (A) β -catenin (marking E-cadherin adhesions), (B) paxillin (marking focal adhesions), and (C) phalloidin (marking actin cytoskeleton). All scale bars are 5 μ m.

In addition, we plated human epithelial A431 cells also in serum free growth culture medium and noticed that focal adhesion formation was totally reduced in all cells (Figure 27).

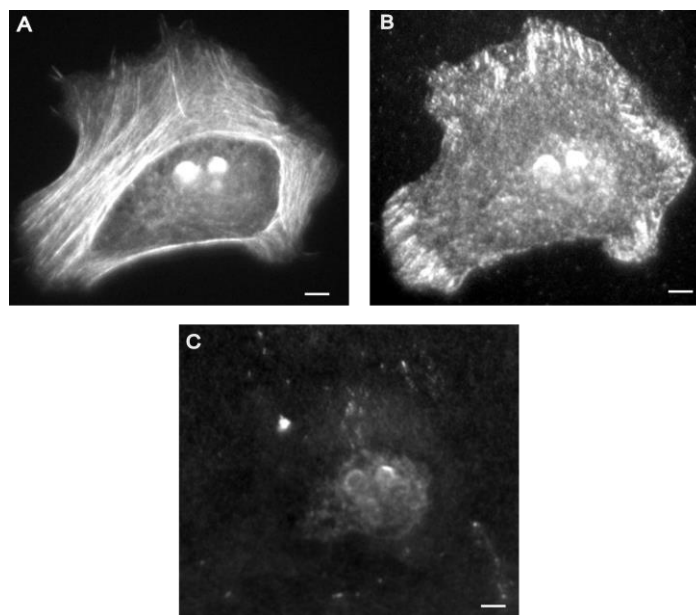


Figure 27: Formation of well-developed E-cadherin adhesions on E-cadherin-Fc glass substrate in serum free medium. (A-C) Immunofluorescence images of A431 cells on E-cadherin glass substrate stained for (A) phalloidin (marking actin cytoskeleton), (B) β -catenin (marking E-cadherin adhesions), and (C) paxillin (marking focal adhesions). All scale bars are 5 μ m.

It is important to note that, serum free media did not affect cells during the entire timescale considered to perform the experiment (Figure 28).

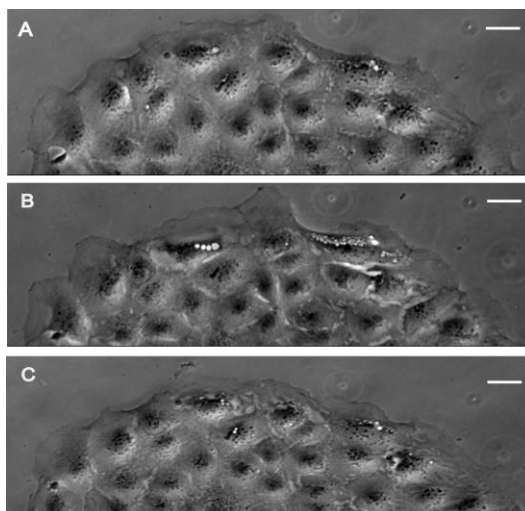


Figure 28: Cell viability is not affected during the experimental time course in the absence of serum. (A) C2BBe cell island at time 0 hour cultured in media with 5% FBS. Same C2BBe cell island after being in culture in serum free medium for 2 hours (B) and 4hrs (C). All scale bars are 10 μm .

4.3.3 Avoiding focal adhesions on E-cadherin-Fc substrate using integrin inhibitors

We tried to use integrin blocking antibodies to see if we can avoid focal adhesion formation [134]. ATN-161 was used to block integrin $\alpha 5 \beta 1$ and was shown to have a cardinal effect in inhibiting metastasis of tumors [135]. SB-273005 was also used as an antagonist of integrin for targeting $\alpha \nu \beta 3$ and $\alpha \nu \beta 5$ integrin receptors [136]. First, we plated C2BBe cells in normal cell culture medium with serum and we treated the cells with a mixture of integrin inhibitors, ATN-161 (20 μM) and SB-273005 (1 μM), for two hours. We observed two kinds of E-cadherin adhesions: adhesions associated with actin foci along circumferential structures of F-actin (Figure 29B) and adhesions associated with the ends of radial orientation of F-actin structures (Figure 29E). However, integrin inhibitors did not preclude focal adhesion formation in all cells.

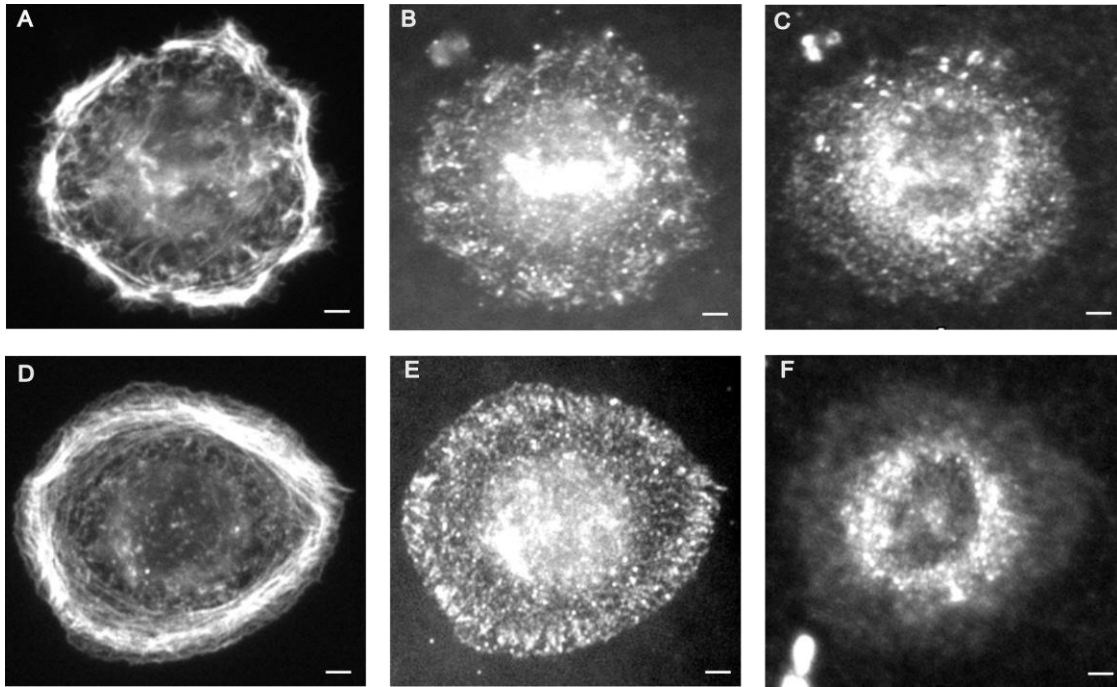


Figure 29: Actin-associated E-cadherin adhesion morphologies after treatment with integrin inhibitors in the presence of fetal bovine serum. (A-F) Immunofluorescence images of C2BBe cells on glass substrate stained for (A, D) phalloidin (marking actin cytoskeleton), (B, E) β -catenin (marking E-cadherin adhesions), and (C, F) paxillin (marking focal adhesions). (B) E-cadherin adhesions associated with actin foci along circumferential structures of F-actin. (E) E-cadherin associated with the ends of radial orientation of F-actin structures. All scale bars are 5 μ m.

Then, we plated C2BBe cells in cell culture medium in the absence of fetal bovine serum and we treated the cells with the same mixture of integrin inhibitors, ATN-161 (20 μ M) and SB-273005 (1 μ M), for two hours. We observed similar results of C2BBe cells treated with integrin inhibitors and plated in cell culture medium with serum (Figure 30). From all the above results,

serum free medium, rather than integrin inhibitors, appeared to be the key factor in avoiding focal adhesion formation.

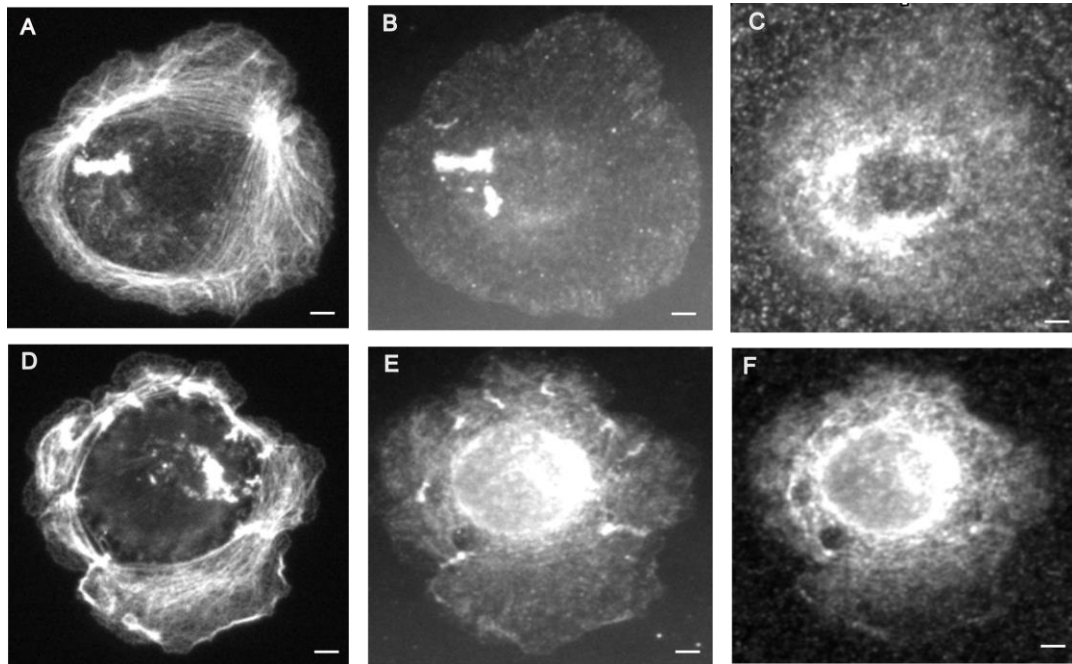


Figure 30: Actin-associated E-cadherin adhesion morphologies after treatment with integrin inhibitors in the absence of fetal bovine serum. (A-F) Immunofluorescence images of C2BBe cells on glass substrate stained for (A, D) phalloidin (marking actin cytoskeleton), (B, E) β -catenin (marking E-cadherin adhesions), and (C, F) paxillin (marking focal adhesions). (B) E-cadherin adhesions associated with actin foci along circumferential structures of F-actin. (E) E-cadherin associated with the ends of radial orientation of F-actin structures. All scale bars are 5 μ m.

4.3.4 Effect of E-cadherin cell-like elastic substrates on the organization of E-cadherin adhesions

One question that we were interested in testing was whether E-cadherin adhesions can sense the elastic microenvironment that imitates the epithelial cells that encircle them. E-cadherin

adhesions are located on the surface of epithelial cells in close vicinity to the cell cortex. Therefore, the stiffness of epithelial cells would be a relevant input for E-cadherin mechanosensing [137]. A survey [36] of many studies [117,118,119,120,138,139,140,141,142,143] that measured the elasticity of cancer and normal epithelial cells from the same tissue origin shows that the stiffness of normal human epithelial cells is in the range of sub-kPa to few-kPa and the stiffness of cancer cells is typically lower than the stiffness of normal cells. It has been shown that E-cadherin adhesions are able to sense applied forces [144] as well as stiffness of tens of kPa [129].

NuSil soft silicone gel was coated with protein A using EDC/sulfo-NHS, and then E-cadherin was immobilized onto protein A using recombinant E-cadherin-Fc. Importantly, mimicking lateral E-cadherin-based cell-cell junctions was recently done using a similar strategy [145]. After performing the in-vitro experiments and plating the cells in normal cell culture medium on two soft silicones [132] that have young's moduli of sub-kPa (0.3 kPa) and few kPa (2.4 kPa), we noticed that after overnight incubation of the cells, focal adhesions were not precluded (Figure 31).

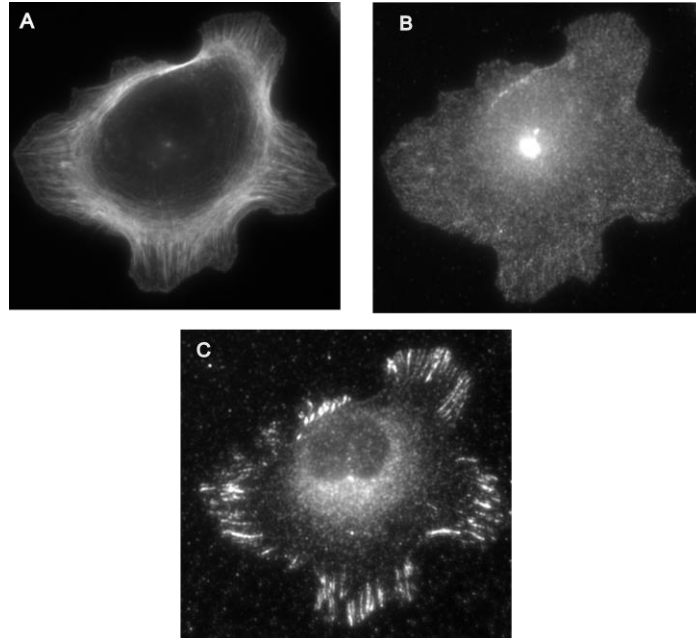


Figure 31: Formation of not well-developed E-cadherin adhesions but prominent focal adhesions on cell-like soft substrate in the presence of fetal bovine serum after overnight incubation. (A-C) Immunofluorescence images of C2BBe cells on 2.4 kPa E-cadherin soft substrate stained for (A) phalloidin (marking the actin cytoskeleton), (B) β -catenin (marking E-cadherin adhesions), and (C) paxillin (marking focal adhesions). All scale bars are 5 μ m.

However, when performing the in-vitro experiments and plating the cells for two hours in serum free medium on the two soft silicones, we noticed two kinds of E-cadherin adhesions via immunofluorescence. We observed linear adhesions associated with the ends of the radial orientation of F-actin structures (Figure 32, 33) and irregular adhesions associated with actin foci adjacent to the circumferences of F-actin structures (Figure 34, 35). Focal adhesions marked by paxillin staining were absent (Figure 32C, 33C, 34C, 35C).

The radial actin bundles (like dorsal stress fibers [146] of cells adherent to the extracellular matrix), where linear adhesions are associated, appeared to be well-integrated with the circumferential orientation of actin bundles (like the transverse arcs [146] of cells adherent to the extracellular matrix). At the circumferential F-actin structures, where irregular adhesions are associated, micrometer-scale regions of F-actin of high intensity were observed, and such foci are not observed at cell-ECM adhesions. Linear and irregular adhesions were present in several cells to different extents based on the dominance of actin foci or radial actin. Also, linear and irregular adhesions were typically largely spatially separated from each other, except for some cases where both linear and irregular adhesions were close to each other.

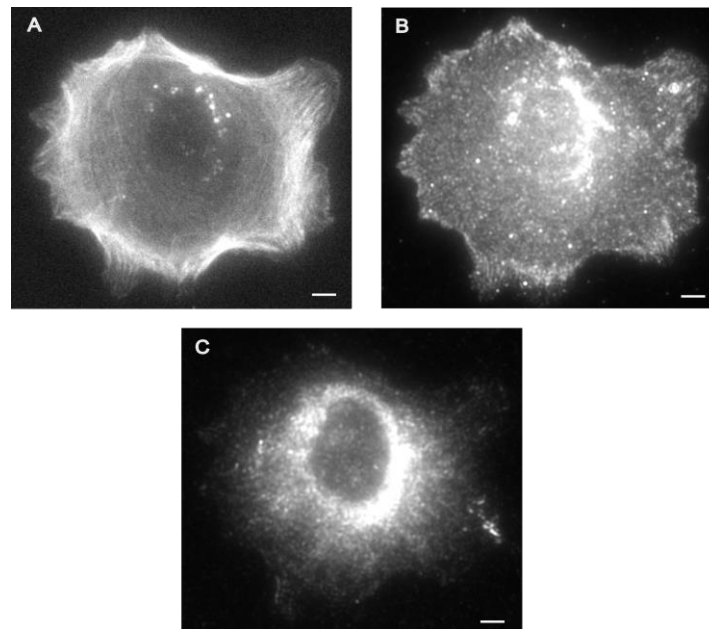


Figure 32: Actin associated with linear E-cadherin morphologies on 0.3 kPa E-cadherin substrates. (A-C) representative immunofluorescence images of C2BBe cells on 0.3 kPa E-cadherin substrate stained for (A) phalloidin (marking actin cytoskeleton) and (B) β -catenin (marking E-cadherin

adhesions), and (C) paxillin (marking focal adhesions). (B) Linear E-cadherin associated with the ends of radial orientation of F-actin structures. All scale bars are 5 μm .

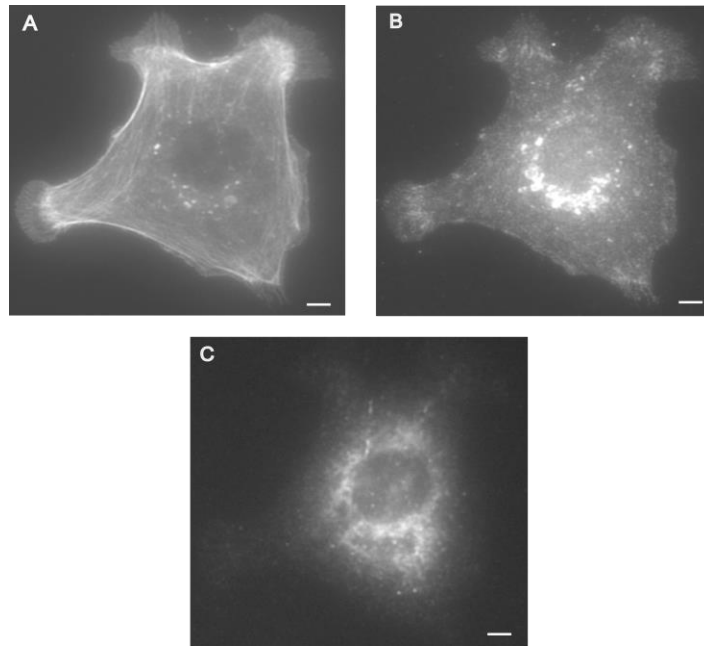


Figure 33: Actin associated with linear E-cadherin morphologies on 2.4 kPa E-cadherin substrates. (A-C) representative immunofluorescence images of C2BBE cells on 2.4 kPa E-cadherin substrate stained for (A) phalloidin (marking actin cytoskeleton) and (B) β -catenin (marking E-cadherin adhesions), and (C) paxillin (marking focal adhesions). (B) Linear E-cadherin associated with the ends of radial orientation of F-actin structures. All scale bars are 5 μm .

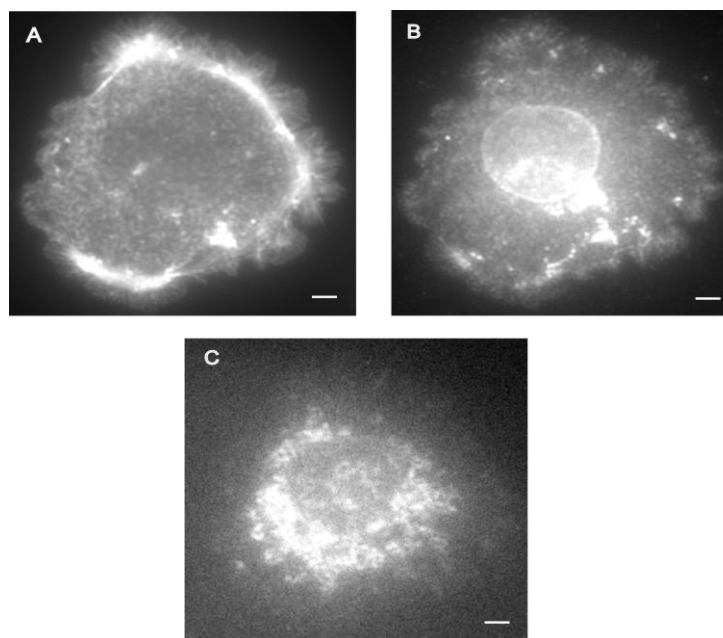


Figure 34: Actin associated with irregular E-cadherin morphologies on 0.3 kPa E-cadherin substrates. (A-C) representative immunofluorescence images of C2BBE cells on 0.3 kPa E-cadherin substrate stained for (A) phalloidin (marking actin cytoskeleton) and (B) β -catenin (marking E-cadherin adhesions), and (C) paxillin (marking focal adhesions). (B) Irregular E-cadherin adhesions associated with actin foci along circumferential structures of F-actin. All scale bars are 5 μ m.

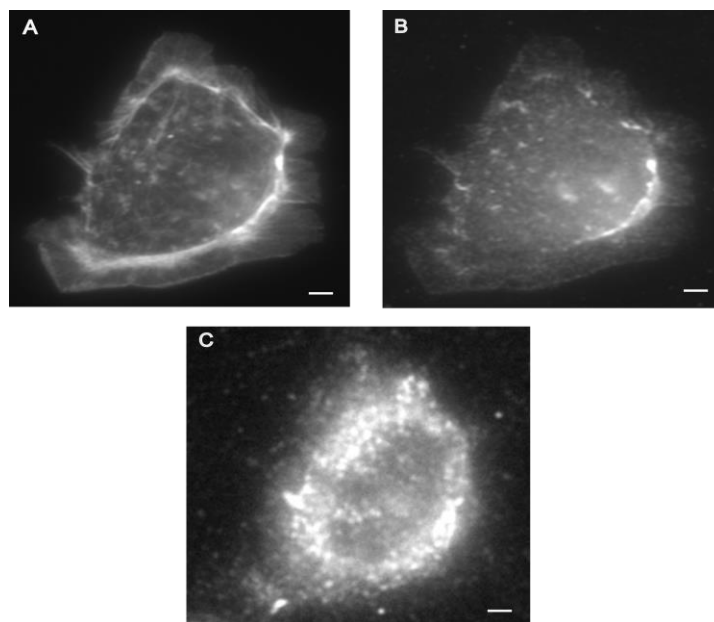


Figure 35: Actin associated with irregular E-cadherin morphologies on 2.4 kPa E-cadherin substrates. (A-C) representative immunofluorescence images of C2BBe cells on 2.4 kPa E-cadherin substrate stained for (A) phalloidin (marking actin cytoskeleton) and (B) β -catenin (marking E-cadherin adhesions), and (C) paxillin (marking focal adhesions). (B) Irregular E-cadherin adhesions associated with actin foci along circumferential structures of F-actin. All scale bars are 5 μ m.

E-cadherin was stained with a specific antibody that was directed against its cytoplasmic domain in order to confirm that β -catenin was a good choice as a marker of E-cadherin adhesions (Figure 36). The presence of linear and irregular E-cadherin adhesions was confirmed respectively as shown in Figure 36. After validating the results, we continued using β -catenin as marker of E-cadherin adhesions as it generated a stained with higher contrast.

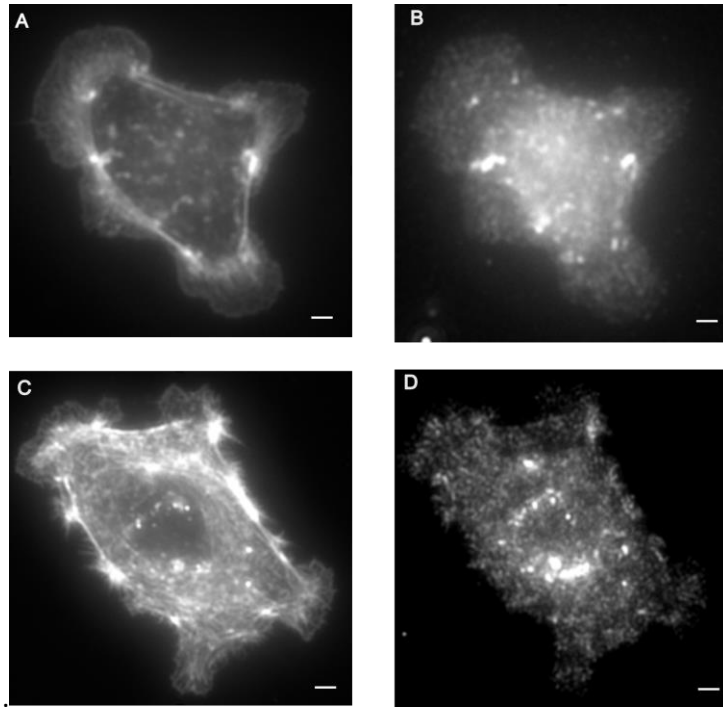


Figure 36: Presence of irregular adhesions associated with circumferential actin foci and linear E-cadherin adhesions associated with radial actin. (A-D) Immunofluorescence images of C2BB7 cells on 2.4 kPa soft substrate stained for (A, C) phalloidin (marking actin cytoskeleton), and (B, D) cytoplasmic domain of E-cadherin. (B) E-cadherin adhesions associated with actin foci along circumferential structures of F-actin. (D) E-cadherin associated with the ends of radial orientation of F-actin structures. All scale bars are 5 μm .

4.3.5 Localization of phospho-myosin in cells on E-cadherin coated cell-like substrates

To determine the mechanisms by which the actin cytoskeleton can be supporting irregular and linear E-cadherin adhesions, we started by testing if the circumferential actin foci are localized in regions of high contractility by staining for phospho-myosin. Irregular adhesions (Figure 37B) colocalized with actin foci (Figure 37A) but did not show any colocalization of phospho-myosin.

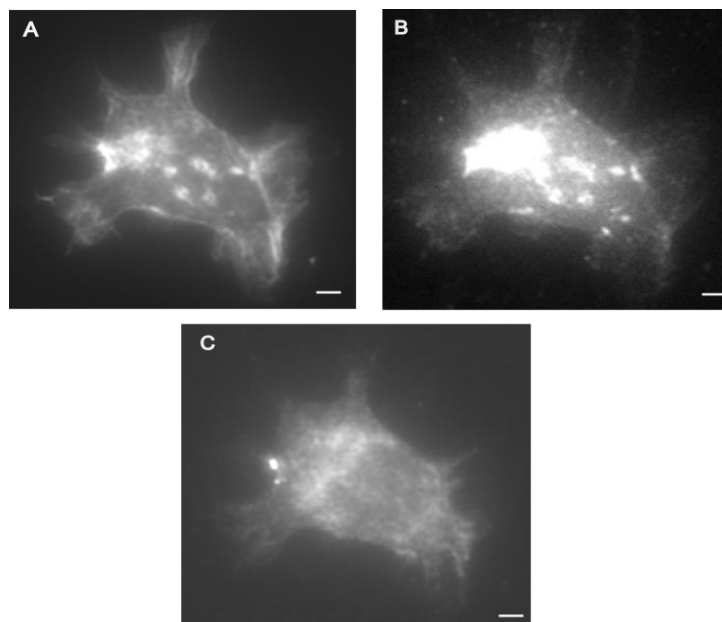


Figure 37: Circumferential actin foci does not colocalize with phospho-myosin. (A-C) representative immunofluorescence images of C2BBe cells on 2.4 kPa E-cadherin substrate stained for (A) phalloidin (marking actin cytoskeleton) and (B) β -catenin (marking E-cadherin adhesions), and (C) phospho-myosin. All scale bars are 5 μ m.

4.3.6 Organization of F-actin in cells on E-cadherin coated cell-like substrates

We hypothesized that at circumferential actin foci, the localization of E-cadherin adhesion is supported by high local actin density. To test this hypothesis, we used jasplakinolide, which is an inducer of polymerization and stabilization of actin cytoskeleton. Jasplakinolide was used at 1 nM for 1 hour to treat C2BBe cells on E-cadherin-coated soft silicone. Note that we observed that treating cells with jasplakinolide over several hours lead to detaching of cells from the substrate over time. However, when C2BBe cells were treated with jasplakinolide for 1 hour, we observed that cells stayed adhered and spread and some cells displayed large actin foci as expected.

Large actin foci supported irregular E-cadherin adhesions on substrate in the range of few-kPa (Figure 38). All these results suggest that local high density of actin was the main reason behind the formation of irregular E-cadherin adhesions.

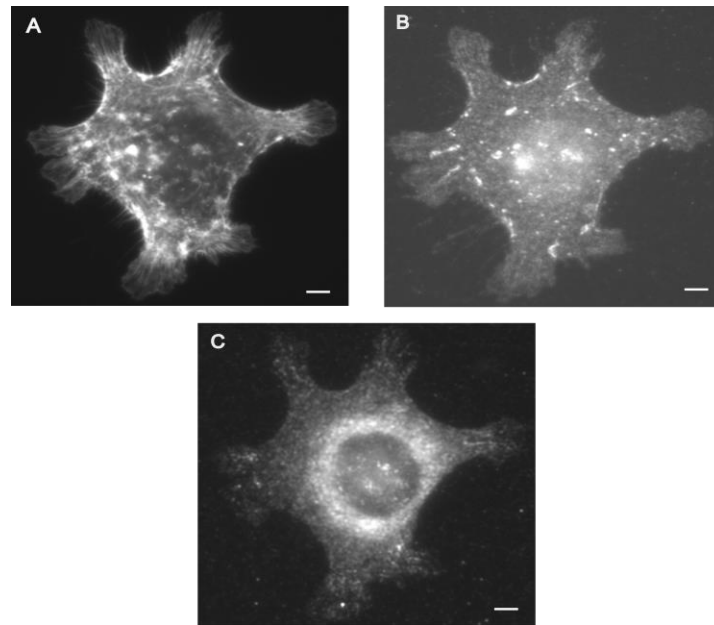


Figure 38: High local actin density supports irregular E-cadherin adhesions on soft substrates. (A-C) representative immunofluorescence images of C2BBE cells on 2.4 kPa E-cadherin substrate treated with Jasplakinolide and stained for (A) phalloidin (marking actin cytoskeleton) and (B) β -catenin (marking E-cadherin adhesions), and (C) paxillin. All scale bars are 5 μ m.

4.3.7 Effect of myosin inhibition on E-cadherin adhesions in cells on E-cadherin coated cell-like substrates

When we treated the cells with the myosin inhibitor blebbistatin (20 μ M), we noticed that cells did not abolish irregular E-cadherin adhesions associated with circumferential actin foci. This

supports the hypothesis that the high density of local actin (rather than contractility) is the main driver behind the localization of irregular E-cadherin adhesions. However, after blebbistatin treatment, linear adhesions were no longer supported (Figure 39).

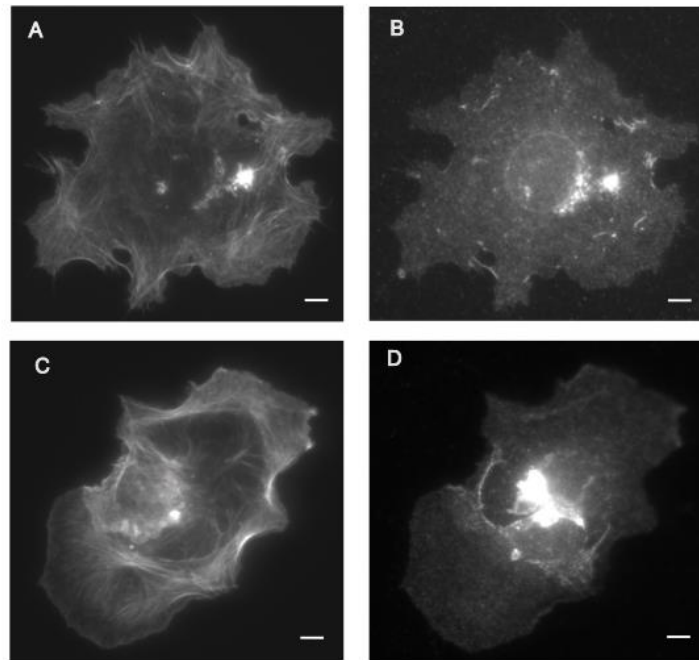


Figure 39: Blebbistatin treatment does not eliminate E-cadherin irregular adhesions but leads to loss of linear adhesions. (A-D) representative immunofluorescence images of C2BBe cells on 2.4 kPa E-cadherin substrate treated with blebbistatin and stained for (A, C) phalloidin (marking actin cytoskeleton) and (B, D) β -catenin (marking E-cadherin adhesions). All scale bars are 5 μ m.

4.3.8 Effect of formin inhibition on the actin organization of cells on E-cadherin coated cell-like substrates

With respect to linear actin adhesions, the linear architecture of the associated contractile actin bundle was apparently significant. We hypothesized that nucleators of linear actin filaments [147], formins, can therefore be important. Therefore, we treated C2BBe cells with a pan-formin

inhibitor [148], SMIFH2 (20 μ M), and we observed that SMIFH2 suppressed the presence of linear E-cadherin adhesions and radial orientation of linear actin structures as well (Figure 40).

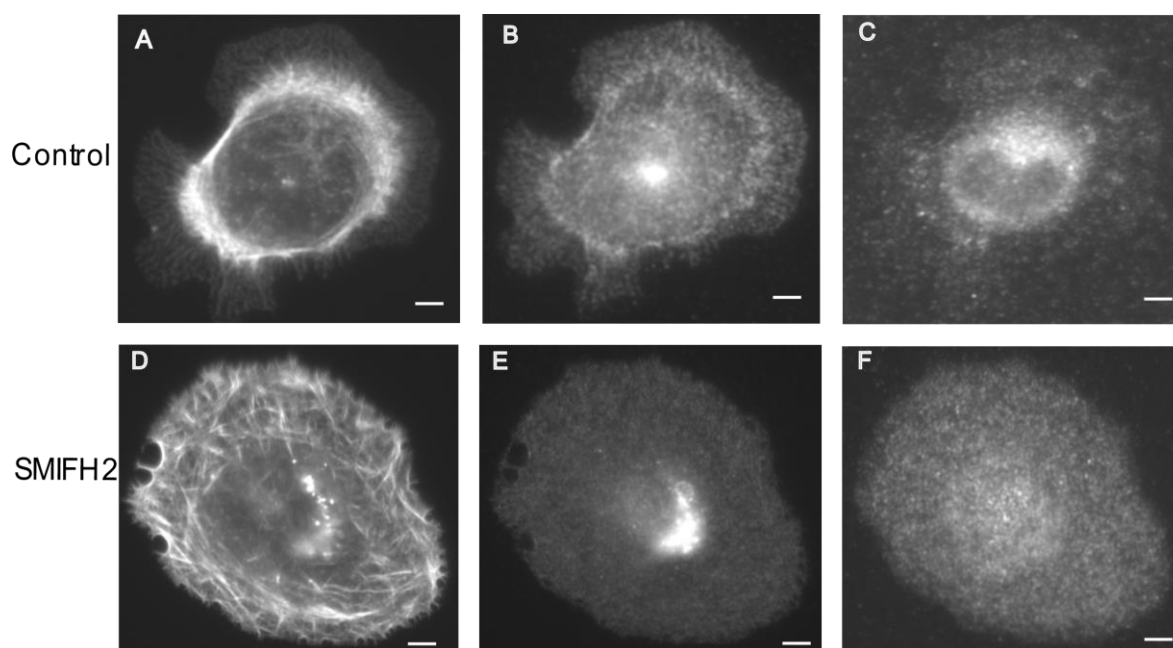


Figure 40: Formin activity is crucial for the formation of linear E-cadherin adhesions associated with the ends of radial orientation of F-actin structures on cell-like soft E-cadherin substrates. (A-F) representative immunofluorescence images of C2BBe cells on 2.4 kPa E-cadherin substrate treated with DMSO (A, B, C) and SMIFH2 (D, E, F) and stained for (A, D) phalloidin (marking actin cytoskeleton) and (B, E) β -catenin (marking E-cadherin adhesions), and (C, F) paxillin. All scale bars are 5 μ m.

The similar results were observed when C2BBe cells were treated with SMIFH2 on E-cadherin substrates in the range of sub-kPa stiffness (Figure 41). This result is consistent with the

fact that formins have been shown to maintain E-cadherin at cell-cell contacts [149]. It is important to note that we used a low concentration of SMIFH2 because it has been shown to have pleiotropic effects [150] at high concentrations.

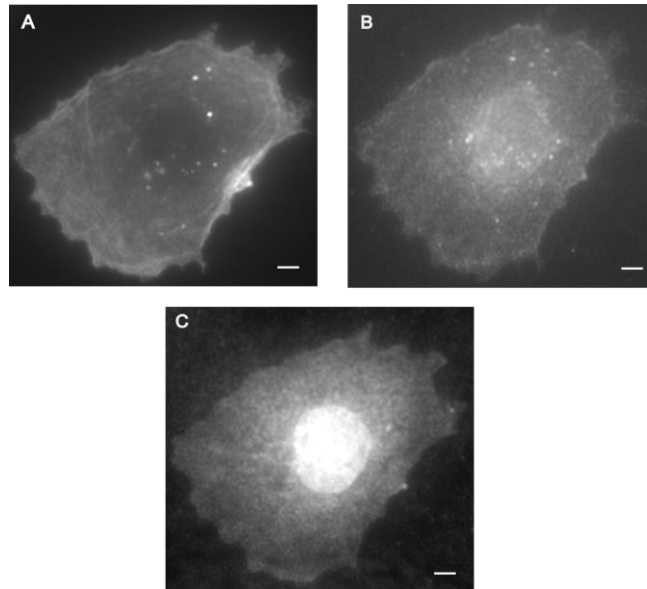


Figure 41: Formin activity is crucial for the formation of linear E-cadherin adhesions on sub-kPa substrates. (A-C) representative immunofluorescence images of C2BBE cells on 0.3 kPa E-cadherin substrate treated with SMIFH2 and stained for (A) phalloidin (marking actin cytoskeleton) and (B) β -catenin (marking E-cadherin adhesions), and (C) paxillin. All scale bars are 5 μ m.

4.3.9 Effect of Arp2/3 inhibition on the actin organization in cells on E-cadherin coated cell-like substrates

Arp2/3 is also a major actin nucleator that is responsible for the nucleation of actin branches[151]. Therefore, we used CK-666, a pharmacological inhibitor of Arp2/3, in order to test the role of this actin nucleator in the formation of E-cadherin adhesions and actin structures.

C2BBe cells plated on E-cad-coated soft substrates were incubated with CK-666 (100 μ M) for 2 hours. We found that actin and E-cadherin organization were not affected by the inhibition of Arp2/3 (Figure 42). C2BBe cells displayed linear adhesions colocalized with radial actin structures as in the control case.

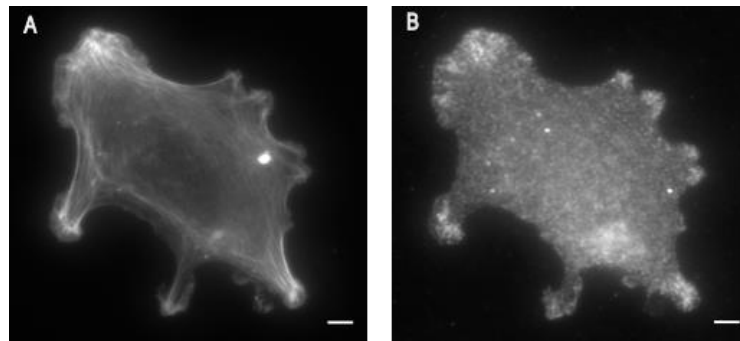


Figure 42: E-cadherin adhesions on cell-like substrates are independent of Arp2/3 actin nucleator. (A-B) Representative immunofluorescence images of C2BBe cells on 2.4 kPa E-cadherin substrate treated with CK-666 and stained for (A) phalloidin (marking actin cytoskeleton) and (B) β -catenin (marking E-cadherin adhesions). All scale bars are 5 μ m.

In addition, we found that a small fraction of C2BBe cells formed irregular adhesions clumps with the corresponding regions of high actin clumps on oriented E-cadherin-Fc coated on 2.4 kPa substrate (Figure 43).

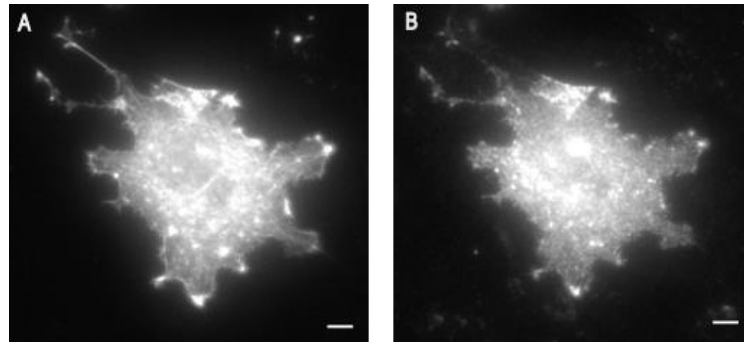


Figure 43: E-cadherin adhesions are localized with actin clumps even under arp2/3 inhibition. (A-B) representative immunofluorescence images of C2BBe cells on 8.7 kPa E-cadherin substrate treated with CK-666 and stained for (A) phalloidin (marking actin cytoskeleton) and (B) β -catenin (marking E-cadherin adhesions). All scale bars are 5 μ m.

4.3.10 Effect of Rho-activation on cells plated on E-cadherin-coated soft substrate

In order to study the effects of Rho activator II activation on the rearrangement of the actin cytoskeleton, we treated the cells with Rho activator (5 μ g/mL). We noticed that the regions of high actin intensity have smaller irregular β -catenin adhesions and some linear β -catenin adhesions (Figure 44).

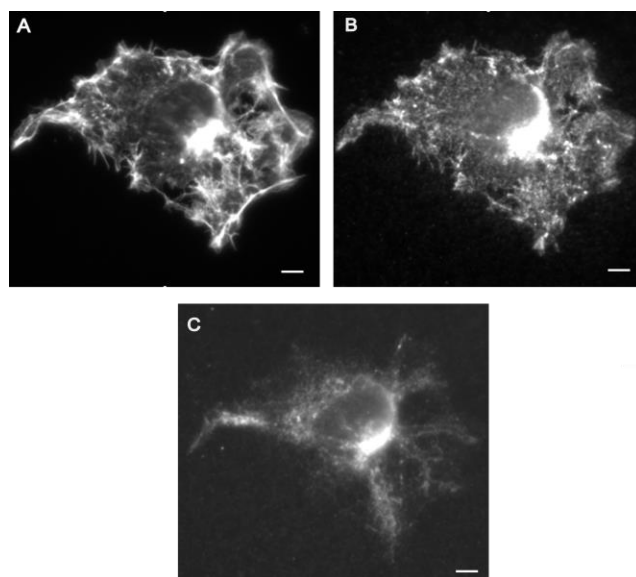


Figure 44: Rho activator promotes the formation of smaller irregular E-cadherin adhesions at regions of high actin density. (A-C) representative immunofluorescence images of C2BBe cells on 2.4 kPa E-cadherin substrate treated with Rho activator and stained for (A) phalloidin (marking actin cytoskeleton) and (B) β -catenin (marking E-cadherin adhesions), and (C) paxillin. All scale bars are 5 μ m.

4.3.11 Soft silicones as possible candidates for E-cadherin coated substrates – Rheology

We were interested in identifying alternative soft silicone substrates whose elasticity could be more broadly tuned. We therefore wondered if could potentially fabricate suitable soft silicone substrates by mixing NuSil gel with a small percentage by weight of Sylgard 184 cross-linking agent, as was done by another group recently [152]. We tried to come up with gel compositions that could be used as E-cadherin substrates going forward. Our aim is to make soft silicones that have a tunable elasticity over a physiological range. We used rheology to characterize the elastic and viscous responses of these soft silicones. G' measures the energy stored by a material during

deformation, while G'' measures the energy lost during the same shear cycle. Storage modulus, $G'(\omega)$, characterizes the elastic behavior of the material at a specific frequency (ω). Loss modulus, $G''(\omega)$, characterizes the material's viscous behavior in response to stress at a particular frequency (ω). The stress response, σ , (in response to an imposed sinusoidal strain) as a function of time t is given by the following equation:

$$\text{For a viscoelastic material: } \sigma(t) = G'(\omega) \gamma_0 \sin(\omega t) + G''(\omega) \gamma_0 \cos(\omega t)$$

where $\gamma(t)$ is sinusoidal strain with amplitude γ_0 . G' and G'' are determined as a function of angular frequency ω , in order to determine how the material behaves. Mixture of NuSil (weigh ratio A:B=1:1) with 0%, 0.15%, 0.5%, 1%, and 2.5% Sylgard 184 respectively were cured in an oven at 100°C for 2.5 hours. Then, the soft gel mixture of roughly mm thickness was loaded on to the rheometer plate. Frequency sweep test was used in order to determine the mechanical properties of the soft silicones. Storage modulus, G' , and loss modulus, G'' , were measured using shear rheology. Strain was set at 0.5% [152] and the range of angular frequencies was chosen to be between 0.1 and 100 rad/s. Then, we calculated the elastic modulus, E , by assuming that the soft silicones used are isotropic and incompressible, (i.e., with a Poisson's ratio, ν , of 0.5) and using the following relation: $E = 2G'(1+\nu)$.

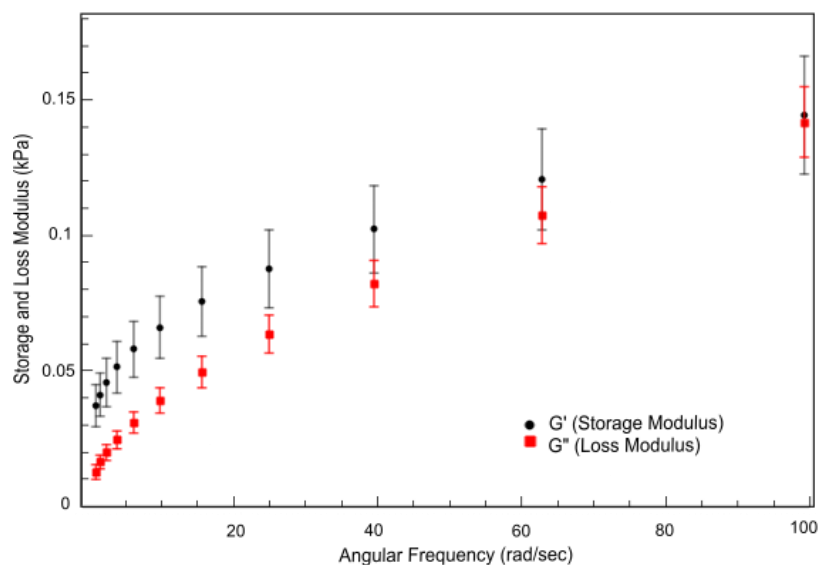


Figure 45: Mechanical properties of NuSil 1.1 with 0% Sylgard 184 with frequency sweep test at 0.5 % strain. Storage modulus, G' , and loss modulus, G'' , in kPa versus angular frequency, ω , in rad/sec. All data points are mean \pm SD.

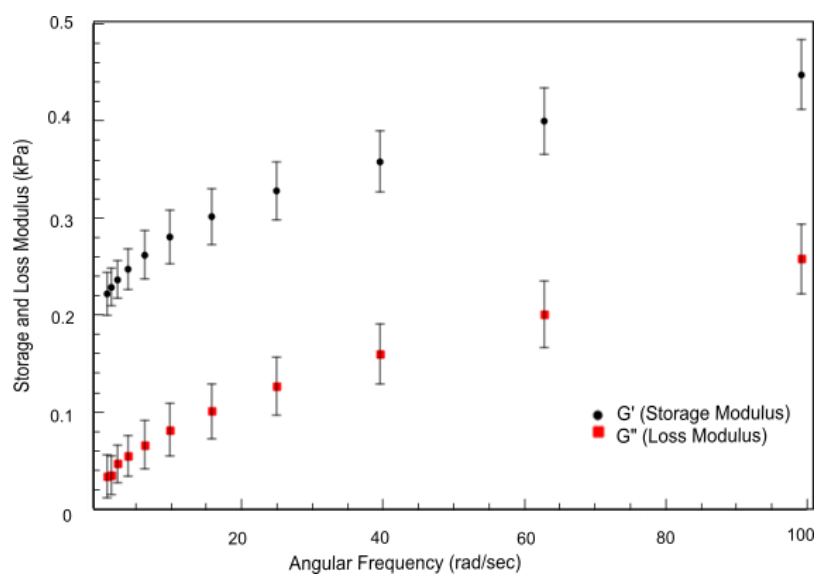


Figure 46: Mechanical properties of NuSil 1.1 with 0.15% Sylgard 184 with frequency sweep test at 0.5 % strain. Storage modulus, G' , and loss modulus, G'' , in kPa versus angular frequency, ω , in rad/sec. All data points are mean \pm SD.

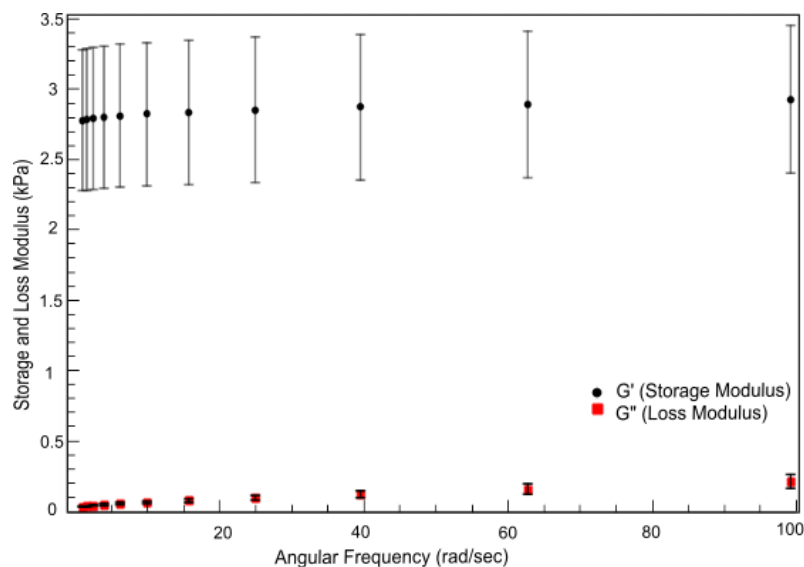


Figure 47: Mechanical properties of NuSil 1.1 with 0.5% Sylgard 184 with frequency sweep test at 0.5 % strain. Storage modulus, G' , and loss modulus, G'' , in kPa versus angular frequency, ω , in rad/sec. All data points are mean \pm SD.

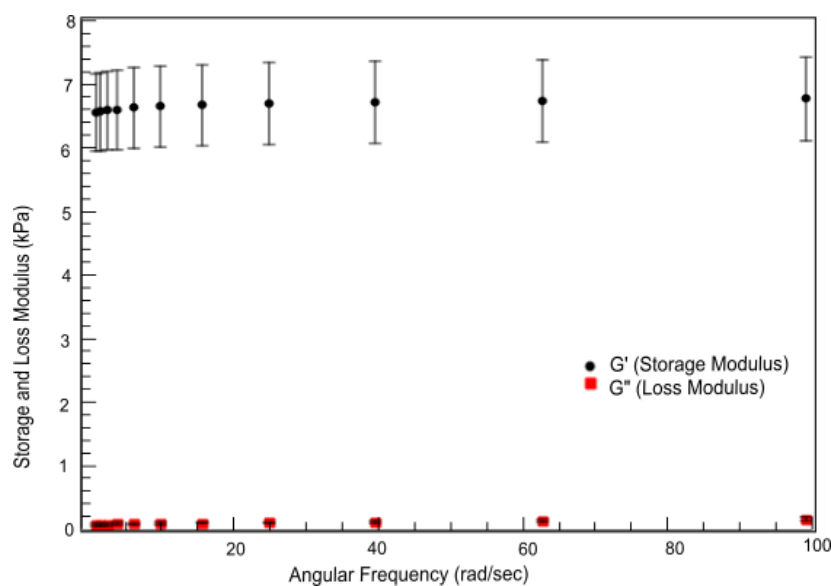


Figure 48: Mechanical properties of NuSil 1.1 with 1% Sylgard 184 with frequency sweep test at 0.5 % strain. Storage modulus, G' , and loss modulus, G'' , in kPa versus angular frequency, ω , in rad/sec. All data points are mean \pm SD.

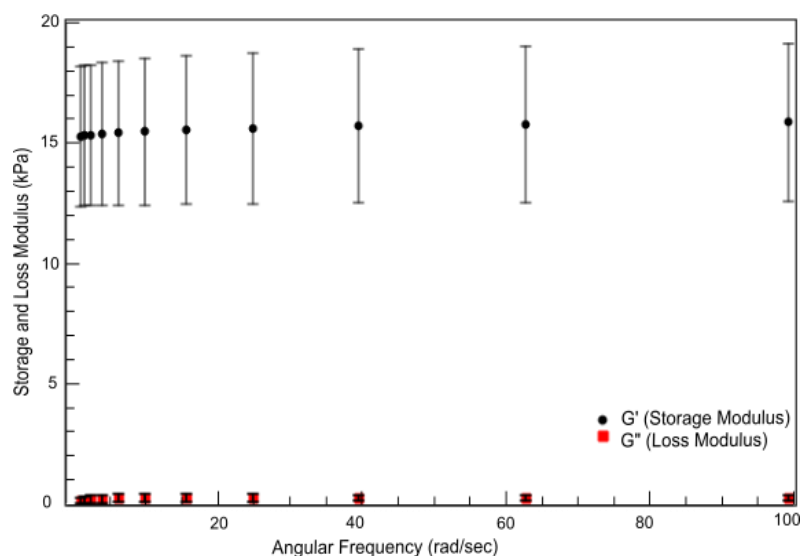


Figure 49: Mechanical properties of NuSil 1.1 with 2.5% Sylgard 184 with frequency sweep test at 0.5 % strain. Storage modulus, G' , and loss modulus, G'' , in kPa versus angular frequency, ω , in rad/sec. All data points are mean \pm SD.

Silicone mixtures	G' : Storage modulus (kPa) (mean = \pm SD)	E: Elastic modulus (kPa) (mean = \pm SD)
NuSil (A: B = 1:1) with 0% Sylgard 184	0.075 \pm 0.013	0.225 \pm 0.039
NuSil (A: B = 1:1) with 0.15% Sylgard 184	0.300 \pm 0.027	0.900 \pm 0.081
NuSil (A: B = 1:1) with 0.5% Sylgard 184	2.830 \pm 0.511	8.490 \pm 1.533
NuSil (A: B = 1:1) with 1% Sylgard 184	6.644 \pm 0.632	19.932 \pm 1.896
NuSil (A: B = 1:1) with 2.5% Sylgard 184	15.484 \pm 3.064	46.452 \pm 9.192

Table 1: Mechanical properties of NuSil soft silicones with 0%, 0.15%, 0.5%, 1%, and 2.5% Sylgard 184. A table of storage modulus, G' , with mean \pm standard deviation and elastic modulus, E, in kPa.

We wanted a substrate with an elastic modulus close to the one we got in NuSil 1:1 with 0.5% Sylgard 184 composition. Therefore, we picked NuSil 1:1 with 0.55% Sylgard 184 and we also changed the curing time to 3 hours instead of 2.5 hours. Based on the obtained stiffness values, we considered NuSil 1:1 with 0.55 Sylgard 184 ($E=6.603$ kPa) as biomimetic substrate for studying force transmission using A431 cells.

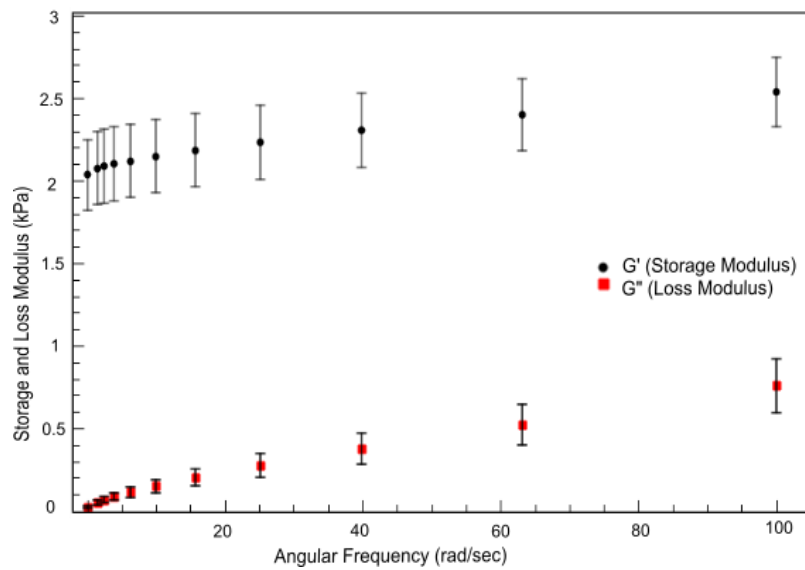


Figure 50: Mechanical properties of NuSil 1.1 with 0.55% Sylgard 184 with frequency sweep test at 0.5 % strain. Storage modulus, G' , and loss modulus, G'' , in kPa versus angular frequency, ω , in rad/sec. All data points are mean \pm SD.

4.3.12 E-cadherin force transmission regulation at the cell membrane and from outside the cell

While we showed that E-cadherin mechanosensors sense epithelial cell-like stiffness, previous studies showed that E-cadherins are also mechanotransduction loci that sense mechanical forces at intercellular junctions [153]. Therefore, we tried to investigate the level of intercellular

forces transmitted through E-cadherin at cell-cell contacts. Previous reports showed that Epithelial Growth Factor Receptor (EGFR) is a crucial factor in the E-cadherin force transduction machinery [43]. Cell-cell adhesions are mediated by the extracellular domains of E-cadherin. The intracellular domain of E-cadherin is mechanically coupled to the actin cytoskeleton through intracellular adaptor proteins such as α -catenin and β -catenin. Under tension at cell junctions, α -catenin unfolds and leads to the recruitment of vinculin in order to reinforce cell junctions. Force fluctuations on E-cadherin result in activating EGFR signaling and integrins in order to form a positive-feedback loop that triggers the activation of Abl, which is necessary for the recruitment of vinculin and actin at stressed E-cadherin junctions [43]. This mechanosensitive pathway connects E-cadherin tugging forces to the activation of EGFR. In addition, previous reports showed that E-cadherin and EGFR form a heterotrimeric complex at the plasma membrane, consisting of a bond between two E-cadherin proteins and one EGFR monomer [130]. Increased junctional tension on homophilic cadherin bonds disrupts E-cadherin/EGFR complex [130]. Tugging forces on homophilic E-cadherin bonds, release EGFR monomers to dimerize, then bind EGF ligand, and signal [130]. These findings show the initial steps in E-cadherin-mediated force transduction which link fluctuations of intercellular force to the activation of signaling cascades. Therefore, we asked if EGFR activity affects the level of endogenous forces transmitted at cell-cell contacts. We first measured the intercellular forces of A431 cells expressing endogenous E-cadherin and high levels of EGFR. Then, we inhibited EGFR in A431 cells to test if perturbations of EGFR potentially affect intercellular forces at cell-cell contacts. A431 cells were plated on Nusil 1:1 with 0.55 Sylgard 184 collagen-I substrate in low serum (0.5 %) with or without 100ng/ml EGFR inhibitor for 30 minutes. Using the traction force imbalance method (TFIM), we found that the average intercellular force of A431 cells is 47.2 ± 20.1 nN and the average intercellular force of A431 cells

treated with EGFR inhibitor is 21.7 ± 10.3 nN (P value= 2×10^{-7}) (Figure 51). These results revealed that EGFR activity affects the level of intercellular forces, presumably by interfering with endogenous mechanotransduction mechanisms.

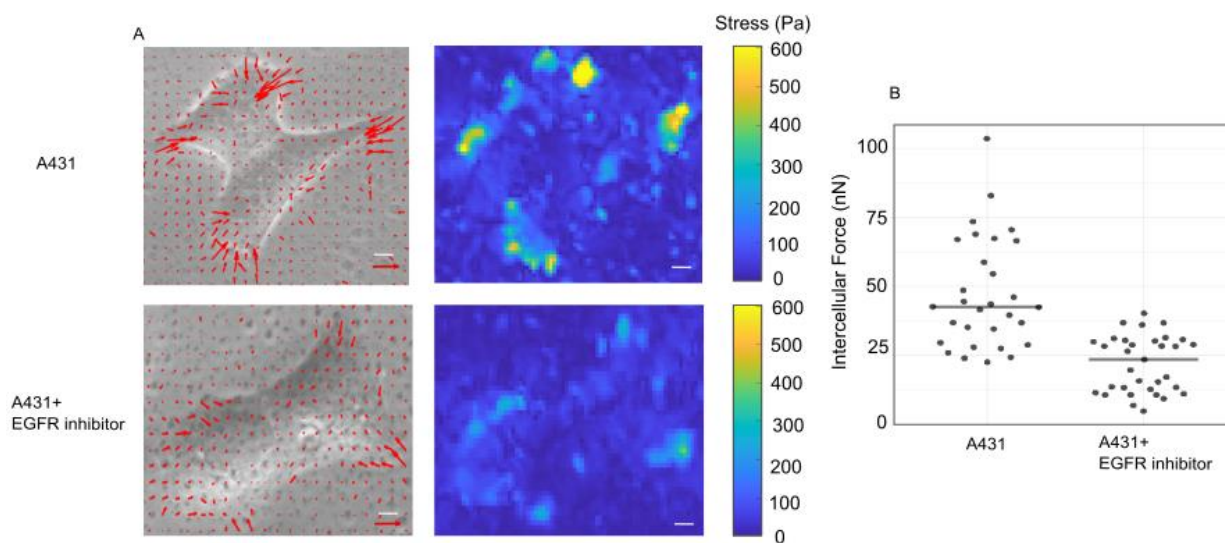


Figure 51: Inhibition of EGFR leads to a decrease in inter-cellular forces. (A) Traction stresses of A431 cell pair (top, left) and A431 cell pair treated with EGFR inhibitor (bottom, left). Traction stress vectors are overlaid (red arrows.). Heat-scale map of the traction magnitude for A431 cell pair (top, right) and A431 cell pair treated with EGFR inhibitor (bottom, right). Scale bar is 5 μ m. Red arrow: 400 Pa. (B) Dot plot of the intercellular forces for A431 cell pair and A431 cell pair treated with EGFR inhibitor cell pairs. Black bar represents the mean value. ($P = 2 \times 10^{-7}$).

While we showed that force transmission is disrupted when inhibiting EGFR bond to E-cadherin at the plasma membrane, what molecule E-cadherin binds to from outside the cell may also influence how much force is transmitted. Previous reports have considered force transmission

at cell-cell contacts mediated by a heterophilic adhesion between E-cadherin and N-cadherin [44]. Studying heterophilic interactions between cadherins is very important for cancer progression and metastasis in which cancer cells interact with their microenvironment [154,155,156]. Several studies have shown heterophilic junctions between two distinct cadherin pairs [157,158,159,160,161,162], and recent structural and energetic analysis demonstrated that heterophilic interaction between E-cadherin/N-cadherin has higher binding affinity compared to homophilic E-cadherin/E-cadherin interaction [131]. Previous reports showed that force transmission is mediated by heterophilic interactions between E-cadherin at the A431 cancer cell membrane and N-cadherin at the Cancer Associated Fibroblast (CAF) membrane [44]. Junctions between E-cadherin from cancer cells and N-cadherin from CAF enable collective cell migration for several hours [44]. While force transmission between heterophilic cadherins in cancer epithelial cells and fibroblasts is well established, the relative force transmission between cadherins in homophilic and heterophilic configurations (E-cadherin/E-cadherin, N-cadherin/N-cadherin, and E-cadherin/N-cadherin) in epithelial cells is not well studied. Therefore, we used human A431D epithelial cells that do not express E-cadherin and we measured the intercellular force between A431D cell pairs transfected with E-cadherin, A431D cell pairs transfected with N-cadherin and heterophilic A431D cells pairs consisting of a heterophilic interaction between A431D cells transfected with E-cadherin and A431D cells transfected with N-cadherin by mixing the former and the later together. Note that all the cells were cultured with 400 $\mu\text{g/mL}$ G418 (Geneticin) so that they continue to express the cadherins. A431D cells transfected with E-cadherin express E-cadherin tagged with Yellow Fluorescence Protein (YFP) could be seen in the green channel using our epifluorescence microscope. To check heterophilic A31D cell pairs, we could therefore check for one YFP tagged cell in the green channel. Using the traction force imbalance method (TFIM),

we found that the average intercellular force of A431D cells transfected with N-cadherin is $28.77 \text{ nN} \pm 15.26$, the average intercellular force of A431 cells transfected with E-cadherin is $21.45 \text{ nN} \pm 12.13$, the average intercellular force of heterophilic A431D cell pairs is $40.3 \text{ nN} \pm 21.05$ (Figure 52). Therefore, the intercellular tension for heterophilic E-cad/N-cad interaction is higher than the homophilic E-cad/E-cad interaction. This has important implications for cancer progression, which often involves epithelial to mesenchymal transition and E-cad to N-cad switch in epithelial cells.

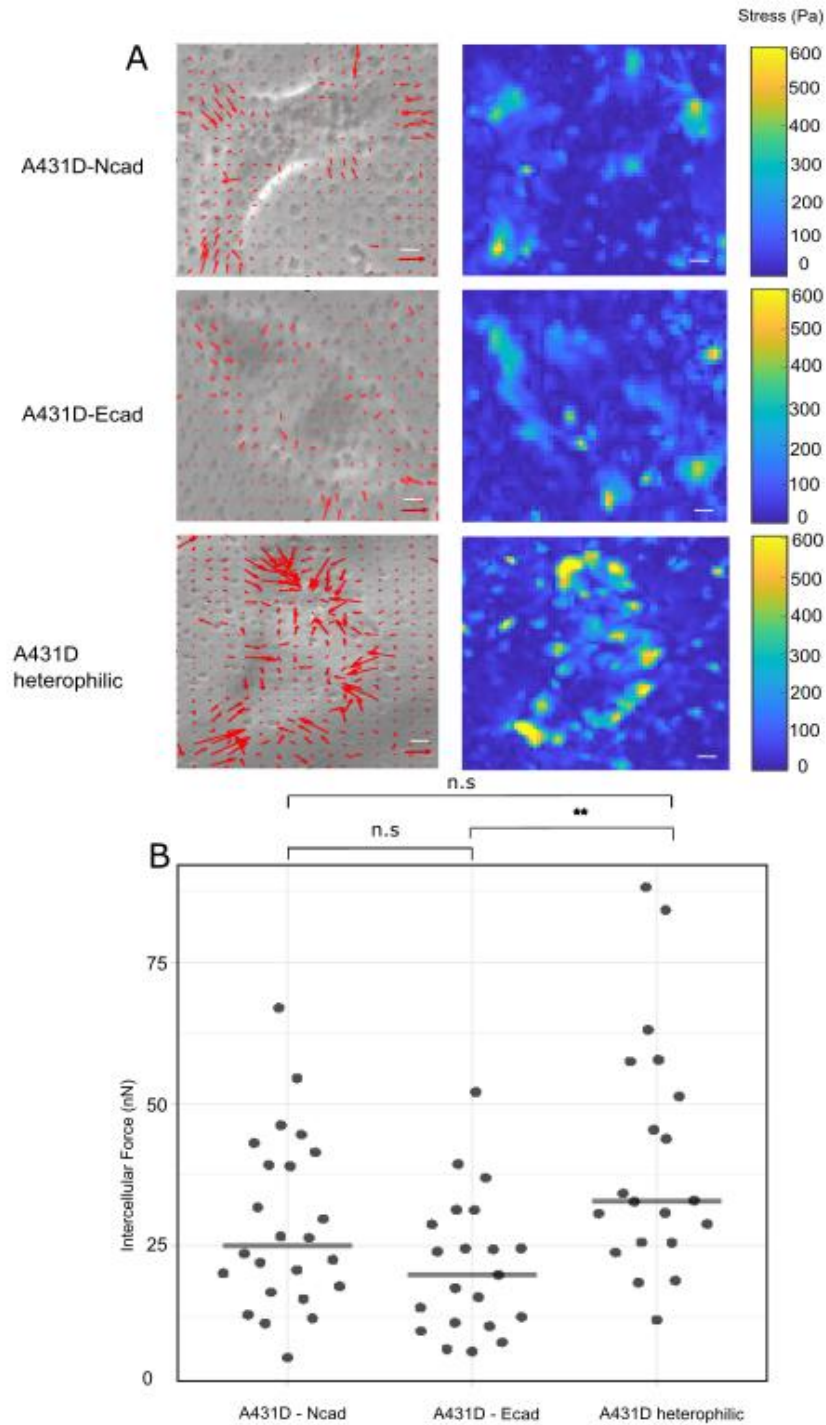


Figure 52: Heterophilic interaction between A431D cells leads to higher inter-cellular forces compared to homophilic interactions between A431D cells. (A) Traction stresses of A431D cell pair transfected with N-cadherin (top, left), A431D cell pair transfected with E-cadherin (middle,

left), and A431D heterogeneous (bottom, left). Traction stress vectors are overlaid (red arrows.). Heat-scale map of the traction magnitude for A431 cell pair transfected with N-cadherin (top, right), A431D cell pair transfected with E-cadherin (middle, right), and A431D heterophilic cell pair (bottom, right). Scale bar is 5 μm . Red arrow: 400 Pa. (B) Dot plot of the intercellular forces for A431D cell pair transfected with N-cadherin, A431D cell pair transfected with E-cadherin, and A431D heterophilic. Black bar represents the mean value. (** corresponds to $p < 0.01$).

4.4 Conclusion

E-cadherin adhesions are very important for cell-cell adhesion as well as mechanical coupling between epithelial cells. E-cadherin adhesions also reside in a microenvironment that is comprised of adjacent epithelial cells. E-cadherin is known to be a mechanosensor, however, it is unknown if E-cadherin adhesions may sense stiffness within the same range of that of epithelial cells. Based on literature, Young's moduli of epithelial cells are in the range of sub-kPa to few-kPa, with cancer cells often being softer than benign/normal cells. We found that E-cadherin adhesions change their organization depending on the magnitude of epithelial cell-like elasticity. E-cadherin adhesions are organized by the actin cytoskeleton in two ways: linear shaped adhesions at the end of linear actin bundles and irregular shaped adhesions colocalized with high actin density. Linear adhesions associated radial actin orientation were more numerous on the higher elasticity substrate with an elasticity of few kPa (compared to sub kPa substrate). Our study suggests that the distribution (density and architecture) of E-cadherin adhesions is modulated by epithelial cell-like elasticity and this has important consequences for several diseases such as carcinomas characterized by altered elasticity of epithelial cells.

In this chapter, we devised biomimetic E-cadherin-coated soft silicone substrates with epithelial cell-like elasticities (sub kPa to few kPa) and showed that discrete E-cadherin adhesions are clearly observed on cell-like silicone soft substrates (unlike previous reports that did not observe well-formed adhesions) [129]. It will be interesting to study the effect of microenvironment elasticity on several cellular factors like actin binding proteins and Rho GTPases and their influence on E-cadherin adhesion organization. The necessity of formin for the proper formation of linear E-cadherin adhesions as well as the enhanced formation of linear adhesions at higher stiffness both point to the possibility that RhoA is activated at E-cadherin adhesions in response to increase in stiffness of the cells [163,164]. E-cadherin sensing of epithelial cell-like stiffness can have consequences in different physiological contexts in which the stiffness of an epithelial cell changes, such as wound healing [115]. In addition, softening of cells during cancer metastasis can decrease cell-cell contact stability and the level of E-cadherin adhesion. In our research study, we also showed that E-cadherin adhesions are supported by actin cytoskeleton in two ways: linear architecture and local high density on both sub-kPa and few-kPa soft substrates. Based on this, we propose that the apical circumferential belt of actin cytoskeleton employs both its linear architecture and high local density in order to support E-cadherin adhesions at cell-cell junctions.

Furthermore, E-cadherin mechanosensors not only sense epithelial-like stiffness but also sense and transmit forces at intercellular junctions. E-cadherin and EGFR form a heterotrimeric complex at the plasma membrane [130]. While previous studies showed that EGFR is involved in force transduction mechanism at interepithelial junctions, we showed that inhibiting EGFR leads to a decrease in intercellular forces between neighboring cells. This suggests a feedback loop between E-cadherin mechanotransduction and EGFR activity. Moreover, it has been reported that

force transmission is mediated by heterophilic adhesion between E-cadherin in cancer cells and N-cadherin in CAFs [44] In this study, we showed that heterophilic interactions in epithelial cells between E-cadherin and N-cadherin result in a higher intercellular force compared to E-cad/E-cad homophilic interaction. E-cadherin adhesions play an important role in organizing cell-cell junctions, coupling adjacent cell cortices, influencing a variety of signaling pathways, and maintaining cell polarity. Based on our results, we suggest that E-cadherin sensing of epithelial like stiffness can be a crucial factor in the function of E-cadherin. The role of EGFR at the plasma membrane and E-cad or N-cad from the neighboring cell all determine the level of force transmitted through E-cadherin. We posit that this enables the cell to sense, respond and give rise to unique biochemical signal combinations in different contexts.

CHAPTER 5

CONCLUSION

In epithelial tissues, cells adhere to each other through cell-cell junctions or to the extracellular matrix (ECM). In addition, cells generate and exert forces on each other or on the extracellular matrix. At cell-cell contacts, cells sense and respond to forces through E-cadherin. Cells also convert mechanical forces into biochemical signals which elicit particular cellular responses. Internal forces are generated by the actomyosin network that regulates force transmission. External forces are transmitted through intracellular and intercellular adhesion proteins. At cell-cell contacts, forces are transmitted through E-cadherin proteins that bind to intracellular proteins which in turn interact with the actin cytoskeleton inside the cell. Therefore, it is very important to study E-cadherin mechanobiology and quantify the level of force transmission through E-cadherin in order to understand the mechanical function of cell-cell contacts in various contexts.

Stiffness sensing and force transmission are two pivotal aspects of E-cadherin mechanobiology. In order to study the stiffness sensing aspect of E-cadherin, we assessed the formation of E-cadherin adhesion on substrates with epithelial cell-like stiffness. We also investigated how these E-cadherin adhesions are supported by the actin cytoskeleton inside the cell on such substrates (chapter 4). E-cadherin has an extracellular region, a transmembrane region and an intracellular region. Here, we assessed factors that can affect the level of force transmission (i) inside the cell, (ii) on the cell membrane, and (iii) outside the cell. To study the level of force transmission inside the cell, we studied the role of vinculin and α -catenin in transmitting endogenous forces at cell-cell contacts (Chapter 2). To study how the level of force transmission

is affected by factors on the cell membrane, we investigated the effect of EGFR on the intercellular forces transmitted at cell-cell contacts (chapter 4). In order to understand how the level of force transmission depends on binding partners from outside the cell, we studied homophilic and heterophilic interactions of cadherins (chapter 4). For quantifying the level of force transmission at cell-cell contacts, we used traction force microscopy (TFM) to determine how EGFR, homophilic E-cadherin interactions, heterophilic E-cadherin interactions, and intracellular adhesion-associated proteins affect the intercellular forces between neighboring cells. In addition, we also devised a modified traction force microscopy method using a novel, simple strategy for coincident immunofluorescence and traction force microscopy (chapter 3).

As detailed in chapter 4, we designed a biomimetic E-cadherin soft substrate of cell-like stiffness and we tested whether E-cadherin senses the elastic microenvironment that mimics the epithelial cells that encircle them. We showed that E-cadherin adhesions change their organization depending on epithelial cell-like elasticity. Linear E-cadherin adhesions associated with radial actin orientation were more common on the higher elasticity substrate (sub kPa). Irregular E-cadherin adhesions associated with actin foci along circumferential structures of F-actin were more common on the lower elasticity substrate (few kPa). To enable better understanding of force sensing by E-cadherin, we addressed the question of what factors determine the level of force transmission through E-cadherin adhesions at cell-cell contacts. We started by inhibiting EGFR and we showed that the intercellular forces transmitted at cell-cell contacts was decreased by the inhibition of EGFR. Thus, EGFR affects not only mechanotransduction via E-cadherin, as shown before, but also the level of force transmission via E-cadherin at cell-cell contacts. We then addressed how E-cadherin's extra-cellular binding partners affect force transmission by quantifying the level of force transmission for homophilic and heterophilic interactions at cell-cell

contacts. Our results revealed that the intercellular tension for heterophilic interactions between E-cadherin and N-cadherin in epithelial cells is higher than homophilic E-cadherin/E-cadherin interaction. In the future, it will be important and interesting to fabricate a biomimetic N-cadherin soft substrate and study the stiffness sensing of neural cells, and to quantify the traction forces of E-cadherin homophilic and heterophilic interactions on N-cadherin soft substrates.

The level of force transmission is also affected by intracellular adhesion-associated proteins. In chapter 2, we showed that knock out of vinculin or both vinculin and α -catenin can significantly decrease the intercellular forces. To study the effect of vinculin binding to α -catenin at intercellular junctions, we examined cells with α -catenin knocked out and expressing α -catenin mutants. The intercellular force in the absence of α -catenin and with α -catenin- Δ VBS were not significantly lesser than the intercellular force for wild-type. Thus, we found that vinculin, and not α -catenin, is responsible for transmitting high endogenous forces at cell-cell contacts. Our result is contrary to the prevailing “textbook picture”, where α -catenin is thought to be more central for force transmission at E-cadherin adhesions. We further showed that vinculin also protects the integrity of cell-cell contacts under mechanical challenges. It will be interesting, to study how force transmission through E-cadherin at cell-cell contacts can be affected when perturbing other intracellular adhesion-associated proteins and determine which other mechanical pathways are important for force transmission through E-cadherin.

Force transmission is quantified using Traction Force Microscopy (TFM). However, the main limitation of this method is that it requires cell removal and substrate relaxation in which cells are removed from the substrate and no further post-processing procedures can be done. As described in chapter 3, we proposed and realized a simple strategy for coincident traction force microscopy and immunofluorescence. This method addressed the aforementioned main limitation

of traction force microscopy and we were able to quantify traction forces without removal of the cells and then obtain protein localization data from cells using immunofluorescence. In the future, it will be interesting to use this method to find the relationship between the localization of different intracellular proteins in cells and the measured traction forces.

Taken together, our studies highlight two main aspects of E-cadherin mechanobiology: stiffness sensing and force transmission at cell-cell contacts. Overall, we showed that vinculin, EGFR, and heterophilic cadherin interactions affect the endogenous force transmission in epithelial cells at cell-cell contacts. We also uncovered the factors that affect E-cadherin adhesion formation on cell-like elastic substrates. Finally, the alternate method we developed for TFM here can be adopted by other labs easily and lead to novel insights in mechanobiology. Our work can thus inform both fundamental and applied research, potentially leading to advances studies in developmental biology (for eg., understanding how inter-cellular forces effect cell shape changes) and tissue engineering (for eg., help in the improved design of artificial skin grafts).

REFERENCES

1. Fenderson BA. MOLECULAR BIOLOGY OF THE CELL, 5TH EDITION. Shock 2008; 30: 100.
2. Khalili A, Ahmad M. A Review of Cell Adhesion Studies for Biomedical and Biological Applications. Int J Mol Sci 2015; 16: 18149–18184.
3. Gumbiner BM. Cell Adhesion: The Molecular Basis of Tissue Architecture and Morphogenesis. Cell 1996; 84: 345–357.
4. de Pascalis C, Etienne-Manneville S. Single and collective cell migration: the mechanics of adhesions. Mol Biol Cell 2017; 28: 1833–1846.
5. Nardini JT, Chapnick DA, Liu X, Bortz DM. Modeling keratinocyte wound healing dynamics: Cell–cell adhesion promotes sustained collective migration. J Theor Biol 2016; 400: 103–117.
6. Dunehoo AL, Anderson M, Majumdar S, Kobayashi N, Berkland C, Siahaan TJ. Cell Adhesion Molecules for Targeted Drug Delivery. J Pharm Sci 2006; 95: 1856–1872.
7. Janiszewska M, Primi MC, Izard T. Cell adhesion in cancer: Beyond the migration of single cells. Journal of Biological Chemistry 2020; 295: 2495–2505.
8. Gao C, Peng S, Feng P, Shuai C. Bone biomaterials and interactions with stem cells. Bone Res 2017; 5: 17059.
9. Muller U, Brandli AW. Cell adhesion molecules and extracellular-matrix constituents in kidney development and disease. J Cell Sci 1999; 112: 3855–3867.
10. Nielsen H, Wennström. Cell adhesion molecules in Alzheimer’s disease. Degener Neurol Neuromuscul Dis 2012; 65.
11. Gumbiner BM. Regulation of cadherin-mediated adhesion in morphogenesis. Nat Rev Mol Cell Biol 2005; 6: 622–634.
12. Wu SK, Gomez GA, Michael M *et al.* Cortical F-actin stabilization generates apical–lateral patterns of junctional contractility that integrate cells into epithelia. Nat Cell Biol 2014; 16: 167–178.
13. Wu SK, Yap AS. Patterns in Space: Coordinating Adhesion and Actomyosin Contractility at E-cadherin Junctions. Cell Commun Adhes 2013; 20: 201–212.
14. Hynes RO. Integrins. Cell 2002; 110: 673–687.
15. Faull RJ, Ginsberg MH. Inside-out signaling through integrins. Journal of the American Society of Nephrology 1996; 7: 1091–1097.
16. Law DA, Nannizzi-Alaimo L, Phillips DR. Outside-in Integrin Signal Transduction. Journal of Biological Chemistry 1996; 271: 10811–10815.
17. Huttenlocher A, Horwitz AR. Integrins in Cell Migration. Cold Spring Harb Perspect Biol 2011; 3: a005074–a005074.

18. Has C, Spartà G, Kiritsi D *et al.* Integrin α_3 Mutations with Kidney, Lung, and Skin Disease. *New England Journal of Medicine* 2012; 366: 1508–1514.
19. Renkawitz J, Sixt M. Mechanisms of force generation and force transmission during interstitial leukocyte migration. *EMBO Rep* 2010; 11: 744–750.
20. Oakes PW, Banerjee S, Marchetti MC, Gardel ML. Geometry Regulates Traction Stresses in Adherent Cells. *Biophys J* 2014; 107: 825–833.
21. Eftekharijoo M, Palmer D, McCoy B, Maruthamuthu V. Fibrillar force generation by fibroblasts depends on formin. *Biochem Biophys Res Commun* 2019; 510: 72–77.
22. Wang X, Ha T. Defining Single Molecular Forces Required to Activate Integrin and Notch Signaling. *Science* (1979) 2013; 340: 991–994.
23. Chowdhury F, Li ITS, Leslie BJ *et al.* Single molecular force across single integrins dictates cell spreading. *Integrative Biology* 2015; 7: 1265–1271.
24. Charras G, Yap AS. Tensile Forces and Mechanotransduction at Cell–Cell Junctions. *Current Biology* 2018; 28: R445–R457.
25. DeMali KA, Sun X, Bui GA. Force Transmission at Cell–Cell and Cell–Matrix Adhesions. *Biochemistry* 2014; 53: 7706–7717.
26. Lecuit T, Lenne P-F, Munro E. Force Generation, Transmission, and Integration during Cell and Tissue Morphogenesis. *Annu Rev Cell Dev Biol* 2011; 27: 157–184.
27. Kechagia JZ, Ivaska J, Roca-Cusachs P. Integrins as biomechanical sensors of the microenvironment. *Nat Rev Mol Cell Biol* 2019; 20: 457–473.
28. Barry AK, Tabdili H, Muhamed I *et al.* α -Catenin cytom mechanics – role in cadherin-dependent adhesion and mechanotransduction. *J Cell Sci* 2014; 127: 1779–1791.
29. Valbuena A, Vera AM, Oroz J, Menéndez M, Carrión-Vázquez M. Mechanical Properties of β -Catenin Revealed by Single-Molecule Experiments. *Biophys J* 2012; 103: 1744–1752.
30. Avvisato CL, Yang X, Shah S *et al.* Mechanical force modulates global gene expression and β -catenin signaling in colon cancer cells. *J Cell Sci* 2007; 120: 2672–2682.
31. Ratheesh A, Gomez GA, Priya R *et al.* Centralspindlin and α -catenin regulate Rho signalling at the epithelial zonula adherens. *Nat Cell Biol* 2012; 14: 818–828.
32. Butler JP, Tolić-Nørrelykke IM, Fabry B, Fredberg JJ. Traction fields, moments, and strain energy that cells exert on their surroundings. *American Journal of Physiology-Cell Physiology* 2002; 282: C595–C605.
33. Maruthamuthu V, Sabass B, Schwarz US, Gardel ML. Cell-ECM traction force modulates endogenous tension at cell–cell contacts. *Proceedings of the National Academy of Sciences* 2011; 108: 4708–4713.
34. Kumar S, Weaver VM. Mechanics, malignancy, and metastasis: The force journey of a tumor cell. *Cancer and Metastasis Reviews* 2009; 28: 113–127.
35. Petrova YI, Schecterson L, Gumbiner BM. Roles for E-cadherin cell surface regulation in cancer. *Mol Biol Cell* 2016; 27: 3233–3244.

36. Alibert C, Goud B, Manneville J-B. Are cancer cells really softer than normal cells? *Biol Cell* 2017; 109: 167–189.
37. Buckley CD, Tan J, Anderson KL *et al.* The minimal cadherin-catenin complex binds to actin filaments under force. *Science* (1979) 2014; 346: 1254211–1254211.
38. Wang A, Dunn AR, Weis WI. Mechanism of the cadherin–catenin F-actin catch bond interaction. *Elife* 2022; 11.
39. Ishiyama N, Sarpal R, Wood MN *et al.* Force-dependent allostery of the α -catenin actin-binding domain controls adherens junction dynamics and functions. *Nat Commun* 2018; 9: 5121.
40. Mandai K, Nakanishi H, Satoh A *et al.* Afadin: A Novel Actin Filament–binding Protein with One PDZ Domain Localized at Cadherin-based Cell-to-Cell Adherens Junction. *Journal of Cell Biology* 1997; 139: 517–528.
41. Abe K, Takeichi M. EPLIN mediates linkage of the cadherin–catenin complex to F-actin and stabilizes the circumferential actin belt. *Proceedings of the National Academy of Sciences* 2008; 105: 13–19.
42. Kobiela A, Fuchs E. α -catenin: at the junction of intercellular adhesion and actin dynamics. *Nat Rev Mol Cell Biol* 2004; 5: 614–625.
43. Sehgal P, Kong X, Wu J, Sunyer R, Trepas X, Leckband D. Epidermal growth factor receptor and integrins control force-dependent vinculin recruitment to E-Cadherin junctions. *J Cell Sci* 2018;
44. Labernadie A, Kato T, Brugués A *et al.* A mechanically active heterotypic E-cadherin/N-cadherin adhesion enables fibroblasts to drive cancer cell invasion. *Nat Cell Biol* 2017; 19: 224–237.
45. Buckley CD, Tan J, Anderson KL *et al.* The minimal cadherin-catenin complex binds to actin filaments under force. *Science* (1979) 2014; 346: 1254211–1254211.
46. Wang A, Dunn AR, Weis WI. Mechanism of the cadherin–catenin F-actin catch bond interaction. *Elife* 2022; 11.
47. Ishiyama N, Sarpal R, Wood MN *et al.* Force-dependent allostery of the α -catenin actin-binding domain controls adherens junction dynamics and functions. *Nat Commun* 2018; 9: 5121.
48. Mandai K, Nakanishi H, Satoh A *et al.* Afadin: A Novel Actin Filament–binding Protein with One PDZ Domain Localized at Cadherin-based Cell-to-Cell Adherens Junction. *Journal of Cell Biology* 1997; 139: 517–528.
49. Abe K, Takeichi M. EPLIN mediates linkage of the cadherin–catenin complex to F-actin and stabilizes the circumferential actin belt. *Proceedings of the National Academy of Sciences* 2008; 105: 13–19.
50. Kobiela A, Fuchs E. α -catenin: at the junction of intercellular adhesion and actin dynamics. *Nat Rev Mol Cell Biol* 2004; 5: 614–625.
51. Yao M, Qiu W, Liu R *et al.* Force-dependent conformational switch of α -catenin controls vinculin binding. *Nat Commun* 2014; 5: 4525.
52. Yonemura S, Wada Y, Watanabe T, Nagafuchi A, Shibata M. α -Catenin as a tension transducer that induces adherens junction development. *Nat Cell Biol* 2010; 12: 533–542.

53. Conway DE, Breckenridge MT, Hinde E, Gratton E, Chen CS, Schwartz MA. Fluid Shear Stress on Endothelial Cells Modulates Mechanical Tension across VE-Cadherin and PECAM-1. *Current Biology* 2013; 23: 1024–1030.
54. Borghi N, Sorokina M, Shcherbakova OG *et al.* E-cadherin is under constitutive actomyosin-generated tension that is increased at cell–cell contacts upon externally applied stretch. *Proceedings of the National Academy of Sciences* 2012; 109: 12568–12573.
55. Shoyer TC, Gates EM, Cabe JI, Conway DE, Hoffman BD. Coupling During Collective Cell Migration is Controlled by a Vinculin Mechanochemical Switch. *bioRxiv* 2023;
56. Ayad MA, Mahon T, Patel M *et al.* Förster resonance energy transfer efficiency of the vinculin tension sensor in cultured primary cortical neuronal growth cones. *Neurophotonics* 2022; 9.
57. Martiel J-L, Leal A, Kurzawa L *et al.* Measurement of cell traction forces with ImageJ. In: 2015: 269–287.
58. Plotnikov S V., Sabass B, Schwarz US, Waterman CM. High-Resolution Traction Force Microscopy. In: 2014: 367–394.
59. Maruthamuthu V, Gardel ML. Protrusive Activity Guides Changes in Cell-Cell Tension during Epithelial Cell Scattering. *Biophys J* 2014; 107: 555–563.
60. Jannie KM, Ellerbroek SM, Zhou DW *et al.* Vinculin-dependent actin bundling regulates cell migration and traction forces. *Biochemical Journal* 2015; 465: 383–393.
61. Thievensen I, Fakhri N, Steinwachs J *et al.* Vinculin is required for cell polarization, migration, and extracellular matrix remodeling in 3D collagen. *The FASEB Journal* 2015; 29: 4555–4567.
62. Holle AW, Tang X, Vijayraghavan D *et al.* In situ mechanotransduction via vinculin regulates stem cell differentiation. *Stem Cells* 2013; 31: 2467–2477.
63. Liu Z, Tan JL, Cohen DM *et al.* Mechanical tugging force regulates the size of cell–cell junctions. *Proceedings of the National Academy of Sciences* 2010; 107: 9944–9949.
64. Barry AK, Tabdili H, Muhamed I *et al.* α -Catenin cytomechanics – role in cadherin-dependent adhesion and mechanotransduction. *J Cell Sci* 2014; 127: 1779–1791.
65. Ozawa M. Nonmuscle myosin IIA is involved in recruitment of apical junction components through activation of α -catenin. *Biol Open* 2018; 7.
66. Peng X, Cuff LE, Lawton CD, DeMali KA. Vinculin regulates cell-surface E-cadherin expression by binding to β -catenin. *J Cell Sci* 2010; 123: 567–577.
67. Thomas WA, Boscher C, Chu Y-S *et al.* α -Catenin and Vinculin Cooperate to Promote High E-cadherin-based Adhesion Strength. *Journal of Biological Chemistry* 2013; 288: 4957–4969.
68. Matsuzawa K, Himoto T, Mochizuki Y, Ikenouchi J. α -Catenin Controls the Anisotropy of Force Distribution at Cell-Cell Junctions during Collective Cell Migration. *Cell Rep* 2018; 23: 3447–3456.
69. Bejar-Padilla V, Cabe JI, Lopez S *et al.* α -Catenin-dependent vinculin recruitment to adherens junctions is antagonistic to focal adhesions. *Mol Biol Cell* 2022; 33.

70. Hazan RB, Kang L, Roe S, Borgen PI, Rimm DL. Vinculin Is Associated with the E-cadherin Adhesion Complex. *Journal of Biological Chemistry* 1997; 272: 32448–32453.
71. Grashoff C, Hoffman BD, Brenner MD *et al.* Measuring mechanical tension across vinculin reveals regulation of focal adhesion dynamics. *Nature* 2010; 466: 263–266.
72. Acharya BR, Nestor-Bergmann A, Liang X *et al.* A Mechanosensitive RhoA Pathway that Protects Epithelia against Acute Tensile Stress. *Dev Cell* 2018; 47: 439–452.e6.
73. Merkel CD, Li Y, Raza Q, Stolz DB, Kwiatkowski A V. Vinculin anchors contractile actin to the cardiomyocyte adherens junction. *Mol Biol Cell* 2019; 30: 2639–2650.
74. Kotini MP, van der Stoel MM, Yin J *et al.* Vinculin controls endothelial cell junction dynamics during vascular lumen formation. *Cell Rep* 2022; 39: 110658.
75. Fournier MF, Sauser R, Ambrosi D, Meister J-J, Verkhovsky AB. Force transmission in migrating cells. *Journal of Cell Biology* 2010; 188: 287–297.
76. Schwarz US, Soiné JRD. Traction force microscopy on soft elastic substrates: A guide to recent computational advances. *Biochimica et Biophysica Acta (BBA) - Molecular Cell Research* 2015; 1853: 3095–3104.
77. Ribeiro AJS, Denisin AK, Wilson RE, Pruitt BL. For whom the cells pull: Hydrogel and micropost devices for measuring traction forces. *Methods* 2016; 94: 51–64.
78. Polacheck WJ, Chen CS. Measuring cell-generated forces: a guide to the available tools. *Nat Methods* 2016; 13: 415–423.
79. Fu J, Wang Y-K, Yang MT *et al.* Mechanical regulation of cell function with geometrically modulated elastomeric substrates. *Nat Methods* 2010; 7: 733–736.
80. Tan JL, Tien J, Pirone DM, Gray DS, Bhadriraju K, Chen CS. Cells lying on a bed of microneedles: An approach to isolate mechanical force. *Proceedings of the National Academy of Sciences* 2003; 100: 1484–1489.
81. Lehnert D, Wehrle-Haller B, David C *et al.* Cell behaviour on micropatterned substrata: limits of extracellular matrix geometry for spreading and adhesion. *J Cell Sci* 2004; 117: 41–52.
82. Kim D-H, Provenzano PP, Smith CL, Levchenko A. Matrix nanotopography as a regulator of cell function. *Journal of Cell Biology* 2012; 197: 351–360.
83. Curtis A, Wilkinson C. Topographical control of cells. *Biomaterials* 1997; 18: 1573–1583.
84. Dembo M, Oliver T, Ishihara A, Jacobson K. Imaging the traction stresses exerted by locomoting cells with the elastic substratum method. *Biophys J* 1996; 70: 2008–2022.
85. Dembo M, Wang Y-L. Stresses at the Cell-to-Substrate Interface during Locomotion of Fibroblasts. *Biophys J* 1999; 76: 2307–2316.
86. Plotnikov S V., Sabass B, Schwarz US, Waterman CM. High-Resolution Traction Force Microscopy. In: 2014: 367–394.
87. Canović EP, Seidl DT, Polio SR *et al.* Biomechanical imaging of cell stiffness and prestress with subcellular resolution. *Biomech Model Mechanobiol* 2014; 13: 665–678.

88. Polio SR, Rothenberg KE, Stamenović D, Smith ML. A micropatterning and image processing approach to simplify measurement of cellular traction forces. *Acta Biomater* 2012; 8: 82–88.
89. Blakely BL, Dumelin CE, Trappmann B *et al.* A DNA-based molecular probe for optically reporting cellular traction forces. *Nat Methods* 2014; 11: 1229–1232.
90. Galliker P, Schneider J, Eghlidi H, Kress S, Sandoghdar V, Poulikakos D. Direct printing of nanostructures by electrostatic autofocussing of ink nanodroplets. *Nat Commun* 2012; 3: 890.
91. Galliker P, Schneider J, Rüthemann L, Poulikakos D. Open-atmosphere sustenance of highly volatile attoliter-size droplets on surfaces. *Proceedings of the National Academy of Sciences* 2013; 110: 13255–13260.
92. Kress SJP, Richner P, Jayanti S V. *et al.* Near-Field Light Design with Colloidal Quantum Dots for Photonics and Plasmonics. *Nano Lett* 2014; 14: 5827–5833.
93. Richner P, Eghlidi H, Kress SJP, Schmid M, Norris DJ, Poulikakos D. Printable Nanoscopic Metamaterial Absorbers and Images with Diffraction-Limited Resolution. *ACS Appl Mater Interfaces* 2016; 8: 11690–11697.
94. Bergert M, Lendenmann T, Zündel M *et al.* Confocal reference free traction force microscopy. *Nat Commun* 2016; 7: 12814.
95. Panciera T, Azzolin L, Cordenonsi M, Piccolo S. Mechanobiology of YAP and TAZ in physiology and disease. *Nat Rev Mol Cell Biol* 2017; 18: 758–770.
96. Dupont S, Morsut L, Aragona M *et al.* Role of YAP/TAZ in mechanotransduction. *Nature* 2011; 474: 179–183.
97. Aragona M, Panciera T, Manfrin A *et al.* A Mechanical Checkpoint Controls Multicellular Growth through YAP/TAZ Regulation by Actin-Processing Factors. *Cell* 2013; 154: 1047–1059.
98. Wang K-C, Yeh Y-T, Nguyen P *et al.* Flow-dependent YAP/TAZ activities regulate endothelial phenotypes and atherosclerosis. *Proceedings of the National Academy of Sciences* 2016; 113: 11525–11530.
99. Wang L, Luo J-Y, Li B *et al.* Integrin-YAP/TAZ-JNK cascade mediates atheroprotective effect of unidirectional shear flow. *Nature* 2016; 540: 579–582.
100. Nakajima H, Yamamoto K, Agarwala S *et al.* Flow-Dependent Endothelial YAP Regulation Contributes to Vessel Maintenance. *Dev Cell* 2017; 40: 523–536.e6.
101. Lin C, Yao E, Zhang K *et al.* YAP is essential for mechanical force production and epithelial cell proliferation during lung branching morphogenesis. *Elife* 2017; 6.
102. Schindelin J, Arganda-Carreras I, Frise E *et al.* Fiji: an open-source platform for biological-image analysis. *Nat Methods* 2012; 9: 676–682.
103. Hartig SM. Basic Image Analysis and Manipulation in ImageJ. *Curr Protoc Mol Biol* 2013; 102.
104. Meng W, Takeichi M. Adherens Junction: Molecular Architecture and Regulation. *Cold Spring Harb Perspect Biol* 2009; 1: a002899–a002899.

105. Gumbiner BM. Regulation of cadherin-mediated adhesion in morphogenesis. *Nat Rev Mol Cell Biol* 2005; 6: 622–634.
106. Wu Y, Jin X, Harrison O, Shapiro L, Honig BH, Ben-Shaul A. Cooperativity between *trans* and *cis* interactions in cadherin-mediated junction formation. *Proceedings of the National Academy of Sciences* 2010; 107: 17592–17597.
107. Briehner WM, Yap AS. Cadherin junctions and their cytoskeleton(s). *Curr Opin Cell Biol* 2013; 25: 39–46.
108. Maître J-L, Berthoumieux H, Krens SFG *et al.* Adhesion Functions in Cell Sorting by Mechanically Coupling the Cortices of Adhering Cells. *Science* (1979) 2012; 338: 253–256.
109. Yap A, Liang X, Gomez G. Current perspectives on cadherin-cytoskeleton interactions and dynamics. *Cell Health Cytoskeleton* 2015; 11.
110. Charras G, Yap AS. Tensile Forces and Mechanotransduction at Cell–Cell Junctions. *Current Biology* 2018; 28: R445–R457.
111. Liu Z, Tan JL, Cohen DM *et al.* Mechanical tugging force regulates the size of cell–cell junctions. *Proceedings of the National Academy of Sciences* 2010; 107: 9944–9949.
112. Ishiyama N, Sarpal R, Wood MN *et al.* Force-dependent allostery of the α -catenin actin-binding domain controls adherens junction dynamics and functions. *Nat Commun* 2018; 9: 5121.
113. Bershadsky AD, Balaban NQ, Geiger B. Adhesion-Dependent Cell Mechanosensitivity. *Annu Rev Cell Dev Biol* 2003; 19: 677–695.
114. Lecuit T, Lenne P-F, Munro E. Force Generation, Transmission, and Integration during Cell and Tissue Morphogenesis. *Annu Rev Cell Dev Biol* 2011; 27: 157–184.
115. Wagh AA, Roan E, Chapman KE *et al.* Localized elasticity measured in epithelial cells migrating at a wound edge using atomic force microscopy. *American Journal of Physiology-Lung Cellular and Molecular Physiology* 2008; 295: L54–L60.
116. Bruner HC, Derksen PWB. Loss of E-Cadherin-Dependent Cell–Cell Adhesion and the Development and Progression of Cancer. *Cold Spring Harb Perspect Biol* 2018; 10: a029330.
117. Cross SE, Jin Y-S, Rao J, Gimzewski JK. Nanomechanical analysis of cells from cancer patients. *Nat Nanotechnol* 2007; 2: 780–783.
118. Xu W, Mezencev R, Kim B, Wang L, McDonald J, Sulchek T. Cell Stiffness Is a Biomarker of the Metastatic Potential of Ovarian Cancer Cells. *PLoS One* 2012; 7: e46609.
119. Prabhune M, Belge G, Dotzauer A, Bullerdiek J, Radmacher M. Comparison of mechanical properties of normal and malignant thyroid cells. *Micron* 2012; 43: 1267–1272.
120. Faria EC, Ma N, Gazi E *et al.* Measurement of elastic properties of prostate cancer cells using AFM. *Analyst* 2008; 133: 1498.
121. Giepmans BNG, van IJzendoorn SCD. Epithelial cell–cell junctions and plasma membrane domains. *Biochimica et Biophysica Acta (BBA) - Biomembranes* 2009; 1788: 820–831.

122. Lambert M, Padilla F, Mege RM. Immobilized dimers of N-cadherin-Fc chimera mimic cadherin-mediated cell contact formation: contribution of both outside-in and inside-out signals. *J Cell Sci* 2000; 113: 2207–2219.
123. McLachlan RW, Kraemer A, Helwani FM, Kovacs EM, Yap AS. E-Cadherin Adhesion Activates c-Src Signaling at Cell–Cell Contacts. *Mol Biol Cell* 2007; 18: 3214–3223.
124. Borghi N, Lowndes M, Maruthamuthu V, Gardel ML, Nelson WJ. Regulation of cell motile behavior by crosstalk between cadherin- and integrin-mediated adhesions. *Proceedings of the National Academy of Sciences* 2010; 107: 13324–13329.
125. Maruthamuthu V, Gardel ML. Protrusive Activity Guides Changes in Cell-Cell Tension during Epithelial Cell Scattering. *Biophys J* 2014; 107: 555–563.
126. Suffoletto K, Jetta D, Hua SZ. E-cadherin mediated lateral interactions between neighbor cells necessary for collective migration. *J Biomech* 2018; 71: 159–166.
127. Kovacs EM, Ali RG, McCormack AJ, Yap AS. E-cadherin Homophilic Ligation Directly Signals through Rac and Phosphatidylinositol 3-Kinase to Regulate Adhesive Contacts. *Journal of Biological Chemistry* 2002; 277: 6708–6718.
128. Cavey M, Rauzi M, Lenne P-F, Lecuit T. A two-tiered mechanism for stabilization and immobilization of E-cadherin. *Nature* 2008; 453: 751–756.
129. Collins C, Denisin AK, Pruitt BL, Nelson WJ. Changes in E-cadherin rigidity sensing regulate cell adhesion. *Proceedings of the National Academy of Sciences* 2017; 114.
130. Sullivan B, Light T, Vu V, Kapustka A, Hristova K, Leckband D. Mechanical disruption of E-cadherin complexes with epidermal growth factor receptor actuates growth factor–dependent signaling. *Proceedings of the National Academy of Sciences* 2022; 119.
131. Vendome J, Felsovalyi K, Song H *et al.* Structural and energetic determinants of adhesive binding specificity in type I cadherins. *Proceedings of the National Academy of Sciences* 2014; 111.
132. Eftekharijoo M, Mezher M, Chatterji S, Maruthamuthu V. Epithelial Cell-Like Elasticity Modulates Actin-Dependent E-Cadherin Adhesion Organization. *ACS Biomater Sci Eng* 2022; 8: 2455–2462.
133. Hinck L, Näthke IS, Papkoff J, Nelson WJ. Dynamics of cadherin/catenin complex formation: novel protein interactions and pathways of complex assembly. *Journal of Cell Biology* 1994; 125: 1327–1340.
134. Muhamed I, Wu J, Sehgal P *et al.* E-Cadherin-mediated force transduction signals regulate global cell mechanics. *J Cell Sci* 2016;
135. Sui A, Zhong Y, Demetriades AM *et al.* ATN-161 as an Integrin $\alpha 5 \beta 1$ Antagonist Depresses Ocular Neovascularization by Promoting New Vascular Endothelial Cell Apoptosis. *Medical Science Monitor* 2018; 24: 5860–5873.
136. WANG S, YANG J, WANG C, YANG Q, ZHOU X. SB-273005, an antagonist of $\alpha v \beta 3$ integrin, reduces the production of Th2 cells and cytokine IL-10 in pregnant mice. *Exp Ther Med* 2014; 7: 1677–1682.
137. Wu P-H, Aroush DR-B, Asnacios A *et al.* A comparison of methods to assess cell mechanical properties. *Nat Methods* 2018; 15: 491–498.

138. Li Y, Schnekenburger J, Duits MHG. Intracellular particle tracking as a tool for tumor cell characterization. *J Biomed Opt* 2009; 14: 064005.
139. Lekka M, Laidler P, Gil D, Lekki J, Stachura Z, Hryniewicz AZ. Elasticity of normal and cancerous human bladder cells studied by scanning force microscopy. *European Biophysics Journal* 1999; 28: 312–316.
140. Omidvar R, Tafazzoli-shadpour M, Shokrgozar MA, Rostami M. Atomic force microscope-based single cell force spectroscopy of breast cancer cell lines: An approach for evaluating cellular invasion. *J Biomech* 2014; 47: 3373–3379.
141. Bastatas L, Martinez-Marin D, Matthews J *et al.* AFM nano-mechanics and calcium dynamics of prostate cancer cells with distinct metastatic potential. *Biochimica et Biophysica Acta (BBA) - General Subjects* 2012; 1820: 1111–1120.
142. Ramos JR, Pabijan J, Garcia R, Lekka M. The softening of human bladder cancer cells happens at an early stage of the malignancy process. *Beilstein Journal of Nanotechnology* 2014; 5: 447–457.
143. Rebelo LM, de Sousa JS, Mendes Filho J, Radmacher M. Comparison of the viscoelastic properties of cells from different kidney cancer phenotypes measured with atomic force microscopy. *Nanotechnology* 2013; 24: 055102.
144. le Duc Q, Shi Q, Blonk I *et al.* Vinculin potentiates E-cadherin mechanosensing and is recruited to actin-anchored sites within adherens junctions in a myosin II-dependent manner. *Journal of Cell Biology* 2010; 189: 1107–1115.
145. Cohen DJ, Gloerich M, Nelson WJ. Epithelial self-healing is recapitulated by a 3D biomimetic E-cadherin junction. *Proceedings of the National Academy of Sciences* 2016; 113: 14698–14703.
146. Hotulainen P, Lappalainen P. Stress fibers are generated by two distinct actin assembly mechanisms in motile cells. *Journal of Cell Biology* 2006; 173: 383–394.
147. Zigmond SH. Formin-induced nucleation of actin filaments. *Curr Opin Cell Biol* 2004; 16: 99–105.
148. Rizvi SA, Neidt EM, Cui J *et al.* Identification and Characterization of a Small Molecule Inhibitor of Formin-Mediated Actin Assembly. *Chem Biol* 2009; 16: 1158–1168.
149. Carramusa L, Ballestrem C, Zilberman Y, Bershadsky AD. Mammalian diaphanous-related formin Dia1 controls the organization of E-cadherin-mediated cell-cell junctions. *J Cell Sci* 2007; 120: 3870–3882.
150. Nishimura Y, Shi S, Zhang F *et al.* The formin inhibitor SMIFH2 inhibits members of the myosin superfamily. *J Cell Sci* 2021; 134.
151. Goley ED, Welch MD. The ARP2/3 complex: an actin nucleator comes of age. *Nat Rev Mol Cell Biol* 2006; 7: 713–726.
152. Yoshie H, Koushki N, Kaviani R *et al.* Traction Force Screening Enabled by Compliant PDMS Elastomers. *Biophys J* 2018; 114: 2194–2199.
153. Leckband DE, de Rooij J. Cadherin Adhesion and Mechanotransduction. *Annu Rev Cell Dev Biol* 2014; 30: 291–315.
154. Egeblad M, Nakasone ES, Werb Z. Tumors as Organs: Complex Tissues that Interface with the Entire Organism. *Dev Cell* 2010; 18: 884–901.

155. McMillin DW, Negri JM, Mitsiades CS. The role of tumour–stromal interactions in modifying drug response: challenges and opportunities. *Nat Rev Drug Discov* 2013; 12: 217–228.
156. Mueller MM, Fusenig NE. Friends or foes — bipolar effects of the tumour stroma in cancer. *Nat Rev Cancer* 2004; 4: 839–849.
157. Apostolopoulou M, Ligon L. Cadherin-23 Mediates Heterotypic Cell-Cell Adhesion between Breast Cancer Epithelial Cells and Fibroblasts. *PLoS One* 2012; 7: e33289.
158. Omelchenko T, Fetisova E, Ivanova O *et al.* Contact interactions between epitheliocytes and fibroblasts: Formation of heterotypic cadherin-containing adhesion sites is accompanied by local cytoskeletal reorganization. *Proceedings of the National Academy of Sciences* 2001; 98: 8632–8637.
159. Ounkomol C, Yamada S, Heinrich V. Single-Cell Adhesion Tests against Functionalized Microspheres Arrayed on AFM Cantilevers Confirm Heterophilic E- and N-Cadherin Binding. *Biophys J* 2010; 99: L100–L102.
160. Straub BK, Rickelt S, Zimbelmann R *et al.* E–N-cadherin heterodimers define novel adherens junctions connecting endoderm-derived cells. *Journal of Cell Biology* 2011; 195: 873–887.
161. Volk T, Cohen O, Geiger B. Formation of heterotypic adherens-type junctions between L-CAM-containing liver cells and A-CAM-containing lens cells. *Cell* 1987; 50: 987–994.
162. Vendome J, Felsovalyi K, Song H *et al.* Structural and energetic determinants of adhesive binding specificity in type I cadherins. *Proceedings of the National Academy of Sciences* 2014; 111.
163. Watanabe T, Sato K, Kaibuchi K. Cadherin-mediated Intercellular Adhesion and Signaling Cascades Involving Small GTPases. *Cold Spring Harb Perspect Biol* 2009; 1: a003020–a003020.
164. Yamada S, Nelson WJ. Localized zones of Rho and Rac activities drive initiation and expansion of epithelial cell–cell adhesion. *Journal of Cell Biology* 2007; 178: 517–527.

VITA

Mazen Mezher
Email: mmezh001@odu.edu
Cell Phone: 757-705-6736

EDUCATION

- Ph.D. candidate in Mechanical Engineering (Fall 2018-Spring 2023), GPA: 4.0
Old Dominion University, Norfolk, VA.
Dissertation: E-cadherin force transmission and stiffness sensing
- M.Sc. in Chemical Engineering (Fall 2014-Spring 2016), GPA: 3.7
Holy Spirit University of Kaslik, Lebanon.
- B.Sc. in Chemical Engineering (Spring 2011-Spring 2014), GPA: 3.01
Holy Spirit University of Kaslik, Lebanon.

PROFESSIONAL EXPERIENCES

- Designing and developing protocols to couple proteins (collagen, fibronectin, N-cadherin and E cadherin) onto soft substrates (Polyacrylamide gels and PDMS) as a biomimetic surface for cell spreading in vitro.
- Quantifying cellular force exertion of different cell types using Traction Force Microscopy (TFM) technique and Traction Force Imbalance Method (TFIM) for several cell types.
- Transiently transfecting cells for DNA plasmids such as vinculin to overexpress vinculin in MDCK vinculin Knock-out cells.
- Quantifying the nucleus and cytoplasmic organization of YAP1 transcription factor of cells using immunofluorescence staining and image processing techniques.
- Investigating the role of molecular keys using various inhibitors
- Fabricating PAA gels and PDMS substrate for extracellular matrix (ECM) of the cells.
- Validating stiffness of PDMS and PAA gels using rheometer instrument and indentation.
- Utilizing biaxial cell stretcher apparatus to study cell-cell adhesion rupturing assays.

SELECTED PUBLICATIONS

- September 2022: Bejar-Pailla, V., Cabe, J. I., Lopez, S., Narayanan, V., Mezher, M., Maruthamuthu, V., Conway, D. E. (2022) α -catenin Dependent Vinculin Recruitment to Adherens Junctions is Antagonistic to Focal Adhesions. *Mol. Biol. Cell*.
- May 2022: Eftekharijoo, M.*, Mezher, M.*, Siddharth, C., and Maruthamuthu, V. (2022) Epithelial Cell-like Elasticity Modulates Actin-Dependent E-cadherin Adhesion Organization. *ACS biomater. Sci. Eng.* 8 2455-62. (Equal Contribution as co-first author.)
- *(Manuscript in progress – will be submitted in Biophysical Journal): Mezher, M., Dumbali, S., Fenn, I., Lamb, C., Miller, C., Cabe, J.I., Conway, D., and Maruthamuthu, V. (2023): “Vinculin is Essential for High Endogenous Force Transmission at Cell-Cell Contacts.”

PRESENTATIONS

- Graduate Student Research Conference (GSRC) at EVMS March 2023, Mazen Mezher, Sandeep Dumbali, Ian Fenn, Carter Lamb, Conrad Miller, Jolene I. Cabe, Daniel Conway, Venkat Maruthamuthu: “Vinculin, but not α -catenin, is Required for High Endogenous Force Transmission at Cell-Cell Contacts.”
- Biomedical Engineering Society (BMES) October 2022, Mazen Mezher, Sandeep Dumbali, and Venkat Maruthamuthu: “Vinculin is Required for High Force Transmission at Cell-Cell Contacts.”
- Engineering Student Projects Expo (ESPEX) April 2022, Mazen Mezher, Daniel Conway, and Venkat Maruthamuthu: “The Protein Vinculin is a Key Link in Cell-to-Cell Force Transmission.”

HONORS AND AWARDS

- %100 ODU Research Foundation scholarship (Spring 2021-Spring 2023)
- Batten College of Engineering and Technology (BCET) graduate student travel award (Fall 2022)
- %100 Tuition waiver scholarship in MAE (Spring 2019-Fall-2020)
- Certified Graduate Teaching Assistant Instructor (GTAI) instructor (Summer 2019)

MEMBERSHIPS

- Biomedical Engineering Society (BMES)